

Electronic Thesis and Dissertation Repository

10-9-2018 10:00 AM

Adsorption kinetics of C9-C12 hydrocarbons on carbonaceous materials

Erfan Pazoki Toroudi
The University of Western Ontario

Supervisor
Pjontek, Dominic
The University of Western Ontario

Briens, Cedric
The University of Western Ontario

Graduate Program in Chemical and Biochemical Engineering
A thesis submitted in partial fulfillment of the requirements for the degree in Master of
Engineering Science
© Erfan Pazoki Toroudi 2018

Follow this and additional works at: <https://ir.lib.uwo.ca/etd>

Recommended Citation

Pazoki Toroudi, Erfan, "Adsorption kinetics of C9-C12 hydrocarbons on carbonaceous materials" (2018).
Electronic Thesis and Dissertation Repository. 5859.
<https://ir.lib.uwo.ca/etd/5859>

This Dissertation/Thesis is brought to you for free and open access by Scholarship@Western. It has been accepted for inclusion in Electronic Thesis and Dissertation Repository by an authorized administrator of Scholarship@Western. For more information, please contact wlsadmin@uwo.ca.

Abstract

Fluid CokingTM reactors are used to convert heavy hydrocarbons to lighter products via thermal cracking. Fouling can occur within the Fluid Coker cyclones, leading to shut down for maintenance and recovery. Hydrocarbon adsorption on carbonaceous materials was thus investigated to identify mitigation strategies for cyclone fouling. A vertically oscillating gas-solid contacting system capable of providing well-mixed conditions has been designed to measure adsorption kinetics on carbonaceous materials under relevant temperatures and pressures. Adsorption kinetics and equilibrium measurements are reported for isothermal conditions. Fluid coke, flexicoke, and coconut shell activated carbon were used as adsorbents. N-decane, n-dodecane, and mesitylene were used as aliphatic and aromatic vapor adsorbates. Adsorption measurements showed much faster kinetics, based on reaching equilibrium values, with coke compared to activated carbon (time constants of 83 s versus 1220 s, respectively). However, equilibrium adsorption uptake of activated carbon is more than an order of magnitude higher than coke.

Keywords

Fluid CokingTM, Cyclone Fouling, Hydrocarbon Adsorption, Adsorption kinetics, Gas-Solid Adsorption, Fluid Coke, Activated Carbon

Dedication

1- In ever loving the memory of my grandmother

For making a wonderful childhood memory

2- To my gracious amazing Mother

For all her sacrifices during my lifetime

3- To my strong, successful Father

For making me feel proud

Acknowledgments

I truly appreciate and acknowledge many people whom this was impossible without their supports:

First, I would like to thank and acknowledge my supervisors Dr. Dominic Pjontek and Dr. Cedric Briens for giving me the opportunity to accomplish my M.E.Sc thesis.

I acknowledge Syncrude Canada and NSERC for trusting and funding this masters study. I truly appreciate the collaboration of Syncrude R&D engineers including Craig McKnight, Jason Wiens, Michael Wormsbecker, and Jennifer McMillan.

I am thankful of my family including my kind mom, my dad, my lovely sister and my brother who have supported me continuously at various stages of my life specifically during these two years being in Canada.

Many ICFAR students and staffs who supported me during these two years, on top of them, Ghazaleh Chegini who was like an older sister for me helping, supporting and advising me technically and emotionally non-stop. Especial thank to Cody Ruthman, and Fransisco Javier Sanchez for building the experimental unit of this project. I appreciate lots of help and supports from Majid, Yohann, Thomas Johnston, Christine Ramsden, Mohammad (Momo), and Flora at different periods of my M.E.Sc thesis study.

Finally, I would like to thank every friend who has supported me toward this path. Hessam Yousefi, I still can't believe that you are gone. Thanks for creating memories in this city and for showing me how to face an unwanted cruel disease while staying extraordinarily successful.

Table of Contents

Abstract	ii
Dedication	iii
Acknowledgment	iv
List of Tables	ix
List of Figures	xi
Chapter 1	1
1 Introduction	1
1.1 General Information on Heavy Oil/ Bitumen Upgrading	1
1.2 Fluid/ FlexiCoking™ Technology	2
1.3 Fluid Coking™ Process	6
1.4 Freeboard of the Fluid Coker	7
1.5 Cyclone Fouling	7
1.6 Dominant Mechanism of the Cyclone Fouling	7
1.7 Necessity of Studying Adsorption	11
1.8 Adsorption system Criteria for the Study	11
1.9 Research Objectives	12
Chapter 2	13
2 Adsorption Literature Review	13
2.1 General Adsorption/ Desorption Definition	13
2.2 Adsorption Isotherms	14
2.2.1 Basic Adsorption Isotherm	15
2.2.2 Langmuir Adsorption Isotherm	16
2.3 Gas-Solid Adsorption Kinetics	17

2.3.1	Adsorption Kinetics Models	17
2.4	Impact of Thermodynamic Parameters on Adsorption.....	17
2.5	Heat of Adsorption.....	18
2.6	Conventional Gas-Solid Adsorption Systems.....	18
26.1	Gas Manometry.....	18
2.6.2	Differential Manometry	19
2.6.3	Gas Flow Technique	21
2.6.4	Volumetric-Chromatographic Method.....	22
2.6.5	Gravimetric Method.....	24
2.6.6	Volumetric-Gravimetric Method	25
2.6.7	Micro Catalytic Reactors	25
2.6.7.1.	Crec Riser Simulator.....	26
2.6.7.1.1	Adsorption Assessment in CREC Riser Simulator.....	26
2.6.7.2	Jiggle Bed Reactor	27
2.7	Comparison of Adsorption Experimental Systems.....	30
Chapter 3	32
3	CO ₂ activation and liquid-solid adsorption	32
3.1	Introduction.....	32
3.2	Material an Methods	32
3.2.1	Adsorbates.....	32
3.2.2	Adsorbents	33

3.2.3	Liquid-solid Adsorption Measurement Procedure.....	35
3.2.4	Experimental Set-Up for Pretreatment and Activation.....	38
3.3	Results and Discussion	40
3.3.1	Activation and Experimental Analysis Results.....	40
3.3.1.1	Raw Fluid Coke Thermogravimetric Analysis.....	40
3.3.1.2	CO ₂ Activation.....	41
3.3.1.3	BET Analysis.....	43
3.3.2	Liquid-Solid Adsorption Results	44
3.3.2.1	Liquid Solid Adsorption Equilibrium.....	44
3.3.2.2	Specific Surface Area (SSA) Estimation.....	48
3.3.3	Liquid-Solid Adsorption Comparison with BET	49
3.3.4	Kinetics of Liquid-Solid Adsorption	50
3.4	Summary.....	52
Chapter 4.....		53
4	Hydrocarbon Adsorption Kinetics with Carbonaceous Materials	53
4.1	Introduction.....	53
4.2	Background Information.....	54
4.3	Material and Methods	54
4.3.1	Experimental Set-up.....	54
4.3.2	Measurement Technique.....	58
4.4	Results and Discussion	63

4.4.1	The Effect of Temperature on Adsorption Kinetics	65
4.4.2	The impact of Molecular Weight and Shape	68
4.4.3	Hydrocarbon Adsorption Kinetics with Coke.....	69
4.4.4	Comparison of Adsorption Kinetics with Different Carbonaceous Materials	71
4.4.5	Gas-Solid Results Comparison with BET and Liquid-Solid Adsorption Result	73
4.5	Summary of the Chapter	75
Chapter 5	77
5	Conclusion	77
	Bibliography	81
6	Appendices.....	87
	Curriculum Vitae	120

List of Tables

Table 1: Fluid and Flexicoking process general comparison.....	6
Table 2. Comparison of adsorption systems available in the literature	30
Table 3. Methylene blue and phenol physical properties (Stoekli et al., 2001; Santamarina et al., 2002)	33
Table 4. Comparison of physical properties of fluid coke with coconut shell activated carbon.....	34
Table 5. Adsorbents surface area and total pore volume along with percentage of micropores, mesopores , and macropores based on BET analysis based on BET analysis	43
Table 6. Activated carbon specific surface area measurement using liquid-solid adsorption method and Langmuir model	49
Table 7. Various coke particles specific surface area measurement using liquid-solid adsorption method with methylene blue and Langmuir model	50
Table 8. Physical Properties of hydrocarbon adsorbates	6464
Table 9. Reproducibility of model parameters	6666
Table 10. Step 1 in liquid-solid error analysis.....	100
Table 11. Step 2 in liquid-solid error analysis.....	101
Table 12. Step 3 in liquid-solid error analysis.....	102
Table 13. Step 4 in liquid-solid error analysis.....	103
Table 14. Step 5 in liquid-solid error analysis.....	104
Table 15. H/C mass ratio comparison of raw coke with activated coke.....	107

Table 16. Elemental analysis with replicates, average and standard deviation.....	108
Table 17. H/C molar ratio comparison of raw coke with activated coke.....	108
Table 18. 2 parameter equilibrium isotherm models.....	111
Table 19. Three parameter equilibrium isotherm models.....	112
Table 20. Kinetic Models.....	113

List of Figures

Figure 1. The schematic of Fluid Coking Process (Modified from Murray R. Gray, 2014)	4
Figure 2. The schematic of the Flexicoking process(Modified from Murray R. Gray, 2014)	5
Figure 3. Six main types of gas adsorption isotherms, according to IUPAC classification (Donohue, 2017)	15
Figure 4. Basic adsorption isotherm (modified from Sing et al., 1985)	16
Figure 5. Simple gas adsorption manometry (adapted from Rouquerol et al., 2014).....	20
Figure 6. Differential gas adsorption manometry (adapted from Haul and Dumbgen, 1960, Camp and Satnley, 1991)	21
Figure 7 Simple gas adsorption flow technique (adapted from Rouquerol et al., 2014) .	22
Figure 8. Schematic diagram for volumetric-Chromatographic measurements (Keller et al., 1999)	23
Figure 9. Schematic for gravimetric-chromatographic method (Keller et al., 1999)	24
Figure 10. schematic for volumetric-gravimetric method (Keller et al., 1999).....	25
Figure 11. Diagram of the Jiggle Bed Reactor (Latifi, 2012).....	2929
Figure 12. Microscope photographs of (a) activated carbon from coconut shell and (b)fluid coke from left to right.	34
Figure 13. Methylene Blue Wavelength Scan at 25 mg/L.....	3636
Figure 14. Phenol Wavelength Scan at 25 mg/L	3636
Figure 15. The time required to reach the equilibrium with activated carbon from coal.	37

Figure 16. Pretreatment/activation unit (JBR) set-up	39
Figure 17. Thermogravimetric Analysis of raw fluid coke.....	4040
Figure 18. Weight loss percentage versus activation temperature.....	4242
Figure 19. Methylene blue and phenol adsorption comparison with coal activated carbon	44
Figure 20. Methylene blue adsorption comparison with coconut shell activated carbon and coal activated carbon.....	46
Figure 21. Adsorption comparison with methylene blue for various coke particles	48
Figure 22. Liquid-solid adsorption results for various adsorbents versus BET surface area	50
Figure 23. Kinetics of methylene blue with activated carbon from coal at an initial concentration of 400 mg/L.....	52
Figure 24. The schematic and detailed dimensions of the unit's vessel.	56
Figure 25. The schematic of the vertically oscillating gas-solid contacting unit for hydrocarbon adsorption kinetic measurement	58
Figure 26. System Set-up: liquid hydrocarbon, solid particles insertion, and system closure.....	59
Figure 27. System Set-Up: Vacuum and nitrogen flush for the burette, solids-cup, and connections	60
Figure 28. Heat Supply: glass beads motions and hydrocarbon phase transition and venting.....	61
Figure 29. Gas-solid contact step in hydrocarbon adsorption kinetics measurement.....	62

Figure 30. Adsorption kinetics of n-decane with coconut shell activated carbon. Hollow and filled in data points are used to compare duplicate runs.	65
Figure 31. N-decane adsorption kinetics in the first 600 seconds with coconut shell activated carbon.	68
Figure 32. Hydrocarbons adsorption kinetics (mg/g) with activated carbon in boiling point +30 °	68
Figure 33. Hydrocarbons adsorption kinetics (mmol/g) with activated carbon in boiling point +30 °C.....	69
Figure 34. Adsorption kinetics comparison of SBC coke and Flexicoke with normal dodecane at 226 °C	70
Figure 35. Initial 100 seconds of coke adsorption kinetics experiment with normal dodecane at 226 °C	71
Figure 36. Adsorption kinetics comparison of raw coke, Flexicoke, and coconut shell activated carbon with normal dodecane at 226 °C.....	73
Figure 37. Comparison of gas-solid adsorption equilibrium with BET surface area ...	7474
Figure 38. Equilibrium gas-solid results versus equilibrium liquid-solid results.	7474
Figure 39. The schematic of delayed coking process.....	88
Figure 40. Coconut Shell Activated Carbon size distribution.....	105
Figure 40. Flexicoke size distribution.....	105
Figure 41. Raw Fluid Coke size distribution.....	106
Figure 43. Elemental Analysis.....	107

Figure 44. Methylene Blue Calibration Curve.....	109
Figure 45. Phenol Calibration Curve.....	110
Figure 46. The actual Ceramic Crucible.....	114
Figure 47. Crucible view from the top.....	115
Figure 48. Solids-cup configuration relative to the lid.....	115
Figure 49. Electromagnet position relative to the crucible lid and char cup.....	116
Figure 50. Pneumatic Valve.....	117
Figure 49. Induction power boar, copper coil and power supply box for induction heat generation.....	118
Figure 50. A scan of motions of stainless steel balls in the transparent vessel.....	118

Chapter 1

1 Introduction

The introduction covers general information about heavy oil upgrading, followed by an explanation about Fluid CokingTM technology, cyclone fouling, the essentiality of experimental adsorption study for proposing a representative model for cyclone fouling. At the end of this chapter, research objectives are explained.

1.1 General Information on Heavy Oil/ Bitumen Upgrading

Canada has some of the largest oil reserves globally, which are estimated to be about 168 billion barrels in the oil sands. Canadian oil production is projected to grow steadily. Although a significant decrease in oil price has slowed down the production rate, still according to CAPP's 2015 Crude Oil Forecast, Markets, and Transportation, total Canadian crude oil production will increase to 5.3 million barrels per day by 2030 from 3.5 million barrels per day in 2013 to meet domestic and international demand for Canadian oil (CAPP, 2015).

Bitumen is heavy crude oil, extracted from oil sands, which has more carbon than hydrogen, accompanied with more impurities, such as sulfur, nitrogen, and heavy metals when compared to conventional crude oil. The main production locations in Canada are Athabasca, Cold Lake, and Peace River. The Wabiskaw-McMurray deposit (in the Athabasca oil sands area) surrounding Fort McMurray is the largest and nearest to the surface (Ancheyta and Speight, 2007).

After extraction of bitumen, it still needs processing, which is called upgrading, for the sake of increasing the value (synthetic crude oil) and more importantly to be pipelined in regular pipelines with no needs of adding diluent and reaching a cleaner product such as gasoline, diesel fuel, kerosene, and petrochemical feedstocks. Through upgrading bitumen is converted into hydrocarbon streams – naphtha, light gas oil (LGO) and heavy gas oil

(HGO) – that are blended to create high quality, light, low-sulfur crude oil. During the upgrading process, large heavy molecules that will not distill (i.e., residue) are cracked to smaller and lighter molecules. This process occurs in the primary upgrading step at over 400 °C (Murray R. Gray, 2014) and may need secondary upgrading to reduce the sulfur concentration to less than 0.5 wt%. Bitumen upgrading is divided mainly into two main parts of separations and reactions. Separation processes include distillation, and asphaltene and solids removal, however, reaction processes branch into four sectors according to the method's operating temperature which are biougrading (ultra-low temperature, < 100 °C), in situ catalysis (low temperature, 100-350 °C), liquid phase reactions without coke (moderate temperature, 350-470 °C), as well as vapor and liquid coking at high temperatures over 470 °C (Murray R. Gray, 2014).

Heavy oil processing is generally divided into two main parts of primary upgrading (PUG) and secondary upgrading (SUG). In the primary upgrading, bitumen conversion to lighter compounds takes place either by carbon removal called coking or hydrogen addition (hydroconversion). Coking process is mainly categorized into three industrial methods: delayed coking, fluid coking, and flexi-coking. Coking processes are carried out under relatively low pressures (up to 350 kPa). Delayed coking is a simple process that is cheaper and easier to implement but produces more waste coke than Fluid Coking. When compared to Fluid Coking, Flexicoking eliminates waste coke by gasifying it (Ellis and Paul, 1998). The delayed coking process has been explained in more details in section 6.1 of appendices.

1.2 Fluid/ FlexiCoking™ Technology

Fluid Coking technology is contemporarily utilized in plants as heavy oil (bitumen) upgrading method which leads to higher distillates yields due to having lower residence times for the cracked vapors (Murray R. Gray, 2014) and operating at relatively higher temperatures (510-540 °C) than delayed coking processes. Fluid Coking is a continuous fluidized bed technology which leads to the production of several valuable products. During the process, it thermally cracks heavy hydrocarbons such as vacuum residues,

atmospheric residues, oil sands bitumen, heavy whole crudes, deasphalter bottoms, or FCC bottoms to lighter products (EMRE Co).

Syncrude Canada Ltd. uses Fluid Coking to upgrade Athabasca oil sands in Alberta, Canada. A typical Syncrude Fluid Coker has a total feed rate of 115 Kbbbl/day, where 75 percent of the feed consists of bitumen and the remainder is LC-Finer residue and purge oil (Murray R. Gray, 2014). Approximately 88.8 Kbbbl/day is produced, where the products consist mainly of combined gas oil (71%) and the rest is naphtha and butane (Murray R. Gray, 2014). The process utilizes reactor and burner vessels, with the overall flow structure shown in Figure 1. The reactor contains a bed of coke particles, fluidized by steam and hydrocarbon vapors. The superficial gas velocity at the top of the reactor is approximately 0.8 m/s, and the solid-to-gas mass flow ratio is 10.7 in the process (Song et al., 2004). The bitumen is atomized with steam and is injected into the bed region, where it contacts and coats the hot coke particles. Endothermic cracking reactions take place on the surface of the coke so that lighter hydrocarbons are created and vaporized. These pass through the freeboard, a horn chamber, cyclones for particle separation, and through a scrubber, while the coke exits the vessel from the bottom. The cold coke is transferred to the burner where it is partially combusted and heated. The hot coke from the burner then passes back into the reactor. Hot coke enters the vessel in the freeboard, with a net downward flow in the vessel. The coke circulation from the burner to the coker provides the required heat for thermal cracking reactions (Solnordal et al., 2012).

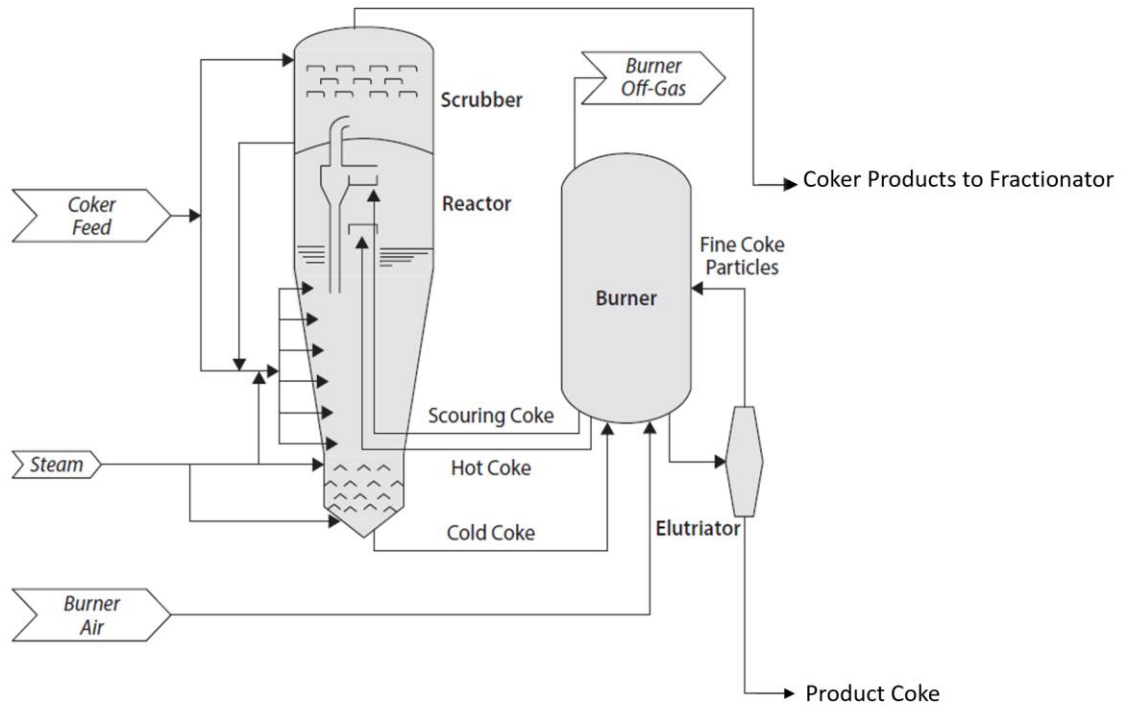


Figure 1. The schematic of the Fluid Coking Process (modified from Murray R. Gray, 2014)

FlexicokingTM technology is a similar process to Fluid Coking. However, a gasifier is included in the process to convert coke to a combination of CO, and H₂. This technology not only produces a clean liquid with about the same yield as with fluid coking but also gasifies the low-value coke to produce flexi-gas, however, this is a low-value gas when compared with relatively low-cost natural gas (EMRE Co; Murray R. Gray, 2014). The diagram of the flexicoking process is shown in figure 2.

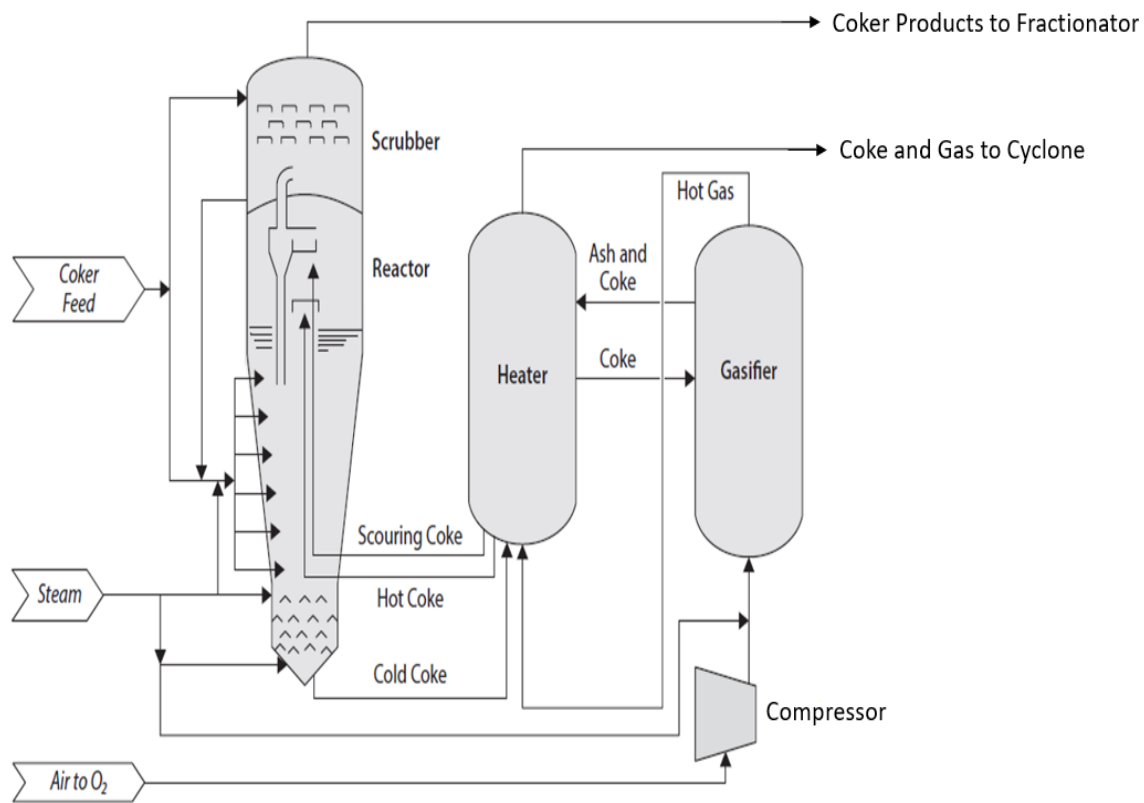


Figure 2. The schematic of the Flexicoking process (modified from Murray R. Gray, 2014)

Table 1. Fluid Coking and Flexicoking process comparison (modified from Murray R. Gray, 2014).

Parameters	Fluid Coking	Flexicoking
Operation Mode	Continuous fluidized bed reactor	Continuous fluidized bed reactor
Operating Pressure (MPa)	0.35	0.35
Reactor Temperature (°C)	510-540	510-540
Burner Temperature (°C)	595-675	595-675
Volume yield per barrel of bitumen	86%	85%
Number of operational units worldwide	8	5
Capital Cost	Medium	Medium

1.3 Fluid Coking™ Process

The reactor is a fluidized bed which is operating at a relatively high temperature of 510-540 °C (EMRE Co). The bed temperature range provides the heat for the thermal cracking reactions, without the presence of a catalyst. At higher temperatures, over cracking to low-value gases is likely to take place. The feed is preheated to 350 °C and is injected through the steam atomization spray nozzles, and fresh hot coke enters in the top of the bed. Bitumen contacts with coke particles and are thermally cracked into volatile compounds.

These compounds are refined downstream, and heavier compounds create solid coke (Pfeifer et al., 1959).

The stripper is located at the bottom of the fluid coker, removes hydrocarbons from coke particles, which are then transferred to the burner. It is important to note that the selection of the bed temperature is a compromise. If the temperature is too high, there is more over-cracking to permanent gases. On the other hand, if it is too low, heavier hydrocarbon survives on the coke particles that flow into the stripper zone, hence, increasing the fouling rate in the stripper sheds. The rate of thermal cracking can be controlled by changing particle's size through injecting attrition stream at high velocities. The purpose of using scrubber at the top of the coker vessel is to remove heavy components coming out of cyclones, by contacting with low-temperature liquid hydrocarbons (Blaser, 1986; Jankovic, 1996; Bi et al. 2008).

1.4 Freeboard of the Fluid Coker

The hydrocarbon vapors and steam rising through the fluidized bed entrain coke particles, thus requiring sufficient space above the bed surface to disengage the coarse particles, allowing them to fall back into the bed. The height of the freeboard is optimized as a long vapor residence time can lead to over cracking to low-value gases. Whereas, if the height is too low, then the flow rate of coke particles entering the cyclones may be higher than can be accommodated by the cyclones. Hot coke particles in the freeboard region are essential by maintaining the elevated temperatures to avoid vapor condensation. Fine particles in this region do not fall back into the bed. Therefore, cyclones are used to separate particles and the vapor phase by utilizing vortex and centrifugal forces. The dipleg at the bottom of the cyclone return particles into the bed based on the collection efficiency. In Canada, Imperial oil operates one fluid coker in its Sarnia refinery, whereas Syncrude Canada Ltd. has three fluid cokers, each of them having a different number of parallel primary cyclones to reach the desirable particle collection efficiency. It should be noted that cyclone diplegs must be submerged into the dense reactor bed to ensure coke stays in the system. The coke particles entering the cyclones are a combination of particles from the fluid bed, from the stream of hot coke entering the freeboard of the reactor, and from scouring coke injected into the horn chamber (Mallory et al., 2000).

1.5 Cyclone Fouling

The condensation of heavy hydrocarbon vapors on the wall of cyclones following by formation of coke deposits referred as cyclone fouling has a significant impact on the reliability of the Fluid Cokers. The coke deposits grow and may cause an uneven blockage of the cyclones, restricting the gas outlet tubes (GOTs). This flow restriction eventually increases the pressure drop to the scrubber, increasing the upstream reactor pressure, and consequently increasing the burner's internal pressure. The increased unit pressure reduces the maximum liquid feed flow rate since the burner air blower maximum output is limited by the unit pressure, where the combustion with air provides the heat for the endothermic cracking reactions. Ultimately, the heavy hydrocarbon feed rate becomes too low, and the unit must be shut down for maintenance and removal of coke. The separate scouring coke transfer line, positioned within the horn chamber, is used to prevent deposits from forming by scouring the surface of the cyclone with additional coke, and by raising the temperature of the hydrocarbon stream (Solnordal et al., 2012).

1.6 Dominant Mechanism of the Cyclone Fouling

Previous studies have identified the main mechanisms for cyclone fouling and proposed mitigation strategies (e.g., adjusting operational conditions) to reduce the amount of coke deposition in the cyclones. Three main possible mechanisms have been identified for cyclone fouling:

1. Liquid feed entrainment
2. Chemical reactions forming condensable species
3. Heavy ends vapor condensation

Feed droplets entrainment into the coker freeboard region was investigated using a chemical liquid tracer placed in the feed atomization nozzles (Watkinson et al., 2004). The liquid tracer at the studied operating conditions of approximately 600-650 °C had negligible volatility. The authors experimentally demonstrated that the tracer concentration in the cyclone deposits was considerably lower than predicted if liquid feed entrainment was the dominant mechanism for cyclone fouling. Another study in this subject changed the filter characteristics between the system's feed section and an exit tube used for

deposition measurement (Zhang and Watkinson, 2005a). By increasing the filter pore size from 10 μm to 3 mm, they showed that feed droplet entrainment was not the main contributor of the observed cyclone fouling.

Following the bitumen injection into the fluidized bed, lighter hydrocarbons will flash to the vapor phase, while heavy hydrocarbons remain on the coke particles for thermal cracking to hydrocarbon vapors. It is possible that some of the heavier hydrocarbon vapors may react under the Fluid Coker operating conditions, potentially forming heavier species which could condense in the vapor phase, and deposit on the surface to form coke. A previous study heated and cooled the resulting vapors which were obtained when atomizing heavy hydrocarbons at a temperature of approximately 535°C (Zhang and Watkinson, 2005a). It was observed that raising the temperature above 535°C did not increase the downstream deposition rate, up to a studied temperature of 680°C. Deposition only increased when cooling the vapor, particularly below a temperature of 510°C. A theoretical study investigated the operating conditions that would favor chemical reactions in the vapor phase leading to condensable hydrocarbon species and aerosols (Gonzalez, 2004). The work concluded that cracking reactions leading to heavy hydrocarbons, and thus condensable species or aerosols, were unlikely at the Fluid Coker operating conditions. Another experimental study showed minimal coke deposition at elevated temperatures (490°C to 560°C) when operating with residence times of approximately 15 seconds, approaching Coker cyclones (Mallory et al., 2000). When increasing the residence time up to around 55 seconds, overall depositions were shown to grow at higher temperatures; however, this increase was observed in the downstream volume of sequential units to measure depositions. The previous results demonstrated that the chemical reaction of hydrocarbons should not dominate for the lower residence times expected in the Fluid Coker cyclones. As such, chemical reactions of the hydrocarbon vapors forming condensable species, although likely participating in the process, were discounted as the dominant mechanism for cyclone fouling.

The released vapors at the Fluid Coker's freeboard conditions are near the vapor-liquid equilibrium. Therefore, any changes in operating conditions such as temperature, pressure, and composition in the downstream may lead to physical condensation, likely starting with

heavier hydrocarbons. The Flexicoking process is like Fluid Coking, however, the coke particles are transported from the burner to a separate fluidized bed gasifier. In this configuration, the low-value rejected carbon (i.e., coke) is gasified to produce flexi-gas. It has been observed during industrial operations that Flexicokers have reduced cyclone fouling (Watkinson et al., 2004), which is believed to occur due to the increased particle porosity and surface area (Furimsky, 2000). In previous experiments, vapors were passed through either a 0.18 kg packed bed of fluid coke, flexi-coke, or a blank control before entering a cyclone. No considerable difference was observed between fluid coke and the empty test section, suggesting that fluid coke did not adsorb significant amounts of heavy hydrocarbon vapors. When using flexi-coke, however, the deposition rate decreased by over 90%. Changes to the particle surface area were measured before and after the previous experimental run, where the flexi-coke surface area dropped from 254 to 3.2-4 m²/g, while the fluid coke decreased from 11.7 to 0.1 m²/g. It was also visually observed that the fluid coke particles agglomerated at the entrance of the packed bed, while this was not observed with the flexi-coke which remained free-flowing. It was thus concluded that the flexicoke could adsorb the heavy hydrocarbon vapors which lead to downstream fouling. The free-flowing behavior of the flexi-coke also indicated that the adsorption likely occurs within the particle pores, while the observed agglomeration with the fluid coke particles concluded that the outer surface might have been coated. To verify the previous results, additional tests were carried out to establish the impact of vapor residence time and dilution effects (Zhang and Watkinson, 2005a). The residence time was varied based on the studied tube diameters when using the same volumetric flow rate, resulting in an eightfold reduction in the residence time, with no significant difference in deposition rate, further confirming that chemical reaction of the vapors is not a dominating fouling mechanism. Lastly, vapor dilution was studied by injecting steam or nitrogen between the experimental coker and the cyclone sections. A strong correlation between vapor dilution and the reduced deposition rate was observed, due to physical dilution of the vapor phase. Chemical reactions such as steam reforming and gasification were discounted since the impact of nitrogen dilution was comparable to that of the same steam dilution.

1.7 The Necessity of Studying Adsorption

It has been already mentioned that the dominant mechanism in cyclone fouling is believed to be due to the physical condensation of heavy hydrocarbons followed by deposition and coke formation. Heavy hydrocarbons, which are present in the Fluid Coker freeboard, are near vapor-liquid equilibrium (i.e., condensable species that could impact cyclone fouling). Adsorption of heavy hydrocarbons on the coke particles in the freeboard, horn chamber, or cyclone could thus reduce the risk of physical condensation, resulting in lower fouling. The primary assumption is that the first hydrocarbons to be condensed in the cyclone gas outlet tube are the ones most likely to be adsorbed, then, even a fraction of 1 % being adsorbed by coke particles is significant since most hydrocarbon vapors do not condense in the cyclone. Experimental hydrocarbon adsorption is thus an important input parameter for the development of a cyclone fouling model (which is a parallel project for this work at Western University on Modeling Fluid Coker Cyclone Fouling). Although the study of adsorption is the priority to understand better the mechanism of cyclone fouling, it is essential to differentiate between adsorption and condensation. Condensation refers to heavy hydrocarbons changing from the vapor to the liquid phase in a specific region followed by deposition and coke formation. Adsorption refers to the transfer of heavy hydrocarbons from the vapor phase to the particle surface and internal pores, which are then bound to the particles themselves. Favorable operating conditions for hydrocarbon adsorption can be combined with the fouling model findings to identify optimal conditions to reduce coke deposition in cyclones. Therefore, experimentally determined adsorption kinetics and equilibrium data are needed to be integrated into the fouling model.

1.8 Adsorption system Criteria for the Study

This thesis aims to provide experimental adsorption kinetic and equilibrium data for the modeling of cyclone fouling. It is essential to consider particles conditions just upstream of the cyclones, so we need to look for the conditions of the fluid coker horn chamber. The kinetic study is particularly important to predict adsorption quantity within a reasonable residence time for the contact between fluid coke particles and the vapors in the freeboard, horn chamber, and cyclones. Particles in the freeboard, whether entrained from the bed

surface inside the horn chamber or transferred directly from the burner to the horn chamber by the scouring coke transfer line, are agitated and well mixed. As such, a fixed bed of particles is avoided, and a fluidized or well-mixed condition is considered to neglect external mass transfer limitations. The particles residence time in the coker can be on the order of minutes. However, the residence time in the horn chamber of the fluid coker is relatively short (on the order of 10 seconds). This further implies that the contacting time between particles and hydrocarbon vapors in the experimental system should reflect these criteria. As such, the experimental system criteria can be summarized as follows:

- 1: Can operate at a uniform temperature that can be set between 50 and 300 °C to avoid thermal cracking
- 2: Operate at a representative hydrocarbon partial pressure (approximately 1 atm)
- 3: Well-mixed conditions, negligible external mass transfer
- 4: Can provide data for adsorption kinetics at a timescale relevant to the Fluid Coker

1.9 Research Objectives

The main objectives of the thesis can be summarized as follows.

1. Study the impact of fluid coke activation on adsorption characteristics. Liquid-solid adsorption with methylene blue will be performed on a range of carbonaceous materials (i.e., activated carbon, fluid coke, activated fluid coke, flexicoke).
2. Design and develop a system for gas-solid hydrocarbon adsorption kinetics and equilibrium.
3. Use model compounds with varying molecular structures (aliphatic, aromatic) to study adsorption rates on coke (Novelty of the research). Compare between carbonaceous materials, including fluid coke, flexicoke, and activated carbon.

There are some previous studies investigating hydrocarbon adsorption on carbonaceous materials (chapter 4), however, this research stands out among literature since we measure C₉-C₁₂ adsorption kinetics on activated carbon, fluid coke, and flexicoke at near atmospheric pressure.

Chapter 2

2 Adsorption Literature Review

This chapter explains the general gas-solid adsorption definition following by introducing various equilibria and kinetics models for gas-solid adsorption, thermodynamic and heat of adsorption. In addition, a comprehensive literature study on potential systems for gas-solid adsorption is investigated and at the end advantages and disadvantages of each system is included, along with the operating conditions required for the actual gas-solid adsorption equipment for the study.

2.1 General Adsorption/ Desorption Definition

Accumulation of molecules of a gas, liquid or dissolved solids on a surface is defined as adsorption. The adsorption process involves two main materials. One is the material on which adsorption occurs, known as an adsorbent. The second is a gas, liquid or solute that gets adsorbed on the surface known as the adsorbate.

There are mainly two terms of adsorption and desorption which are usually used to show the direction from which the equilibrium states are reached. In the mid-1980s a committee of IUPAC published a set of recommendations to guide the use of gas adsorption measurements (especially for nitrogen at its normal boiling point of 77 K) for porous materials characterization. The classification introduced for pores based on their size: micropores for pores with diameters less than 2 nm; mesopores for pores with diameters in the range 2–50 nm and macropores for pores with diameters greater than 50 nm). Adsorption hysteresis (where adsorbent loading and regeneration follow some different trend versus partial pressure) arises when the amount adsorbed is not brought to the desired level by the adsorption and desorption approach to a given equilibrium pressure or bulk concentration. The relation, at a constant temperature, between the amount adsorbed and the equilibrium pressure, or concentration, is known as adsorption isotherms (F. Rouquerol et al., 1999).

There are two types of adsorption, mainly known as physical adsorption (physisorption) or chemical adsorption (chemisorption). Physisorption forces are equal to those for condensation of vapors and deviation from an ideal gas. However, chemisorption interactions are essentially those responsible for the formation of chemical compounds (F. Rouquerol et al., 1999).

2.2 Adsorption Isotherms

The amount of gas adsorbed, X , per unit mass of solid, m , is dependent on the nature of the system, temperature, and pressure, so considering a specified system in an isothermal condition will lead to having the amount of adsorption as a function of pressure.

There is a wide variety of forms for measurement of gas-solid adsorption in the literature review, however, according to IUPAC classification, most of these physical adsorption isotherms can be classified into main six groups representing in figure 3. Type I approaches the limiting value at $P/P^\circ \rightarrow 1$ (P is the operating pressure, and P° is the saturation pressure). Type II represents the completion of the monomolecular layer (monolayer) and also beginning of the formation of multicomponent layer (multilayer). This type occurs when using nonporous or macroporous adsorbents and allow monolayer-multilayer adsorption to occur at high P/P° . Complete reversibility of adsorption-desorption isotherm is the first condition to be satisfied for normal monolayer-multilayer adsorption on an open and stable surface. Type III isotherm indicates weak adsorbent-adsorbate interactions. A real type III isotherm is not typical. The loop is usually associated with filling and emptying of the mesopores by capillary condensation (hysteresis). The exact shape of the loop varies from one system to another. Type V isotherm as type III shows weak adsorbent-adsorbate interactions. The type V hysteresis loop is associated with the mechanism of pore filling and emptying. Type VI adsorption isotherm which is known as stepped isotherm is associated with layer-by-layer adsorption on a highly uniform surface (F. Rouquerol et al., 1999).

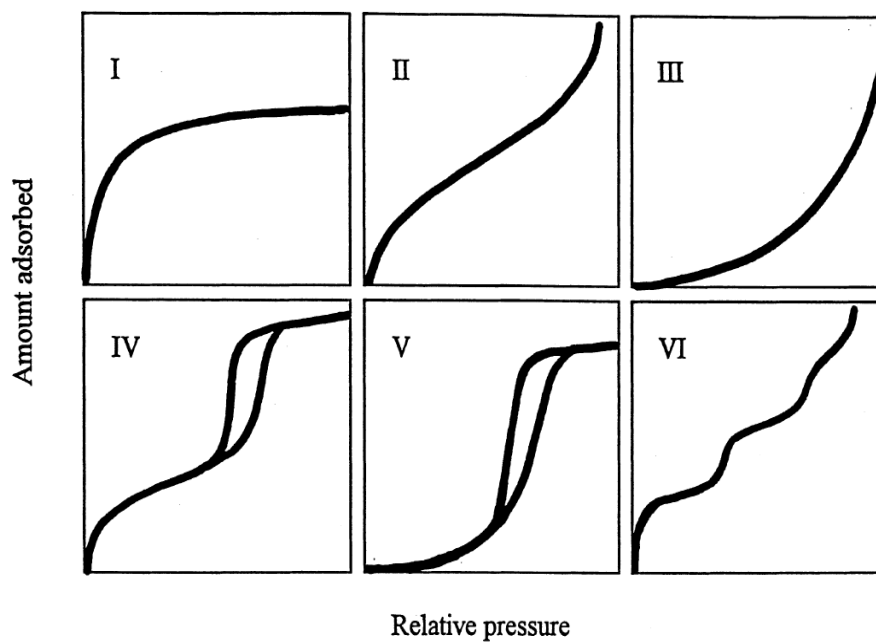


Figure 3. Six main types of gas adsorption isotherms, according to IUPAC classification (Donohue, 2017)

2.2.1 Basic Adsorption Isotherm

In this isotherm, the amount of adsorption increases by an increase of pressure, until P_s (P_s is the saturation pressure), however, after this pressure, increasing the pressure does not affect adsorption amount, since the adsorbent has reached its maximum capacity for the adsorption. (Sing et al., 1985)

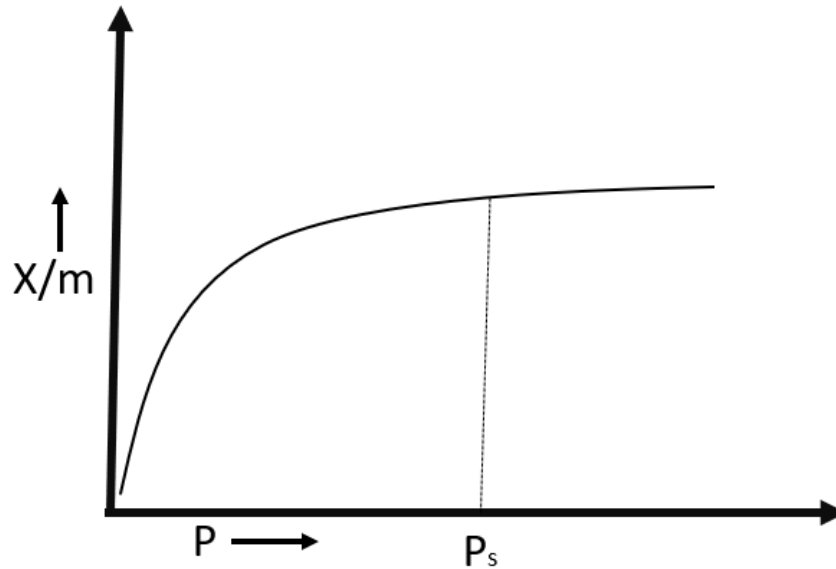


Figure 4. Basic adsorption isotherm (modified from Sing et al., 1985)

It is shown by figure 4 that after saturation process, adsorption does not occur, which can be explained due to the filling of limited numbers of vacancies in the surface (Peter Atkinson).

2.2.2 Langmuir Adsorption Isotherm

Langmuir assumed that an adsorbate behaves as an ideal gas at a constant temperature. In that condition, adsorbate's partial pressure is related to the volume of it which is adsorbed onto the adsorbent. Original derivation of Langmuir correlation is a kinetic-based equation by considering that the adsorbent surface has an array of N^s vacancies and considering N^a of these vacancies are occupied by molecules, then the fractional occupancy is defined ($\theta = \frac{N^a}{N^s}$). Considering that equilibrium will be reached when rates of adsorption and desorption are equal, so Langmuir isotherm can be expressed as (Langmuir, Irvine 1918);

$$\theta_A = \frac{V}{V_m} = \frac{K_{eq}^A P_A}{1 + K_{eq}^A P_A} \quad (1)$$

Where, θ_A = Fractional occupancy of adsorption sites, V = adsorbate volume which is adsorbed on the adsorbent, V_m = Volume of the monolayer, K_{eq} = equilibrium Langmuir constant, and P_A = adsorbate's partial pressure.

Langmuir assumed that the energy of adsorption in the first layer is much higher compared to the other layers, then multilayer formation is possible at higher pressure compared to the pressure required for completion of the monolayer. Indeed, this situation coincides with stepwise in type VI isotherm, however, Langmuir isotherm is not able to predict adsorbate-adsorbate interactions accurately. Besides, it has been considered that adsorbed molecules in this isotherm are immobile. A detailed explanation on the other types of equilibrium isotherm models including Freundlich model, the Brenner-Emmet-Teller (BET), and Dubinin-Astakhov (D-A) Isotherm has been investigated at the end of the thesis in the section 6-3, 6-4, 6-5 and 6-12 of the appendices.

2.3 Gas-Solid Adsorption Kinetics

Adsorption kinetics study is the investigation of adsorption as a function of time on the solid surface. Along with equilibria study of adsorption, kinetics study is essential to understand how fast this process is taking place. We can consider four distinct stages for adsorption kinetics, which are (Lazaridis and Asouhidou, 2003):

1. External Diffusion: Diffusion of molecules from the bulk phase towards the interface space
2. Internal diffusion: Diffusion of molecules inside the pores
3. Surface diffusion: Diffusion of molecules in the surface phase
4. Adsorption/desorption elementary processes

There are many adsorption kinetics models in the literature (Banat *et al.*, 2003; Sunand Yang, 2003; Aksu and Kabasakal, 2004; Hamadi *et al.*, 2004; Jain *et al.*, 2004; Min *et al.*, 2004; Shin *et al.*, 2004; Namasivayam and Kavitha, 2005; Chen *et al.*, 2008; Cheng *et al.*, 2008; Hameed, 2008; Huang *et al.*, 2008; Wan Ngah and Hanafiah, 2008; Rosa *et al.*, 2008;

Tan *et al.*, 2008). A range of kinetic models have been represented and compared in section 6.12 of appendices which includes Pseudo-first-order-rate, Pseudo-second-order-rate, Elovich, modified second-order, n^{th} order, and intraparticle diffusion. Among different models which used with experimental results, pseudo-first-order-rate fit reasonably well, therefore we used this model with all experimental results. The model is explained in the following subsection.

2.3.1 Adsorption Kinetics Model (Pseudo-First-Order-Rate)

The Pseudo-first-order rate kinetic model is the earliest model (Lagargen,1898) which is calculating the adsorption rate based on the adsorption capacity. The primary, integrated and linearized equations are as following:

$$\frac{dq}{dt} = K_{p_1}(q_e - q_t) \quad (2)$$

$$\text{Ln} \left(\frac{q_e}{q_e - q_t} \right) = K_{p_1} t \quad (3)$$

$$\text{Log} (q_e - q_t) = \text{Log} q_e - \frac{K_{p_1}}{2.303} t \quad (4)$$

Where q_e (mg/g) and q_t (mg/g) are the adsorption capacities at equilibrium and at time t . K_{p_1} (min^{-1}) is the pseudo first order rate constant. Boundary conditions are: $q_t = 0$, at $t=0$ and $q_t=q_t$ at $t=t$.

2.4 Impact of Thermodynamic Parameters on Adsorption

One of the crucial parameters which is affecting the adsorption is temperature. Temperature does not work in favor of adsorption which essentially means by increasing the temperature; less adsorption is likely to occur (for gaseous adsorbates). However, the trend is in opposite for partial pressure (gas phase) and concentration (in the liquid phase), and by increasing partial pressure (concentration or adsorbate's moles), it is expected to have more adsorption taking place. Two main thermodynamic parameters impacting on adsorption process are temperature and partial pressure. Since in most equilibrium studies,

the objective is to investigate adsorption capacity as a function of partial pressure, therefore, the temperature is stabilized on a certain amount in each experiment to investigate the adsorption data properly and model the obtained results with an isotherm.

The adsorption process is an exothermic reaction, hence, ΔH (enthalpy change known as heat of adsorption) is always negative in a process. In addition, while adsorption is taking place, the adsorbate molecules have less freedom to move which makes entropy change (ΔS) negative as well.

On the other hand, adsorption is an instantaneous process, therefore, (ΔG) is always negative based on Gibbs-Helmholtz laws ($\Delta G = \Delta H - T\Delta S$). During the process $|\Delta H| > |T\Delta S|$ and the more process continues $|\Delta H - T\Delta S|$ would be less. Finally, at equilibrium, ΔH is equal to $T\Delta S$ to make $\Delta G = 0$. At this stage maximum adsorption has occurred and no adsorption will take place after then.

2.5 Heat of Adsorption

Molar heat or molar enthalpy of adsorption is the amount of heat released when 1 mole of gaseous adsorbate is adsorbed on the surface of the adsorbent. The amount of heats of adsorption in the case of chemisorption is much more than physisorption. Since in chemisorption we have chemical bonds which are noticeably stronger than weak van der Waals forces in the physisorption.

Heats of adsorption are twice as large as heats of condensation and range between 10 KJ/mole to 100 KJ/mole (Zimmermann and Keller, 2003). A full description of the measurement of the heat of adsorption along with corresponding differential equations is explained in the appendices of the thesis in section 6.7.

2.6 Conventional Gas-Solid Adsorption Systems

In this section, we will review equilibria systems for single-component adsorptive and consequently multi-component adsorptive.

2.6.1 Gas Manometry

In the gas manometry measurement, the basic idea is to measure the changes in a system's internal pressure in a calibrated, constant volume and at a known temperature. Once the adsorptive contacts the adsorbent, experiment starts and in case adsorption occurs, there should be a decreasing trend from initial to a final equilibrium pressure. Figure 5 shows the diagram of the gas adsorption manometry system (Rouquerol et al., 2014).

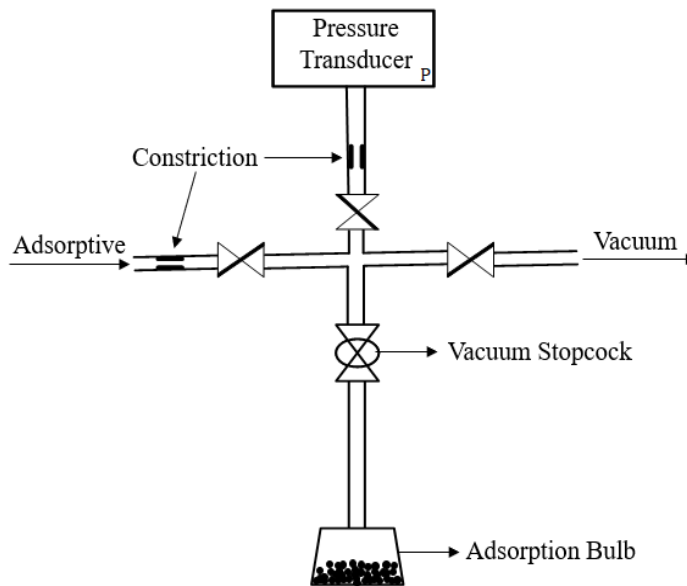


Figure 5. Simple gas adsorption manometry (adapted from Rouquerol et al., 2014)

2.6.2 Differential Manometry

In the differential manometry measurement, the idea is to use two separate vessels, one with the adsorbate and the other one with glass beads (which does not adsorb). Using a differential pressure transducer is of necessity in this method (glass beads container with higher pressure). We should note that in this method ensuring the same conditions (temperature, particle's mass, and adsorptive's partial pressure) in both containers is a necessary requirement that should be satisfied for the reasonable comparison between the

two vessels. Figure 6 shows a possible mechanism for differential gas adsorption manometry (Haul and Dumbgen, 1960).

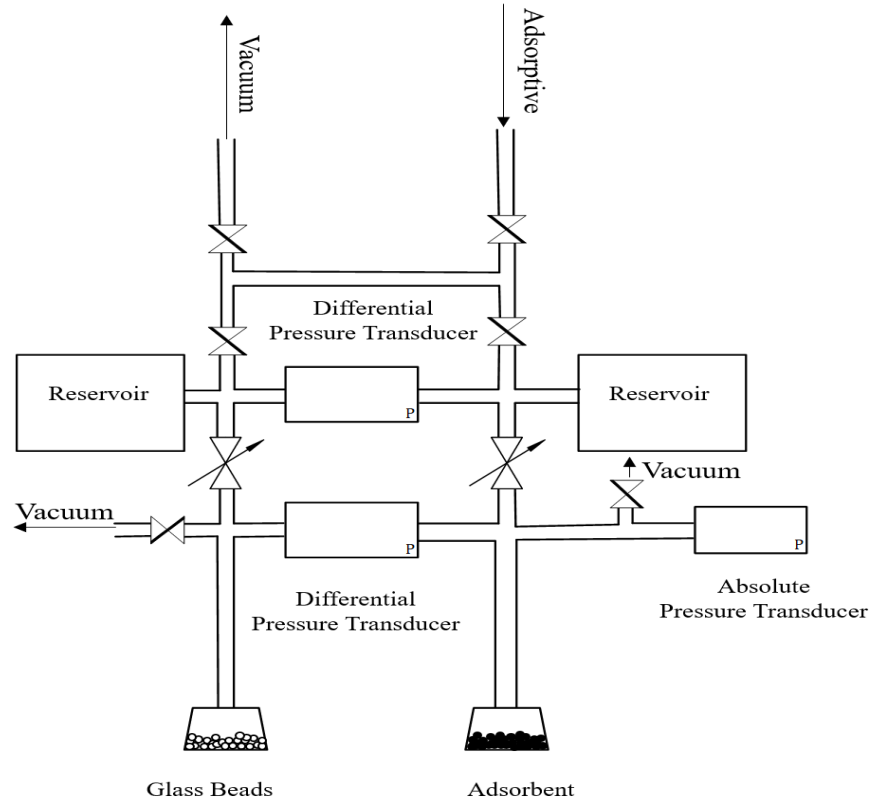


Figure 6. Differential gas adsorption manometry (adapted from Haul and Dumbgen, 1960)

2.6.3 Gas Flow Technique

In the gas flow technique, the measurement is based on the volume of gas that replaces the adsorbed adsorptive. The same amount of mole should flow to the system as the number of moles that is adsorbed. There are different measurement types including a differential gas flowmeter and a thermal flowmeter, etc. Figure 7 shows a possible simple system which can be used for the gas flow technique adsorption measurement (Rouquerol et al., 2014).

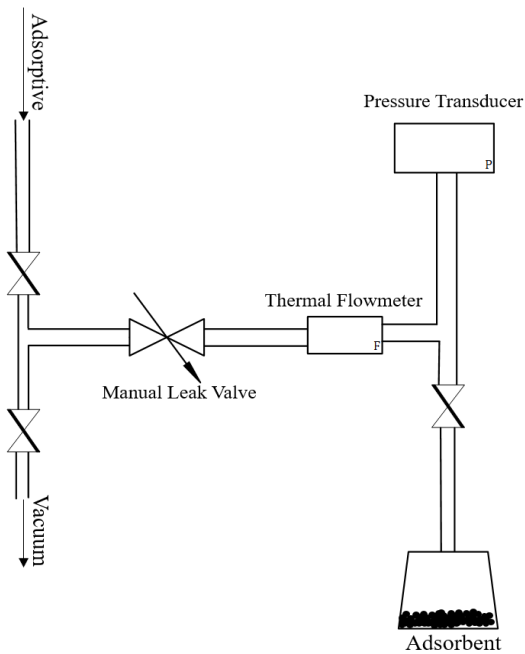


Figure 7. Simple gas adsorption flow technique (adapted from Rouquerol et al., 2014)

2.6.4 Volumetric-Chromatographic Method

This method will lead to the measurement of reduced mass Ω_i , not the absolute mass adsorbed m_i . In this method specified amount of a gas mixture with masses m_i^* , $i=1, \dots, N$ prepared in a storage vessel of volume (V_{Sv}) and is expanded into an adsorption chamber of volume (V_{AC}) and partly adsorbed in a sorbent. Wait to equilibrium reaches, i.e., constant values of pressure and temperature in the system attained. Then, the molar or mass concentration of all components of remaining adsorptives are measured by taking a sample and sending it to a gas chromatograph (GC) or a mass spectrometer (Keller et al., 1999).

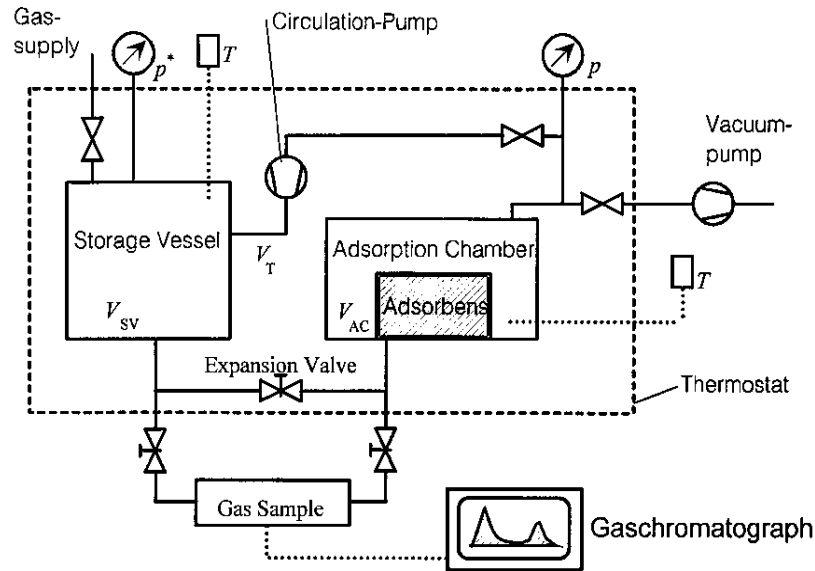


Figure 8. Schematic diagram for volumetric-Chromatographic measurements (Keller et al., 1999)

General concepts of mass spectrometer and gas chromatograph are based on Gibb'sian excess mass m_{iG} ($m_i = m_{iG} + \rho_i^f V^a$) where $V^a = (V^V - V^S)$, is the volume of inaccessible to adsorptive when equilibrium reaches and $V^S = V_{He}^S$ is calculated using helium in the system, because helium is not adsorbed and the volume of catalyst considering the voidage can be evaluated, however, it is suggested that helium is adsorbed very slowly with negligible amount, hence, using Argon in some cases is more logical, since it adsorbs almost half of the amount nitrogen is adsorbed.

Before taking gas samples for concentration measurements, circulation of the adsorptive in the installation is recommended to avoid local concentration differences and to enhance equilibrium. A disadvantage of this system for our study is that it only works fine for equilibrium, not kinetics. Therefore, considering this system, we will have a deficiency with two of our essential criteria that are operating at elevated temperature and measurement as a function of time.

2.6.5 Gravimetric Method

This measurement procedure is like the volumetric-chromatographic method, however here we have only one vessel for the adsorption chamber and a microbalance for knowing the exact weight of particle before and after adsorption (Keller, Dreisbach, Rave, Staudt, & Tomalla, 1999).

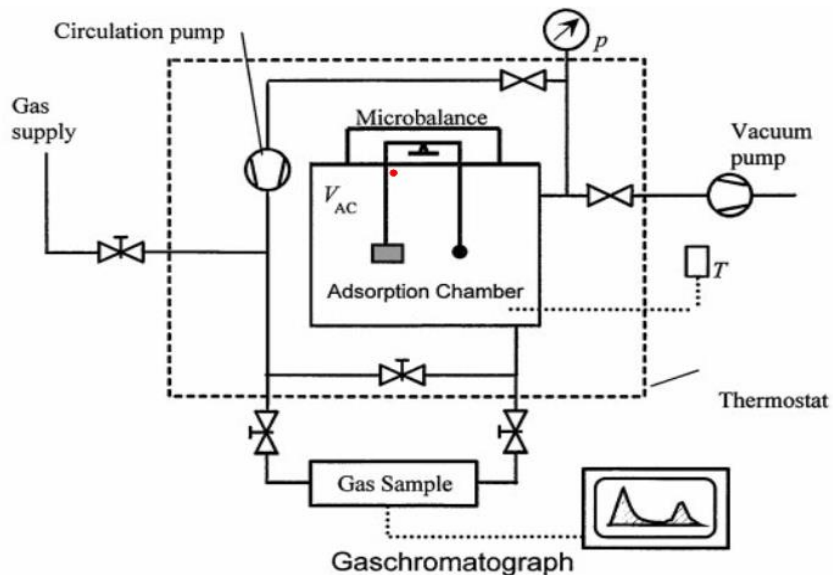


Figure 9. Schematic for gravimetric-chromatographic method (Keller et al., 1999)

It should be noted that this system works fine only for the fixed bed system, considering the microbalance usage.

2.6.6 Volumetric-Gravimetric Method

As an advantage of combining volumetric and gravimetric methods in one system, we can refer to making system free of the chromatography process. However, this system only works fine for co-adsorption of a binary gas mixture (Keller, Dreisbach, Rave, Staudt, & Tomalla, 1999).

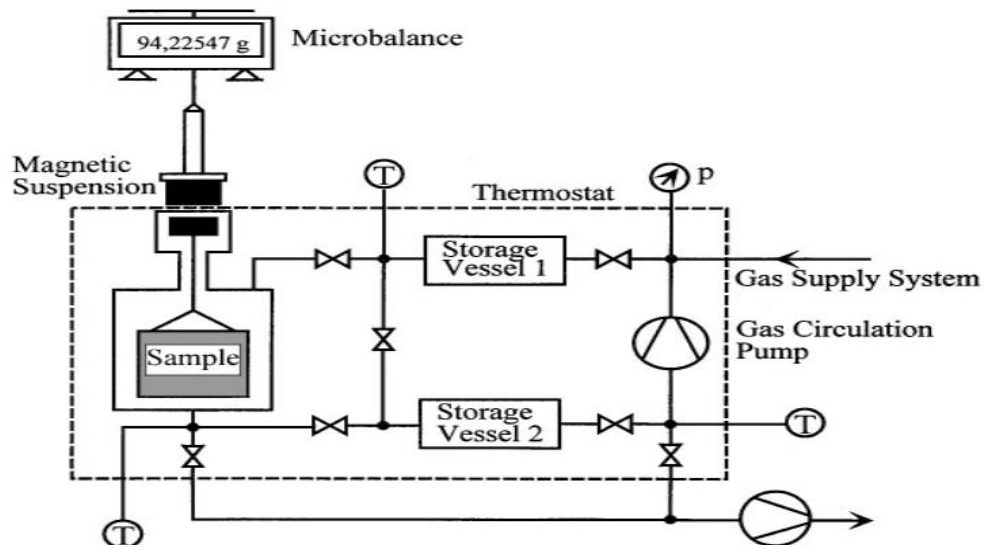


Figure 10. schematic for volumetric gravimetric method (Keller et al., 1999)

2.6.7 Micro Catalytic Reactors

Micro catalytic reactors are widely used for their ability for the measurement of rapid reactions and obtaining experimental data in the minimum allowable time in petroleum and catalysis study. As their advantages to previous systems, we can refer to (1) ability to control contact time and kinetics study due to not having dead space volume and having an instant gas-solids contact and (2) no internal pressure drop (Reactors and Tracers, 1970).

The reactor is mainly a vertical vessel containing ports for thermocouples for knowing the internal temperature. Providing heat is of important priority in micro catalytic reactors.

Providing a uniform temperature for an isothermal reaction is necessary. However, keeping the adsorption process in an isothermal condition might need a perfect controlling system to compensate the generated heats of adsorption and system's heat losses. Therefore, usually, these reactors have more extended height than the internal diameter to have the same temperature on the wall and in the center. Often, a large thickness from a material that reduces heat losses (for instance ceramic) is designed to minimize the amount of heat losses. Some possible methods for the heat supply are (1) induction heating systems (2) band heaters (3) fluidized bed sands bath. We illustrate two examples of successful micro catalytic reactors which are used previously for gasification of catalysts and are most relevant to our study in the following sections.

2.6.7.1 CREC Riser Simulator

The CREC Riser Simulator is a bench scale mini-fluidized bed unit with a capacity of 52 cm³. The unit allows the loading of 1 g of catalyst. An impeller is located in the upper section and a basket containing the catalyst is placed in the central part. Due to rotation of the impeller at high speeds, gas is forced both outward in the impeller section and downwards in the outer reactor annulus which makes the simulator to be a simple well-mixed device that allows for the contact chemical species with the fluidized catalyst in a predetermined time. This creates a lower pressure in the center region of the impeller with a spiraling upwards flow of gas in the catalyst chamber. Therefore, the impeller provides a fluidized bed catalyst particles, as well as intense gas mixing inside the reactor (Ginsburg and Lasa, 2003; McCoy and Madras, 2003)

Pressure transducers are installed in both chambers of the reactor and vacuum box to monitor the progress of a reaction run. Before the injection of reactants, the vacuum box is maintained at low pressure (around one psi), and the reactor is set at atmospheric pressure. Once the operation is completed, a product sample collected in the sampling loop and is sent to the gas chromatograph for further analyses.

2.6.7.1.1 Adsorption Assessment in CREC Riser Simulator

Catalytic cracking takes place on the active sites of the catalyst, and reactant molecules (adsorbates) need to be adsorbed on the surface of the particle before catalytic conversion.

The idea of measuring adsorption is done by calculating the difference in concentration between the thermal and catalytic experiments. Therefore, Atias & De Lasa, 2004, performed experiments under the same conditions with and without catalyst loaded into the basket. Besides, they obtained a quantitative relation between the amount of a species adsorbed on the solid surface and its corresponding gas-phase partial pressure according to ideal gas law, hence, there is no need for microbalance in this study which is impossible to be used in a fluidized bed and this correlation helps in the investigation of the kinetics of reactions. They used Henry's law as linear adsorption isotherm under the relatively low-pressure conditions of FCC.

They used temperature compensated anemometry for the gas velocity measurements. By sensing the changes in heat transfer from a heated sensor exposed to the fluid motion, thermal anemometers measure fluid velocity according to recorded voltage. In order to have consistent measurements of the selected conditions, fluid temperature and composition should be kept close to constant. The system consists of a sensor and a control box that supplies current across a thin wire to keep the temperature level unchanged around the sensing element. The heater heats the wall on the outside of the recirculation chamber or that the heat transfer is wall to gas and then gas to solids. For an absolute velocity of gas passing by the sensor, a specific current is required to maintain a constant temperature. Thus, the gas velocity can be inferred from the voltage output. This anemometer was certified by the manufacturer to measure single component air velocity measurements at ambient temperatures up to 150°C. However, this temperature range is limited for our study and is not sufficient.

Furthermore, using a wire for heat supply in the wall might result in over cracking of the vapor close to the wall in higher temperature. (Ginsburg and Lasa, 2003)

2.6.7.2 Jiggle Bed Reactor (JBR)

The jiggle bed reactor (JBR) is a batch microreactor developed by (Latifi, 2012) for the study of gasification catalysts and hydrodynamic studies, further studies on this device have been done to investigate the adsorption of CO₂ on activated carbon. Biochar activation

and production of activated carbon was another application of JBR (Colomba, 2015). There is also an ongoing project producing biochar with different heating rate with JBR.

A linear pneumatic actuator is successfully designed in the system to reach fluidization conditions in a mechanical approach (vibration) without using a fluidization gas. Catalyst particles are fluidized inside the ceramic crucible because of alternating vertical motion created by a pneumatic actuator which is installed below crucible.

One of the critical matters in the study of elevated temperature is the supply of heat. The main problem of microreactors with endothermic reactions is poor heat transfer that is due to the much higher temperature on the surface of the catalyst bed. Latifi et al. studies show that induction heating provides a minimum temperature difference between the wires and catalyst bed. Therefore, induction heating is a method utilized in the jiggle bed reactor to supply heat for the system. Induction heating is a high-speed heating method. However, if we provide a high amount of power, then the internal wires of the reactor could reach a very high temperature after a few seconds which results in the temperature difference between wires and particles. Initial developments by Rohani et al. shows that external induction field can heat-up vertical fluidization which is generated rapidly and uniformly disturbed particles avoiding creation of hot spots and high-temperature gradients, besides to prevent shielding of the induction field, the body of the reactor cannot be metallic. Moreover, the material used in the reaction chamber must withstand the high temperature of 550-600 °C and also it should be non-porous and robust enough to sustain the vibrating conditions (Latifi, 2012).

The jiggle bed reactor contains three sections: the linear pneumatic actuator, the reaction zone, and the induction heating system. Vibrating motion is transferred to the crucible through a scalloped shape stainless steel on top; three stainless steel threaded support rods and around aluminum seat underneath the crucible, which is mounted directly on the air cylinder of the actuator. The schematic of the Jiggle Bed Reactor is shown in figure 11 (Latifi, 2014).

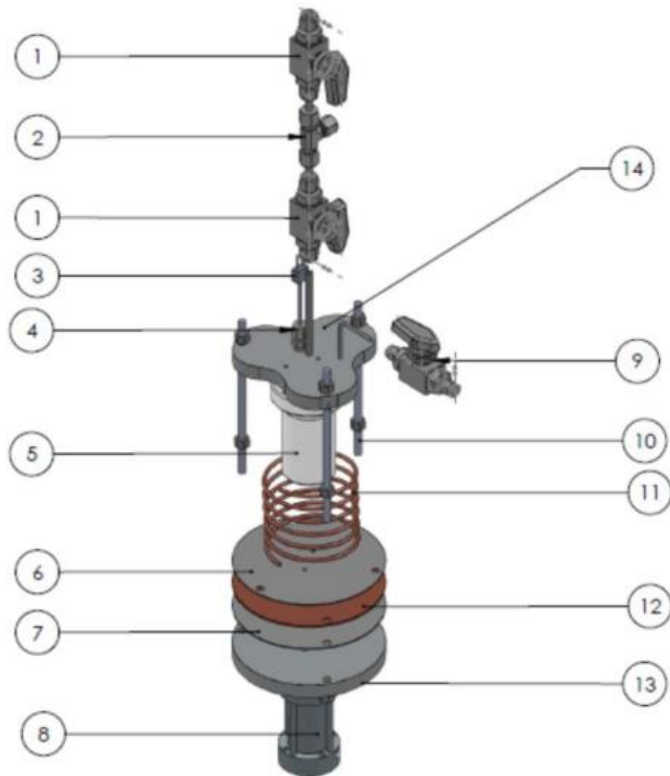


Figure 11. Diagram of the Jiggle Bed Reactor (1) on/off feed valves; (2) Inlet of carrier gas; (3) Thermocouple; (4) Inlet of feed and carrier gas; (5) Ceramic crucible with insulation; (6) Insulation disk; (7) Insulation disk; (8) Linear pneumatic actuator; (9) Outlet gas valve; (10) Stainless steel support rods; (11) Copper coil; (12) Copper disk; (13) Aluminum disk mounted on the actuator; and (14) Stainless steel scalloped disk.

(Latifi, 2014)

2.7 Comparison of Adsorption Experimental Systems

This section compares different adsorption systems measurements and illustrate their advantages and drawbacks and explain their deficiencies with our four essential criteria for the proposed system. Table 2 compares the benefit and disadvantages of different systems.

Table 2. Comparison of adsorption systems available in the literature

Experimental System	Advantage	Drawbacks
Gas manometry	Straightforward system	1-It is a fixed bed (not well-mixed). 2-No control over gas-solid contacting time (kinetics) 3-Hydrocarbon condensations
Differential Manometry	An accurate system with a differential pressure transducer	Difficult to make same operating conditions in both chambers
Gas Flow Technique	No concern for condensation, although still a uniform and steady temperature is required	Flowmeter is not ideal for kinetics measurement

Volumetric-Chromatographic	multicomponent equilibrium adsorption measurement	<ol style="list-style-type: none"> 1- It is not designed for high boiling point vapors 2- Limited with equilibrium measurement
Gravimetric-Chromatographic	multicomponent equilibrium adsorption measurement	<ol style="list-style-type: none"> 1- Microbalance is not suitable with providing well-mixed conditions and uniform temperature 2- Limited with equilibrium measurement
Volumetric-Gravimetric	Binary equilibrium adsorption measurement	<ol style="list-style-type: none"> 1- No uniform temperature 2- Only works for equilibrium (not kinetics)
CREC Riser Simulator	Using the gas carrier in a microreactor for kinetics study and instant gas-solid contact	<ol style="list-style-type: none"> 1. Heat supply is not ideal (heat transfer is from wall to gas and then gas to solids) 2. Measurement in the first few seconds is challenging (phase transition is required for the gas-solid contact)
Jiggle Bed Reactor (JBR)	Uniform temperature, and capable of being operated in elevated temperatures (900 °C)	<ol style="list-style-type: none"> 1. Hydrocarbon gas-solid contacting (phase transition) is not utilized with the system. 2. A designed measurement system is required for adsorption kinetics measurement.

Chapter 3

3 CO₂ Activation and Liquid-solid Adsorption

3.1 Introduction

The purpose of this chapter is, first to activate the carbonaceous materials used in our gas-solid study (chapter 4), to increase their specific area, and then to characterize the properties of the original and activated materials. Two different activation types are used: first, the temperature of the material is increased to desorb contaminants and, second, carbon dioxide at high-temperature acts as a mild oxidant to convert parts of the material. Liquid-solid adsorption is commonly used to estimate the specific surface area of carbonaceous materials (Santamarina et al., 2002; Nunes and Guerreiro, 2011).

This chapter uses two adsorbates: phenol and methylene blue.

The objectives of this chapter are summarized as follows:

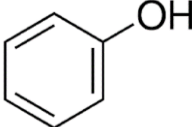
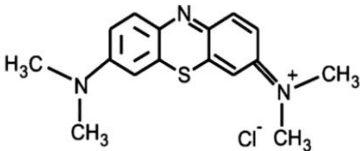
1. Determine the impact of activation methods on the adsorption capacity of fluid coke.
2. Characterize the adsorption characteristics of fluid coke, flexicoke, activated fluid coke, and commercial activated carbons as a reference.

3.2 Material and Methods

3.2.1 Adsorbates

Two conventional liquid dye adsorbates were used in our study. Most previous experiments use only methylene blue, but we also used phenol, a smaller molecule compared to methylene blue, to verify and compare our results. Table 3 provides relevant adsorbate properties including formula, chemical structure, molar mass, cross-sectional area, and molecular diameter.

Table 3. Methylene blue and phenol physical properties (Stoeckli et al., 2001; Santamarina et al., 2002)

Properties	Phenol	Methylene Blue
Formula	C ₆ H ₆ O	C ₁₆ H ₁₈ ClN ₃ S
Chemical structure		
Molar mass (g/mole)	94.11	319.85
Cross sectional area (Å ²)	41.2	130
Molecular diameter (Å)	7.2	9.8

3.2.2 Adsorbents

Various carbonaceous particles were used as our potential adsorbents. This includes activated carbon from coal, activated carbon from coconut shell, raw fluid coke (taken from the burner of the Fluid cokingTM process), pretreated fluid coke, activated coke and flexicoke (combination of the burner and flexicoke taken from the burner of the FlexicokingTM process (explained in chapter 1)). Pictures of activated carbon and fluid coke were taken with a Keyence's VHX-6000 series microscope for comparison in the 100-micrometer scales, as shown in figure 12.

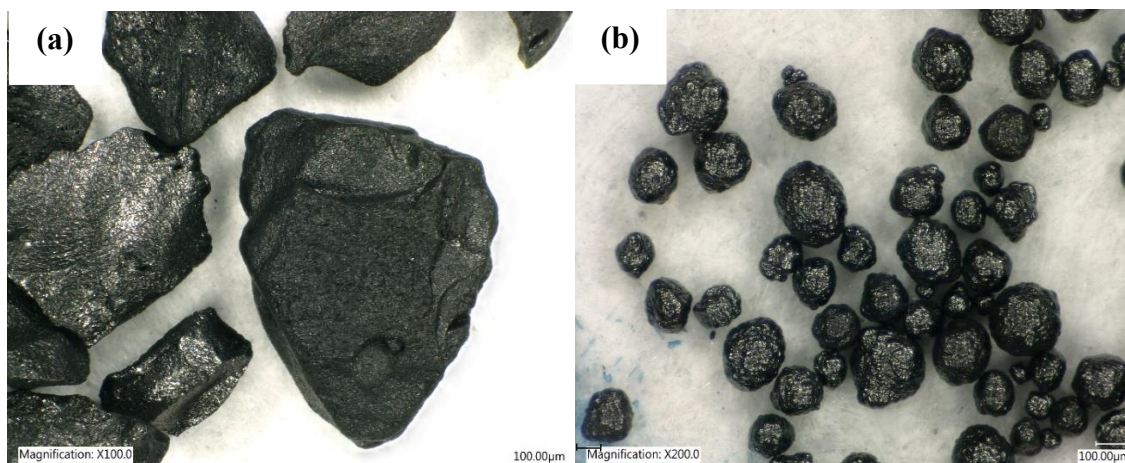


Figure 12. Microscope photographs of (a) activated carbon from coconut shell and (b) fluid coke from left to right.

The physical property of (a) coconut shell activated carbon is compared with (b) raw fluid coke as well as with coal activated carbon in Table 4.

Table 4. Comparison of physical properties of fluid coke with coconut shell activated carbon

Physical Properties	Coconut shell Activated Carbon	Coal Activated Carbon	Raw Fluid Coke
Carbon Content wt. %	90-100	-----	84
Hydrogen Content %	0-1	-----	1.8
Density (kg/m³)	470-530	540 (Apparent)	1600
Sauter Mean Diameter (µm)	600-700	600-700	150-170
BET Surface Area (m²/g)	809.25	850 (min)	6.68
Ash Content wt.%	12 (max)	-----	8

3.2.3 Liquid-solid Adsorption Measurement Procedure

To perform liquid-solid adsorption, a stock liquid solution is made. From the stock solution, different samples in selective concentrations are prepared (dilution). The selected initial dye concentration range for activated carbon experiments is 100 to 800 mg/L. This range in case of using coke particles is between 2.5 to 100 mg/L (the empirical concentration ranges chosen to monolayer equilibrium adsorption falls within the range). In each sample, a known volume of liquid dye adsorbate (V) (methylene blue, phenol) is inserted and measured the mass of particles added afterward.

A Thermo Fisher Scientific BNIS-100 Shaker was then used to maintain samples at 1000 rpm (maximum capacity of the equipment) for five days, and the temperature was set at 25 °C. Before liquid sampling for dye concentration measurement, samples were transferred to a centrifuge for the separation of the liquid and solid phase. They were kept in a Thermo Fisher Scientific Sorval Legends X1 centrifuge for 1 hour at a frequency of 3000 rpm. A Thermo Scientific Evolution 220 UV spectrophotometer was used to measure the adsorbate concentration in the liquid phase. Figures 13 and 14 show the peak adsorption wavelength for dilute solutions of methylene blue (670 nm) and phenol (270 nm). To measure samples concentration, UV spectrophotometer calibration curves, obtained for methylene blue and phenol, are used (section 6-11 of appendices).

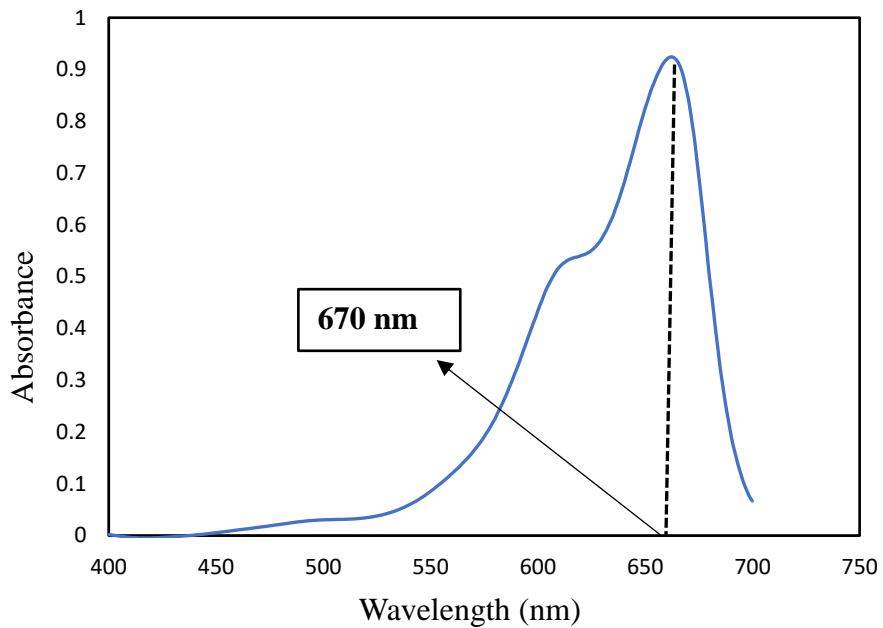


Figure 13. Methylene Blue Wavelength Scan at 25 mg/L

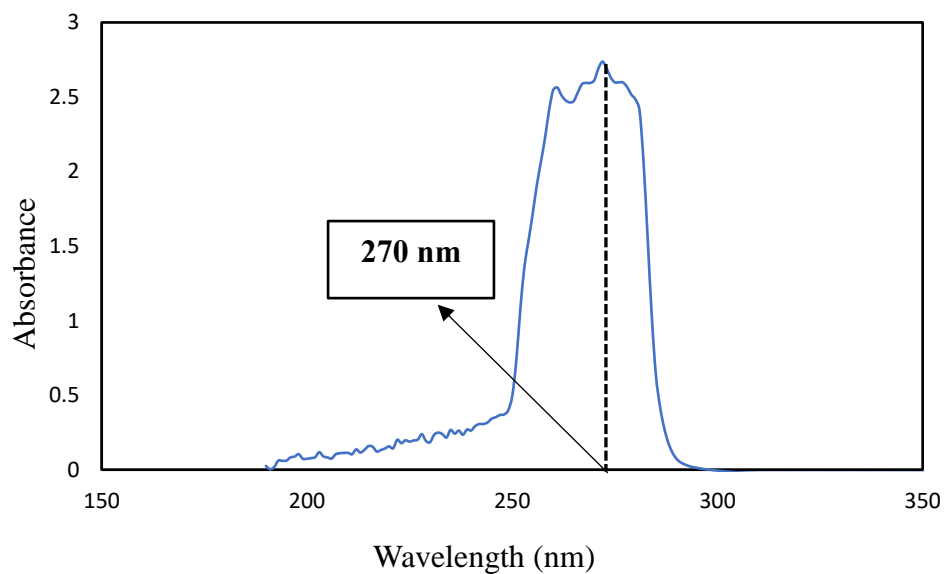


Figure 14. Phenol Wavelength Scan at 25 mg/L

The length of time required to reach equilibrium was studied based on five samples with the same initial concentration of methylene blue (800 mgL^{-1}) and same mass of activated carbon (0.1 g). Figure 15 shows the measurements based on samples obtained on different

days. A plateau is achieved after four days, thus sampling for equilibrium adsorption measurements was taken after keeping samples five days in the shaker (figure 15).

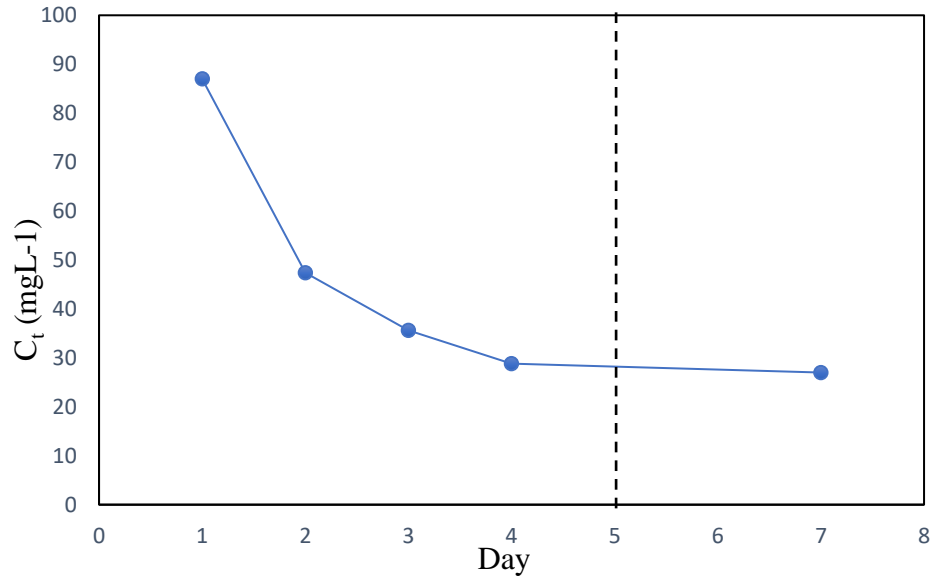


Figure 15. The time required to reach the equilibrium with activated carbon from coal.

Equation 5 is used to calculate the equilibrium adsorption for each sample from the equilibrium concentration (measured from UV spectrophotometer calibration curve).

$$q_e(\text{mg/g}) = \frac{(C_0 - C_e) \times V}{M} \quad (5)$$

Where M (g) is the mass of particles used in the sample and V (mL) is the volume of solution, q_e (mg/g) is the equilibrium adsorption, C_0 (mg/L) is the initial dye concentration and C_e (mg/L) is the equilibrium concentration of the sample. A complementary liquid-solid adsorption measurement procedure along with error studies is provided in the appendices at the end of the thesis.

3.2.4 Experimental Set-Up for Pretreatment and Activation

The Jiggle Bed Reactor (JBR), is equipment that other researchers have shown is ideal for the production of biochar, and activated carbon from biomass (Latifi, 2012; Colomba, 2015). In this study, the JBR was used for both thermal pretreatment and activation.

Thermal pretreatment was used to desorb potential volatile materials out of the fluid particles before liquid-solid adsorption measurements. Simulated burner coke (SBC Coke) was produced using the JBR at 650 °C (a typical operating temperature for the burner of a fluid coker) under a nitrogen environment to avoid combustion. The JBR reached 650 °C within 10-11 minutes (the heating rate was set at 60 °C/min) and was kept at the set point for 1 hour. The system provides shaking during the entire run using a pneumatic actuator. Nitrogen flow for all experiments was set at 7.9×10^{-6} m³/s. The schematic of the JBR set-up is presented in figure 16.

In the case of CO₂ activation, raw fluid coke was used in the JBR (one-third of the volume of crucible). The JBR was operated under a nitrogen environment with a temperature ramp of 60 °C/min to reach the desired activation temperature. Once the system was reached to the activation temperature set-point, the gas was changed from nitrogen to CO₂. Activated coke then was produced by keeping the reactor under CO₂ environment (flowrate= 7.9×10^{-6} m³/s) for 1 hour at activation temperature set point. In all experiments, the JBR was flushed with nitrogen while it was cooling down avoiding CO₂ adsorption on particles. A condenser was used in the downstream of JBR for collecting the desorbed volatile material during activation (figure 16).

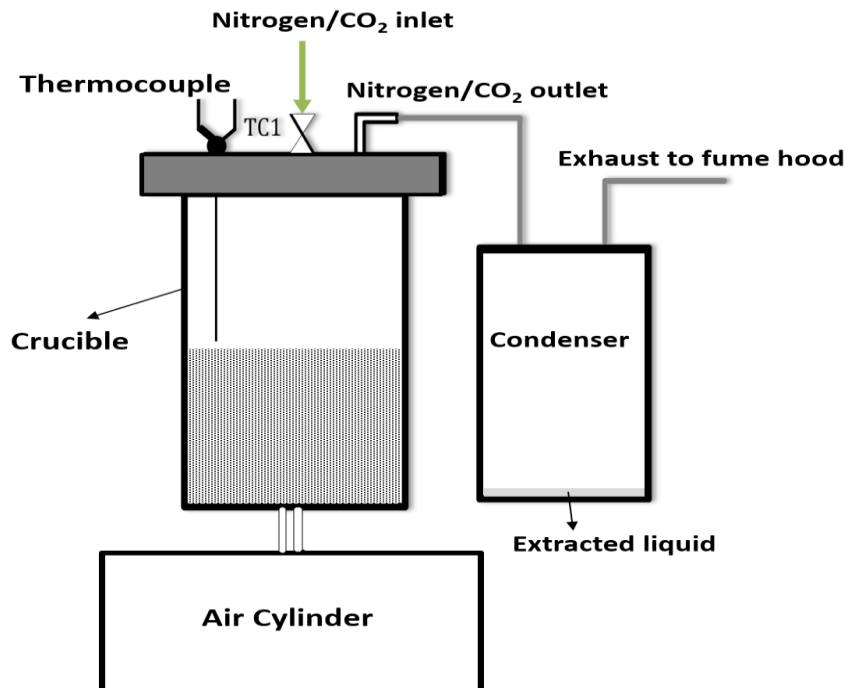


Figure 16. Pretreatment/activation unit (JBR) set-up

The mass of coke was recorded before and after each experiment, and the extracted liquid was recovered in each test.

BET analysis was performed as a conventional method with coconut shell activated carbon and different coke particles activated and preheated at different conditions to measure the BET surface area and total pore volume for different adsorbents. The results will be compared with the liquid-solid estimated surface area. To do this, a Nova Quntchrome 11.03 was used. The samples are outgassed for 17.5 hours at 250 °C initially. After then, Nitrogen is used as an adsorbate for BET analysis. The experiments are carried out with liquid nitrogen at the boiling point of nitrogen (77.35 K) for three hours. The results will be used as a validation to compare the effect of pretreatment, and activation in creating porosity and increasing the surface area.

3.3 Results and Discussion

3.3.1 Activation and Experimental Analysis Results

3.3.1.1 Raw Fluid Coke Thermogravimetric Analysis

Thermogravimetric Analysis measures the mass reduction of particles as a function of a predetermined temperature increase. It provides an estimate of the lower and higher volatile materials in the fluid coke. A Perkin-Elmer Pyris 1 TGA was used for the analysis of raw fluid coke. Figure 17 provides the TGA of raw fluid coke up to 800 °C with a temperature ramp of 10 °C/min under the nitrogen environment. The coke loses approximately 8% of its total mass when is heated up to 800°C. The curve shows 3 steps: (i) mass reduction due to temperature increase up to 130 °C, due to lower boiling points volatile materials desorbing, including water, (ii) mass reduction in the temperature variation range between 130-600 °C, due to loss of lighter hydrocarbons, and finally (iii) a noticeably sharp increase from 600 to 800 °C is likely associated with residue and pitch materials.

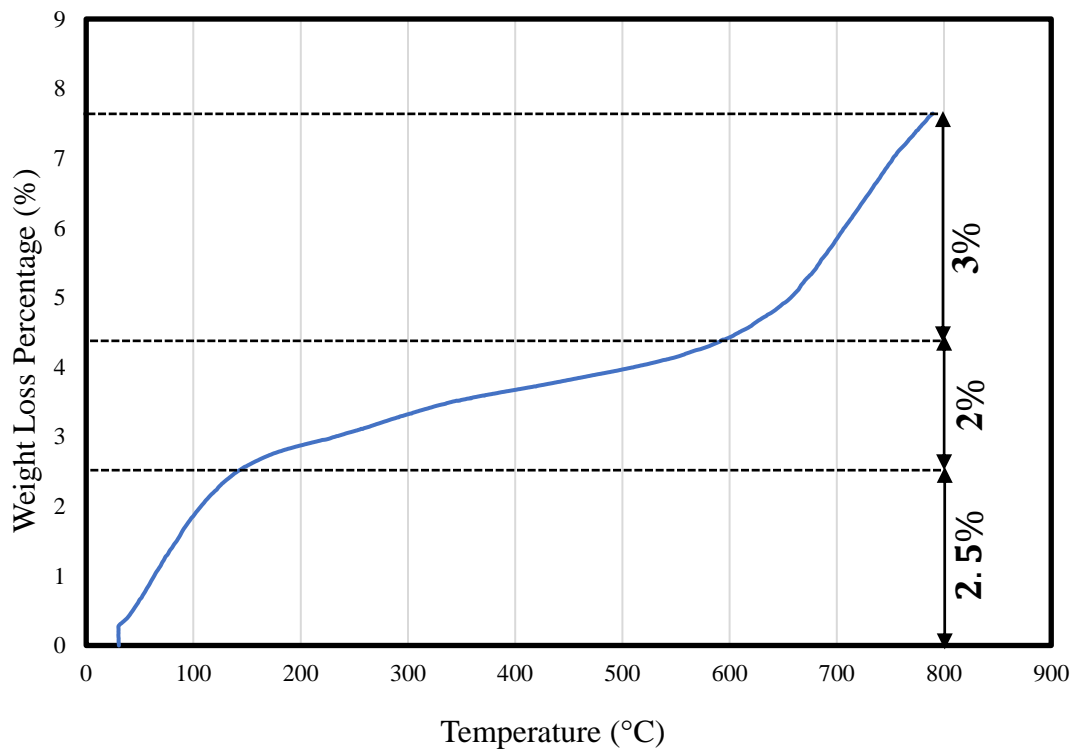
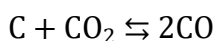


Figure 17. Thermogravimetric Analysis of raw fluid coke

3.3.1.2 CO₂ Activation

Numerous conventional methods can be used to make active sites in carbonaceous materials, including CO₂ activation, thermal activation, photoactivation, and plasma activation over catalyst surface (Álvarez et al., 2017). CO₂ gasification is a method to increase particles porosity through a reaction between the carbon content of particle and CO₂, removed carbon from the particle and creating porosity according to the following reaction:



The reaction moves toward the production of CO in the 800 to 900 °C temperature range (Karimi et al., 2013). The reaction is reversible and produces unstable CO, which may decompose. Among available CO₂ activation studies in the literature, Karimi et al. studied activated carbon production from oil sands coke which is interesting for our study. In their study, they investigated the impact of coke particle size distribution (20–45, 45–90, 90–150, 150–300 and 300–600 μm size ranges), the flow rate of CO₂ (75 mL/min, 150 mL/min, and 250 mL/min), and the time of activation (2- 15 h). The activation in this study is done at 900 °C with CO₂, however, prior activation, particles are pre-oxidized with air (160 mL/min). The temperature ramp they used is 10 °C/min, and they keep particles at 270 °C for 24, 72 and 120 h for pre-oxidization. During these conditions, they have measured the weight loss percentage after activation as a function of time of activation and concluded that it varies from 10- 80 % from 2 to 15 hours of CO₂ activation for different particle size cuts. Then, they measured the surface area as a function of weight loss percentage. The obtained activated carbon surface area ranges from 30 m²/g to 650 m²/g (the initial raw coke surface area in this study is 0.2-3.5 m²/g). They have also concluded that the overall weight loss percentage is highly dependent on the time of peroxidization and it increases significantly by increasing the time of pre-oxidization.

In our study, CO₂ activation was performed in the Jiggle Bed Reactor (JBR) at three different temperatures of 650 °C, 750 °C, and 850 °C for 1 hour. Figure 18 shows the weight loss percentage at different activation temperatures. The weight loss increased from 8.5 to 10.5 % when increasing the temperature from 650 to 850 °C.

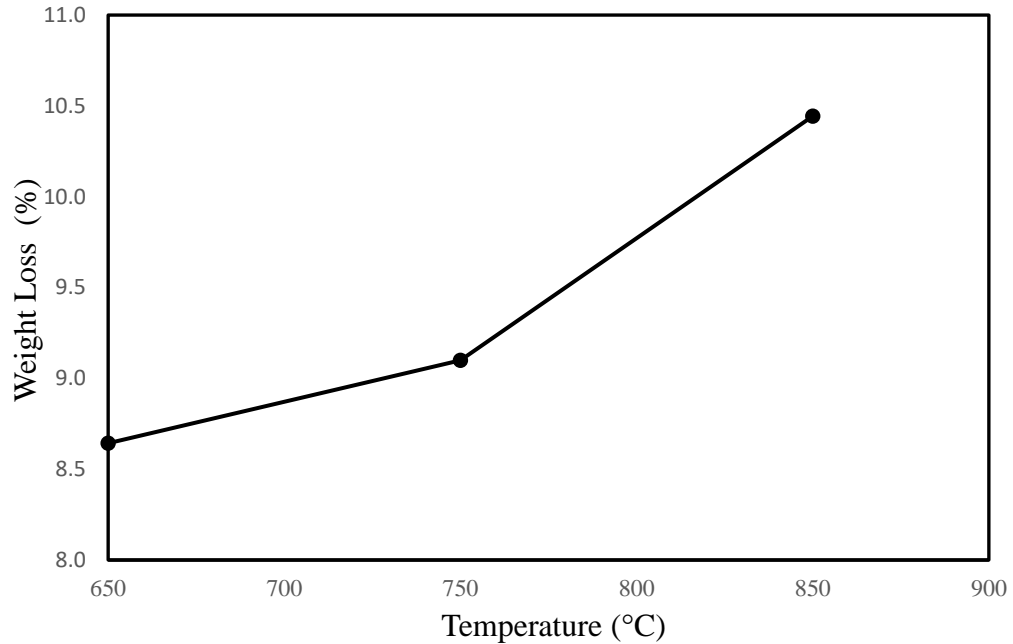


Figure 18. Weight loss percentage versus activation temperature.

3.3.1.3 BET Analysis

BET analysis results are summarized in Table 5. The coconut shell activated carbon surface area ($809.254 \text{ m}^2/\text{g}$) is 34 times that of the flexicoke ($23.67 \text{ m}^2/\text{g}$) and 121 times that of the raw fluid coke ($6.678 \text{ m}^2/\text{g}$). The activation with CO_2 at $850 \text{ }^\circ\text{C}$ and activation with air at $650 \text{ }^\circ\text{C}$ increased the surface area coke to $11.046 \text{ m}^2/\text{g}$ and $10.246 \text{ m}^2/\text{g}$ respectively. The process to produce SBC coke noticeably increases porosity, demonstrated by comparing the total pore volume of SBC coke (0.006 mL/g) with raw fluid coke (0.0027 mL/g). The BET surface area of SBC coke has also increased to $12.354 \text{ m}^2/\text{g}$. However, results suggest that activation with CO_2 at $750 \text{ }^\circ\text{C}$ is not sufficient and reduces the total pore volume and surface area of the coke. Another important finding from the BET analysis is the pore size distribution of different adsorbents. This can be evaluated regarding the distribution of micropores (pores with an average diameter of less than 2 nm), mesopores (pores with an average diameter of 2 to 50 nm) and macropores (pores with an average diameter of more than 50 nm). The table demonstrates the volumetric percentage of micropores, mesopores, and macropores for each adsorbent.

The table is obtained via evaluating BJH adsorption pore size distribution. The table concludes that micropores and mesopores are covering almost for all adsorbents most of the volumetric portion of the particles' pore volume and macropores only stand for 8-20 percent of the total pore volume. A key finding of this table is that the distribution of micropores, mesopores, and macropores does not seem to change significantly. Therefore the observed adsorption changes are believed to be due to the surface area difference of adsorbents.

Table 5. Adsorbents surface area and total pore volume along with the percentage of micropores, mesopores, and macropores based on BET analysis

Adsorbents	BET Surface Area (m ² /g)	Total Pore Volume (mL/g)	Micropores %	Mesopores %	Macropores %
Coconut Shell Activated Carbon	809.3	0.430	45.6	38.3	16.1
Flexicoke	23.7	0.020	32.4	43.7	23.9
SBC coke	12.4	0.0060	47.1	44.6	8.4
Activated Coke with CO ₂ at 850 °C	11.0	0.0074	35.3	42.4	22.3
Activated coke with air at 650 °C	10.2	0.0059	41.6	48.9	9.5
Raw fluid coke	6.7	0.0027	49	33.8	17.2
Activated Coke with CO ₂ at 750 °C	4.9	0.0026	44.9	45.9	9.1

3.3.2 Liquid-Solid Adsorption Results

3.3.2.1 Liquid-Solid Adsorption Equilibrium

Liquid-solid equilibrium adsorption measurements were carried out with the various adsorbents. Adsorbents were divided into two categories: activated carbons (i.e., activated carbon from coal, activated carbon from coconut shell) and coke (i.e., raw fluid coke, flexicoke, and activated coke at 750 °C and 850 °C).

Two parameter isotherm models including Langmuir, Freundlich and BET and three model isotherms, Redlich Peterson, Stips, and Toth, were compared (appendices section 6-12). Langmuir model assumes monolayer adsorption coverage, therefore, allowing an estimate of the specific surface area. Furthermore, Langmuir gives a reasonably good model fit with our experimental results, hence, in this chapter we used Langmuir as a potential model fit with experimental results. In section 6-12 of appendices, the rest of the isotherm models explained with details in two tables and corresponding figures of isotherm models are illustrated. The Langmuir isotherm equation is as follows:

$$q_e = \frac{q_m \cdot K_L \cdot C_e}{1 + K_L \cdot C_e} \quad (6)$$

Where in the Langmuir equation, q_e (mg/g) is the equilibrium adsorption, C_e (mg/L) is the equilibrium concentration of adsorbate, K_L (L/g) is the Langmuir constant and q_m (mg/g) is the maximum uptake per unit mass of carbon.

The following figures show the adsorption of methylene blue and phenol with different adsorbents. Figure 19 is indicating that methylene blue adsorption more with activated carbon than phenol in mass basis, which is reasonable due to be a heavier molecule, however, converting the equilibrium adsorption q_e (mg/g) to n_e (mmol/g), activated carbon adsorbs more moles of phenol (3.15 mmol/g) compared to methylene blue (1.19 mmol/g). Phenol potentially due to having a smaller molecule to methylene blue adsorbs more (diffusion to mesopores/micropores.) Langmuir is used to fit with experimental results.

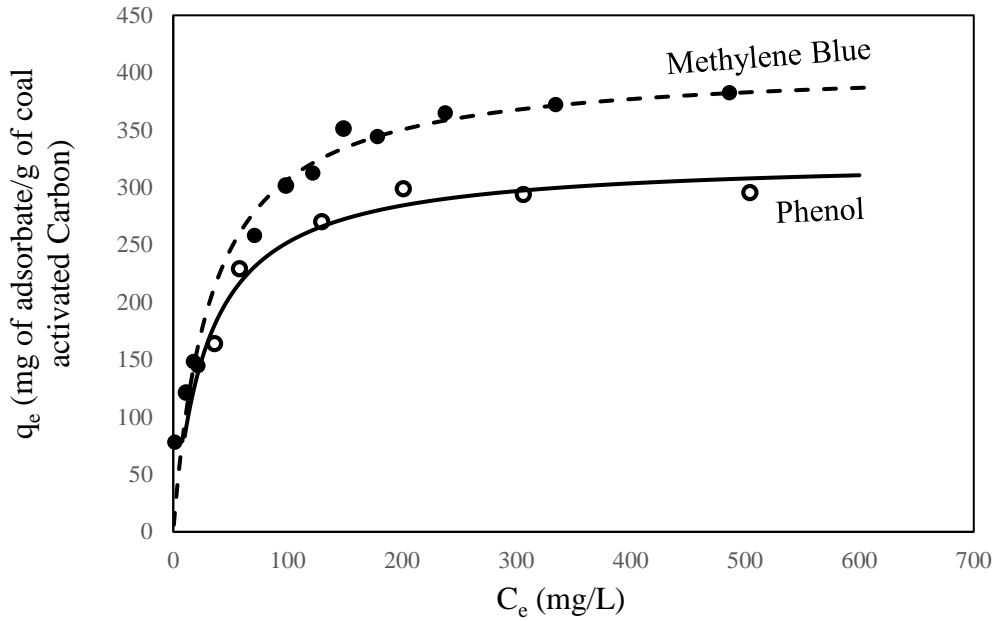


Figure 19. Methylene blue and phenol adsorption comparison with coal activated carbon, experimental results fitted with Langmuir isotherm

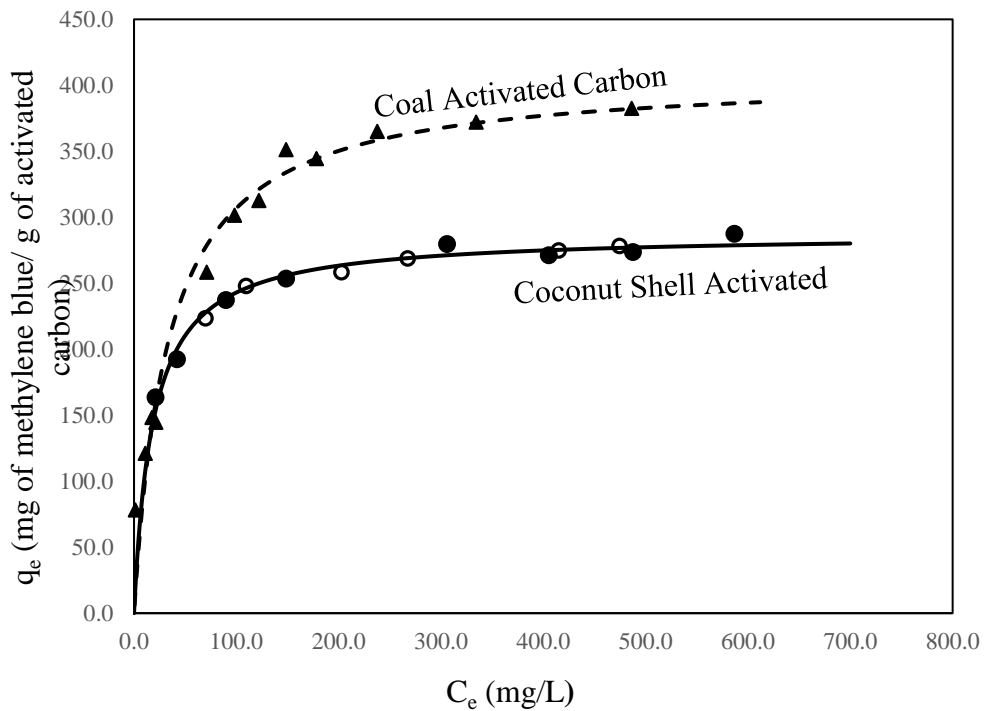


Figure 20. Methylene blue adsorption comparison with coconut shell activated carbon and coal activated carbon, experimental results fitted with Langmuir isotherm.

The coconut shell activated carbon has been used for hydrocarbon adsorption study widely in chapter 4. Hence, a replicate carried out to prove the accuracy of results and Langmuir isotherm model fitted with both series. According to figure 20, coal activated carbon adsorption with methylene blue is relatively higher than coconut shell activated carbon in equilibrium. Langmuir has fitted relatively well again with experimental results in this graph. An equilibrium study on adsorption of methylene blue onto activated carbon produced from steam activated bituminous coal shows that the activated carbon adsorbs 250-350 mg/g of methylene blue in equilibrium. In this study, Langmuir, Freundlich and Redlich-Peterson isotherms fit relatively well with experimental results (Qada et al., 2006). This study shows that we have also gathered methylene blue equilibrium adsorption on activated carbon in the expected range that agrees with literature.

Figure 21 compares the adsorption of different coke particles (including raw fluid coke, activated coke at 750 °C, and activated coke at 850 °C and flexicoke) with methylene blue. Raw fluid coke adsorbed 0.89 mg/g at equilibrium. On the other hand, it is observed that CO₂ activation process at 850 °C had a significant impact on increasing porosity and adsorption capacity since the adsorption uptake doubled at equilibrium (1.7 mg/g). However, results suggest that activation at 750 °C was not sufficient (as in the literature also suggested to perform CO₂ activation at above 800 °C to be effective (Karimi et al., 2013)) and decreased the fluid coke adsorption capacity to 0.56 mg/g. The figure illustrates that the flexicoke had the highest methylene blue adsorption at equilibrium among coke adsorbents (2.05 mg/g). Langmuir is fitted with each experimental set in figure 21.

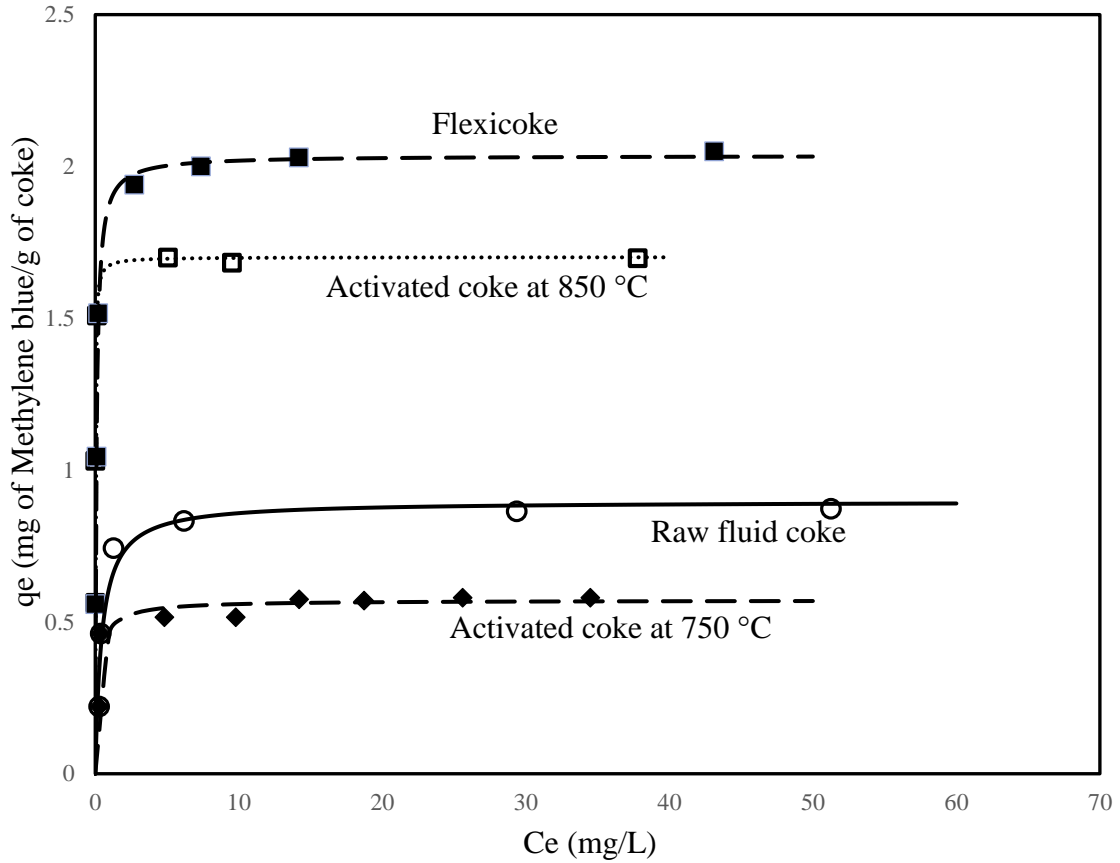


Figure 21. Adsorption comparison of methylene blue for various coke particles, experimental results fitted with Langmuir isotherm.

3.3.2.2 Specific Surface Area (SSA) Estimation:

The specific surface area for different adsorbents can be estimated from the monolayer adsorption assumption of the Langmuir model. From the Langmuir model fits, maximum adsorption uptake q_m (mg/g) is estimated. Specific surface area (SSA) (m^2/g) is measured using the following equations.

$$n_m \text{ (mole/g)} = (q_m/M) \times (10^{-3}) \quad (7)$$

$$SSA = n_m \times N \times A \quad (8)$$

Where SSA (m^2/g), n_m (mole/g) is the maximum molar adsorption uptake, M (g/mole) is the molar mass of the adsorbate, $N = 6.022 \times 10^{23}$ (atom/mole) is the Avogadro constant,

and A (m^2/atom) is adsorbate cross-sectional area taken from literature (Santamarina et al., 2002; Hamdaoui and Naffrechoux, 2007)

In table 6 and 7, the estimated surface area is compared for each adsorbent. The adsorption capacity difference between activated carbon and coke shows the reduced adsorbent quality of coke relative to activated carbon. Coke adsorption capacity is more than two orders of magnitude less than activated carbon. Liquid-solid adsorption method also suggests that coal activated carbon adsorbs more than coconut shell activated carbon. Activation with CO_2 at 850°C approximately doubled the surface area, and the flexicoke has the highest surface area among coke adsorbents.

Table 6. Activated carbon specific surface area measurement using liquid-solid adsorption method and Langmuir model

Parameters	Methylene Blue-Activated Carbon (Coal)	Phenol-Activated Carbon (Coal)	Methylene Blue-Activated Carbon (coconut shell)
q_m (mg/g)	408	325	283.8
n_m (mole/g)	0.001276	0.003453	0.000887
A (m^2/atom)	130×10^{-20}	41.2×10^{-20}	130×10^{-20}
SSA (m^2/g)	998.6	856.8	694.6

Table 7. Various coke particles specific surface area measurement using liquid-solid adsorption method with methylene blue and Langmuir model

Parameters	Raw Fluid Coke	Activated Coke at 750 °C	Activated Coke at 850 °C	Flexicoke
q_m (mg/g)	0.87	0.57	1.7	2.03
n_m (mole/g)	0.000003	0.0000017	0.0000053	0.0000063
A (m ² /atom)	130×10^{-20}	130×10^{-20}	130×10^{-20}	130×10^{-20}
SSA (m ² /g)	2.1	1.4	4.16	4.96

3.3.3 Liquid-Solid Adsorption Comparison with BET

Equilibrium liquid-solid adsorption results obtained for different adsorbents is compared with the BET surface area. As figure 22 shows, the liquid-solid adsorption results can be correlated with the BET surface area accurately for all the adsorbents. A logarithmic scale figure is used to compare all different adsorbents in one graph (figure 22).

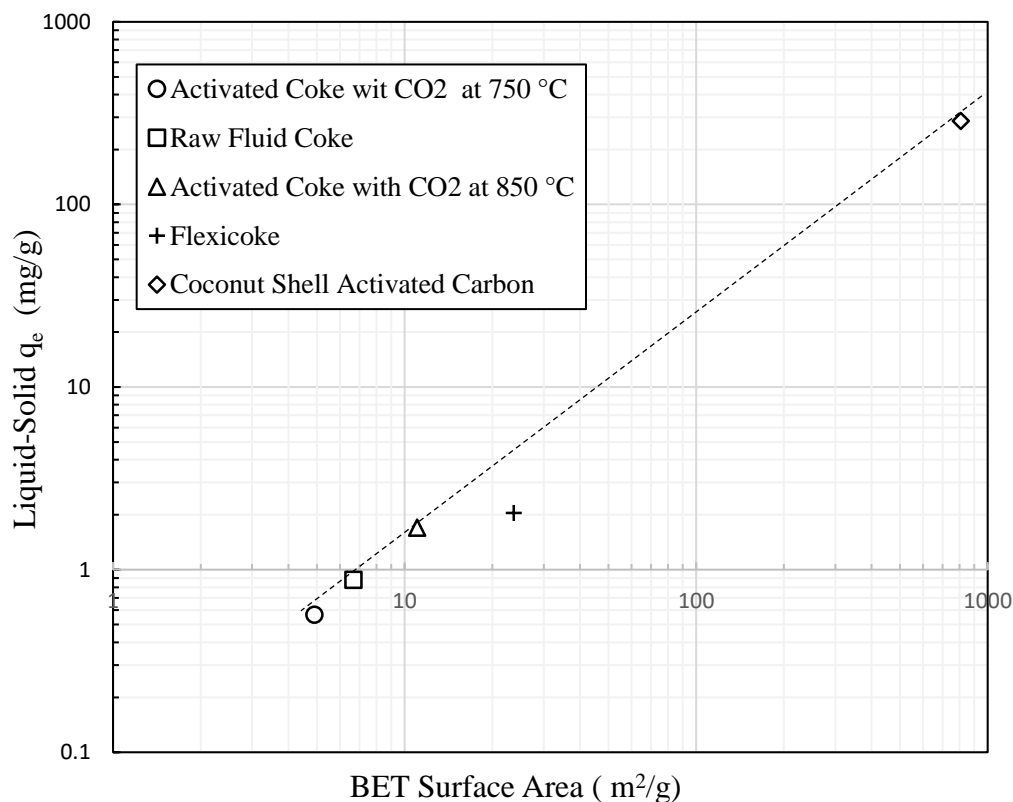


Figure 22. Liquid-solid adsorption results for various adsorbents versus BET surface area

3.3.4 Kinetics of Liquid-Solid Adsorption

An adsorption kinetics study was carried based on measurements at different time intervals. A 10 mL solution of methylene blue with a concentration of 400 mgL⁻¹ was prepared. 0.01 grams of activated carbon from coal was used in the sample. Sampling was done in time intervals of 10 min, 20 min, 40 min, 1 hour, 2 hours, 3 hours and 4 hours. Various kinetic models were compared with the experimental results. Pseudo-first-order model was chosen to fit with experimental results as it is a well-known simplified kinetic model (the pseudo-first-order model has been selected since this model also fits with many of hydrocarbons adsorption study in chapter 4). The model was developed for the first time by Lagergren (1898) to explain the adsorption kinetics of oxalic acid and malonic acid onto charcoal. In the literature, a comparison of Pseudo-first order rate and Pseudo-second order rate is

available. Although at some point in literature, the superiority of pseudo-second order to pseudo-first order has been found, it is recommended that closeness of model to data in equilibrium for determination of the best kinetics model is not reasonable and this idea has unfairly promoted the Pseudo-second order rate to a better model (Simonin, 2016). The Pseudo-first order rate model is widely used to explain the adsorption of liquid adsorbates. However, the model works fine for gaseous adsorbate as well (Rao, 2010). It has been shown that in case film diffusion is the rate-limiting step, particle size and film thickness work inversely with the pseudo-first order constant. Should the process be chemically rate controlled, the pseudo-first-order constant is independent of particle size and flow rate, however, is a function of partial pressure (or concentration in case of liquid adsorbate) and temperature (Ho and Mckay, 1999). Furthermore, It is believed that this model is applicable in initial 20-30 minutes of contact and in a timescale wider than this boundary, the error is going to increase (Aly et al., 2013). The shorter residence time in coke experiments compared to activated carbon in chapter 4 also lead to having a better model fit in coke experiments compared to activated carbon. The general pseudo-first-order kinetics model is expressed as follows:

$$\frac{dq_t}{dt} = K_1(q_e - q_t) \quad (9)$$

By integrating the equation (5), the pseudo-first-order rate kinetics model will be

$$q_t = q_e(1 - e^{-t.k_1}) \quad (10)$$

Where in this model q_t (mg/g) is adsorption capacity at t , q_e (mg/g) is the adsorption capacity at equilibrium, K_1 is the Pseudo-first order rate adsorption constant and t (min) is the time. Additional kinetics models are explained in the appendices.

Figure 23 shows the pseudo-first-order kinetics model fitted with experimental kinetics results. The amount of adsorption uptake after 5 hours is equal to 280.47 mg/g.

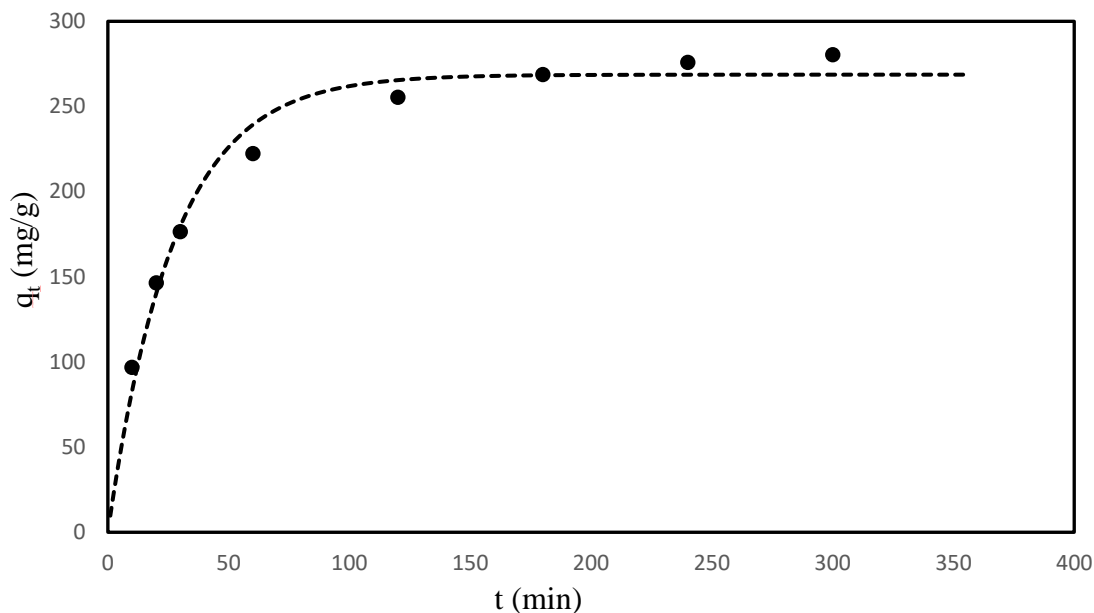


Figure 23. Kinetics of methylene blue with activated carbon from coal at an initial concentration of 400 mg/L. Experimental results fitted with Pseudo-first-order rate model.

3.4 Summary

Coke Activation carried out with CO₂ at 650 °C, 750 °C, and 850 °C as well as with nitrogen (SBC coke) and air at 650 °C for 1 hour at set-point with JBR. The effect of activation on creating porosity and increasing the surface area was tested via BET and liquid-solid adsorption with methylene blue and phenol. Commercial activated carbons were also used to be compared with results. Other experimental analysis including TGA and BET was performed to understand the characteristics of the different adsorbents better.

Chapter 4

4 Hydrocarbon Adsorption Kinetics with Carbonaceous Materials

4.1 Introduction

In this chapter, we aim to experimentally measure hydrocarbon adsorption kinetics in a novel well-mixed system in a time scale relative to Fluid Cokers (0-10 seconds for the freeboard, and up to 600 seconds for the entire Fluid Coker). A vertically oscillating gas-solid contacting unit was designed to carry out this measurement. The equipment was initially tested using coconut shell activated carbon, which allowed us to measure adsorption kinetics and test for reproducibility. The objectives of the chapter are mainly organized into four sections which are described as follows:

1. Designing a system that experimentally measures hydrocarbon adsorption kinetics in the time scale resolution of seconds, under elevated temperatures condition (up to 300 °C) with a vapor pressure of up to 1 atm.
2. Investigating the effect of temperature on adsorption kinetics (adsorption at temperatures of 10°C, 30°C, and 50°C above the hydrocarbon boiling point), to relate adsorption results with the model that uses a boiling point distribution.
3. Determine the impact of hydrocarbon adsorbate molecular weight (Mesitylene (C_9H_{12})-n-decane ($C_{10}H_{22}$)- n-dodecane ($C_{12}H_{26}$)) and molecular shape (Mesitylene is an aromatic adsorbate derived from benzene, looks like a ring with three methyl substituent positioned around the ring, while n-decane and n-dodecane are aliphatic hydrocarbon adsorbate which they have an open chain linear structure) on adsorption kinetics.
4. Comparing hydrocarbon adsorption kinetics with various carbonaceous materials, and relate the results based on the measured surface areas.

4.2 Background Information

Previous adsorption kinetics studies on activated carbon are confined to lighter hydrocarbons (e.g., methane, ethane, and propane), which are in the gaseous phase at ambient conditions. These conditions avoid the risk of hydrocarbon condensation in the experimental system. The operating temperatures for such experiments range from 25 to 50°C (Costa and Sotelo, 1981; Malek, 1997; Choi et al., 2003). Although Al-muhtaseb et al. investigated the adsorption of heavier hydrocarbons, including C₆H₁₄ and C₇H₁₆, the study only measured adsorption equilibrium (i.e., no kinetic measurements) in vapor pressures ranging up to a maximum of 0.2 atm. The effect of temperature (285-350 °C) on equilibrium adsorption uptake of n-heptane in much lower partial pressures compared to our study (0-0.8 kPa) with Polyvinylidene chloride-based microporous activated carbon investigated (Jiménez-Cruz et al., 2007). Effect of pore structure and temperature (280-350 °C) on VOC including benzene adsorption on activated carbon is investigated (Chiang et al., 2001). Laredo et al., studied gas-phase diffusion of linear and multi-branched alkanes on carbon molecular sieve and as an important finding, they showed that in a given hydrocarbon family, increasing the branch and carbon number will slow down the diffusion.

Furthermore, useful literature found to investigate the kinetics of hydrocarbon adsorption with activated carbon but only with propane (Wang and Do, 1999). In the Fluid Coker, bitumen is injected onto the hot coke particles and is vaporized following thermal cracking, and finally exists in the vapor phase through the freeboard and downstream cyclones. The hot coke particles contact with vapors in fluid coker's horn chamber before entering cyclones is very short (few seconds). As such, it is necessary to investigate the adsorption kinetics of hydrocarbon vapors, at representative partial pressures (approximately 1 atm.) with fluid coke.

4.3 Material and Methods

4.3.1 Experimental Set-up

As a reminder, the experimental adsorption equipment must meet the following criteria:

1. Well agitated conditions for negligible external mass transfer and uniform temperature,

2. Operating at elevated temperatures while also avoiding thermal cracking,
3. Operating at a maximum hydrocarbon partial pressure of approximately 1 atm,
4. Capable of measuring the adsorption kinetics study.

A novel vertically oscillating gas-solid contacting unit was designed to satisfy the previous requirements. The unit includes an internal stainless-steel cup which is held within a thick ceramic vessel to minimize heat losses to the surrounding. The internal stainless-steel cup gives an internal volume of 500 mL for the vaporization vessel. A solids-cup with an internal volume of 10 mL (2% of the total volume) was placed at the top of the vaporization vessel and attached to the bottom of the vessel lid. A round DC electromagnet capable of 180 lbf was positioned above the vessel lid and used to pull the solids-cup lid upwards via the resulting magnetic force. A Viton O-ring was applied between the solids-cup and its lid to make a seal between the vaporization vessel inner cup and solids-cup. General dimensions of the system, as well as the definition of different sections, are provided in figure 24.

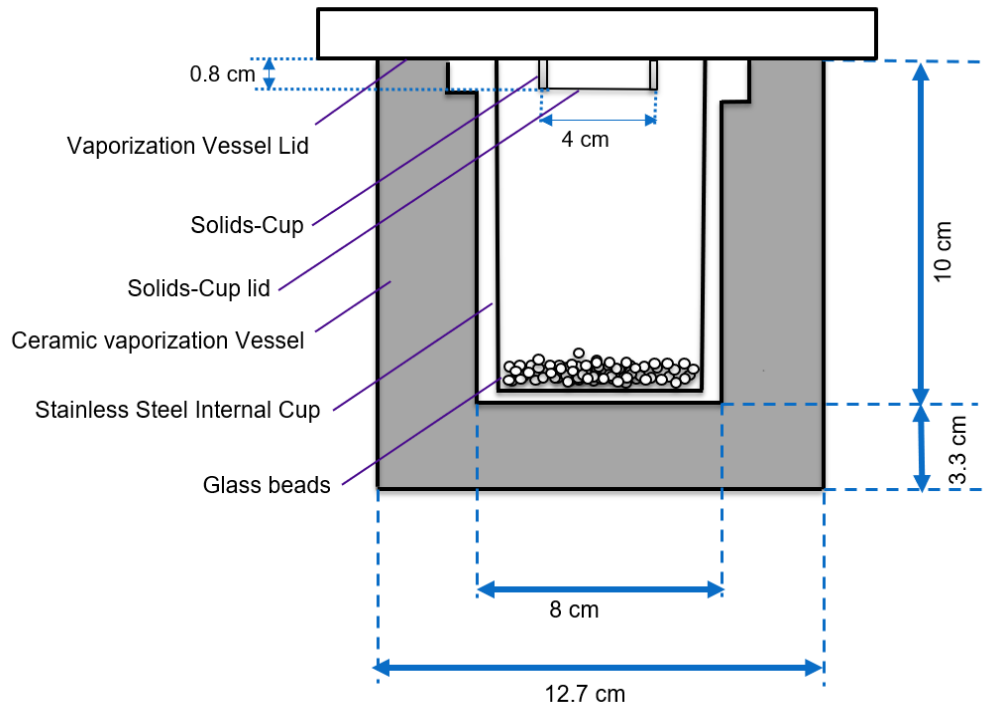


Figure 24. The schematic and detailed dimensions of the unit's vessel.

A pneumatic actuator was used to provide the required gas-solid mixing to reduce the external mass transfer resistance and to provide a uniform temperature (requirements 1). Once the particles expand over the height of the crucible, the gas which is located initially at the top of the vessel moves downward. The opposite occurs when the bed contracts downward, providing good mixing and gas-solid contacting (Latifi, 2012).

A single rod air cylinder, a solenoid valve, reed switches, and a controller box were used to obtain the needed vertical oscillations. The amplitude of the unit was altered by changing the position of the reed switches, and the required frequency was set by the air pressure regulator attached to the controller box. Inert glass-beads were used in the system to improve mixing and to maximize heat transfer before gas-solid contact. The required frequency and amplitude for the system were tested with a transparent vessel with stainless steel balls based on conditions where steel balls hit the top of the vessel. The frequency of the system was also examined by recording a video of the vertical oscillation of the ceramic

vessel. The video shows that the frequency of the vessel is estimated to be approximately 3 Hz. A 48 VDC/1 kW power supply was used to heat the system to the necessary temperatures (requirement 2) via induction.

4.3.2 Measurement Technique

The overall schematic of Vertically Oscillating Gas-Solid Contacting system is shown in figure 25. The idea behind the design of the system for hydrocarbon adsorption kinetics measurement clearly expressed. The step by step procedure and techniques that used for adsorption kinetics measurement is explained in detail afterward.

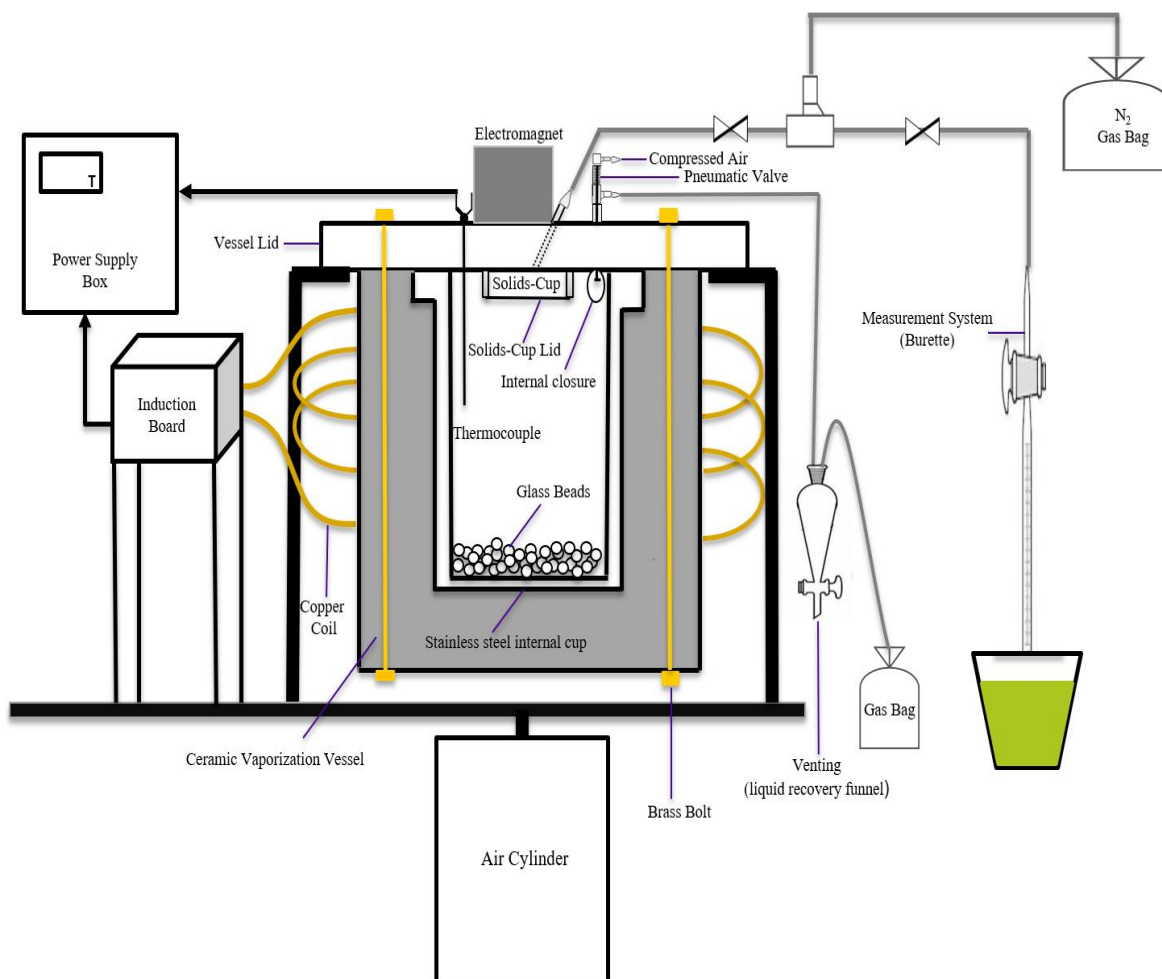


Figure 25. The schematic of the vertically oscillating gas-solid contacting unit for hydrocarbon adsorption kinetic measurement

Adsorption kinetic analysis is based on the simple gas flow technique measurement system explained in chapter 2. However, the system upgraded in here to be capable of adsorption kinetics measurement at an isothermal condition. The idea behind the gas flow technique for adsorption kinetics measurement is to keep the system at a hydrocarbon partial pressure of 1 atmosphere. Then the adsorbed hydrocarbon moles create a driving force to nitrogen enter the system and replace the adsorbed hydrocarbon moles. The calculation is based on a simple mole balance of the semi-batch system. The equal number of nitrogen moles will be entering the system instantaneously while adsorption is taking place. This calculation method will enable us to record the nitrogen volumetric changes versus time and measure the adsorption kinetics consequently.

4.3.2.1 Step1: System Set-up

In each run, the required mass of carbonaceous particles is inserted and sealed inside the solids-cup by enabling the electromagnet on top of the vessel lid. The required amount of liquid (5-6 grams, this is a function of hydrocarbon boiling point and molar mass of each hydrocarbon, calculated using simple ideal gas law) inserted in the crucible to generate a vapor volume of approximately three times of the internal vessel volume, flushing out the air from the vessel via external venting. Brass bolts were used to make a proper seal between the crucible and the lid, without being heated via induction. Figure 26 shows the vessel which is filled with an adequate amount of liquid hydrocarbon and solids-cup holding particles using a plugged electromagnet. The pneumatic valve is kept fully open for the required venting.

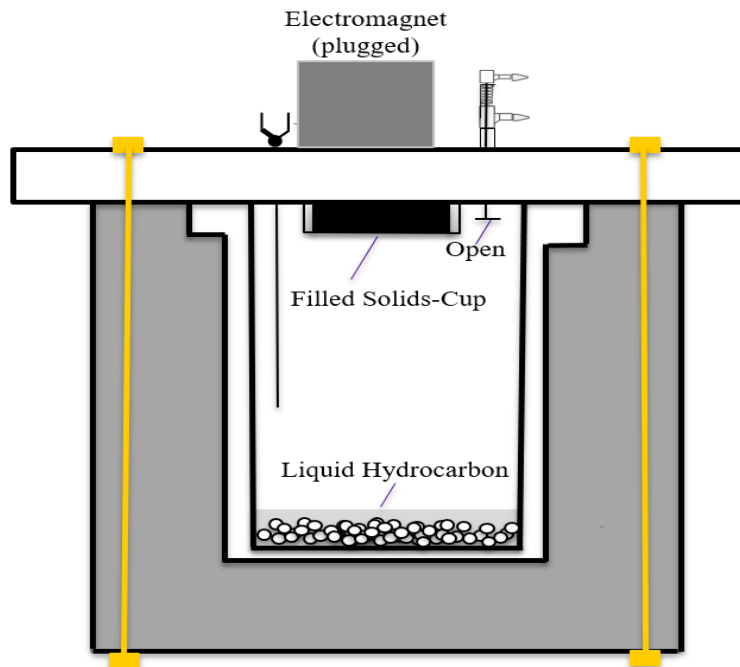


Figure 26. System Set-up: liquid hydrocarbon, solid particles insertion, and system closure

Before the heating-up step, the burette, solids-cup, and connections from the burette to solids-cup are going under vacuum to provide the required driving force for flushing with nitrogen to remove the oxygen present and eliminate the risk of combustion. The zones which are flushed with nitrogen are distinguished using a dashed line in figure 27. Initially, valve 1 is closed to shut off the connections to solids-cup, then vacuum and nitrogen flushing are performed for burette. After then, valve 3 is closed to shut off the burette and make nitrogen environment in the solids cup using vacuum and nitrogen gas bag subsequently. Before the heating stage, the connection to vacuum ejector is removed, and valve 1 and 3 are switched to open. Valve 2 and 4 remain open to the nitrogen gas bag ensuring that all the connections will stay under nitrogen environment for the whole run. After this stage, the system is ready to be heated.

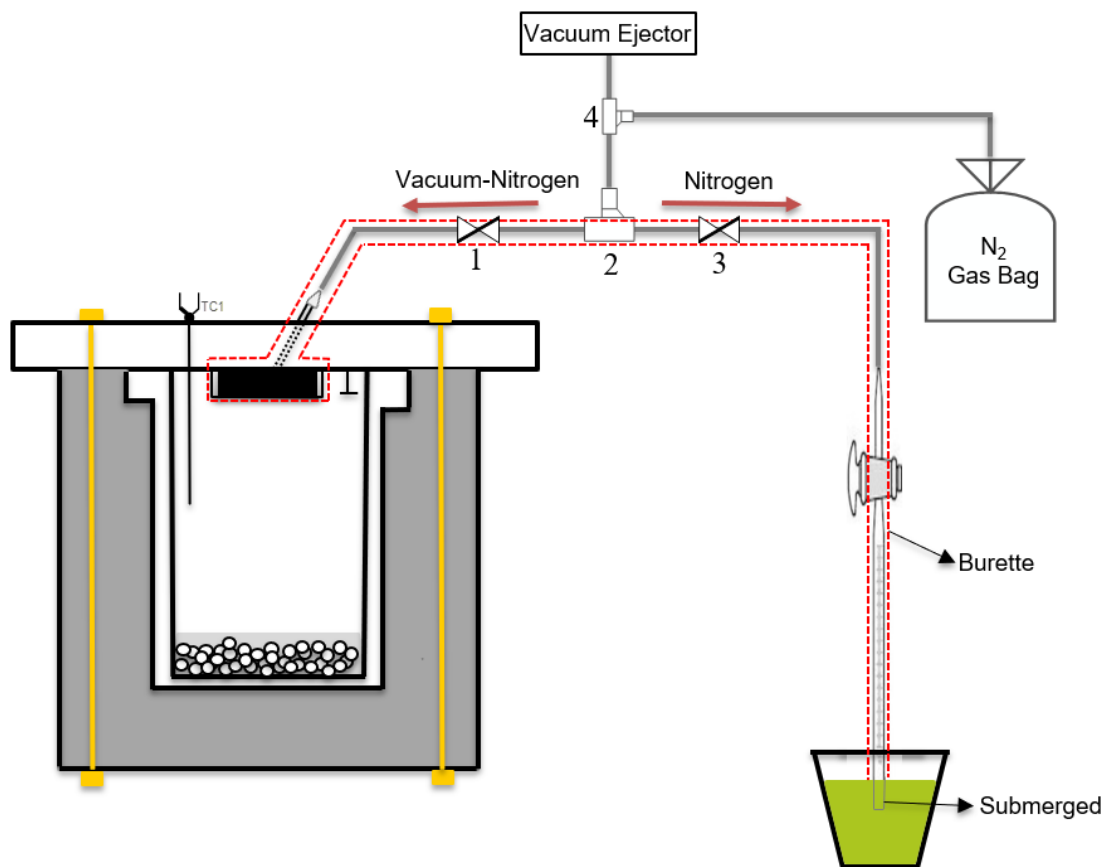


Figure 27. System Set-up: Vacuum and nitrogen flush for the burette, solids-cup, and connections

4.3.2.2 Step 2: Heat Supply

During the heating step, the hydrocarbon phase is vaporized inside the vessel via induction heating while the system is well mixed (vertical oscillations and inert glass beads). A pneumatic valve is used to allow for venting while the system is heating thus reaching a partial pressure of 1 atm. (requirement 3), which is then closed to avoid condensation inside the crucible. The mole fraction of the hydrocarbon vapor is then equal to 1 everywhere, which eliminates external mass transfer effect (requirement 1). An undiluted hydrocarbon atmosphere inside the crucible is thus obtained at the end of this step. The exhaust line is connected to a funnel to collect the condensed hydrocarbons. Figure 28 shows the motions of the inert glass beads particle inside the vaporization vessel thanks to utilizing the air cylinder and illustrates the hydrocarbon phase transition and recovery in the funnel.

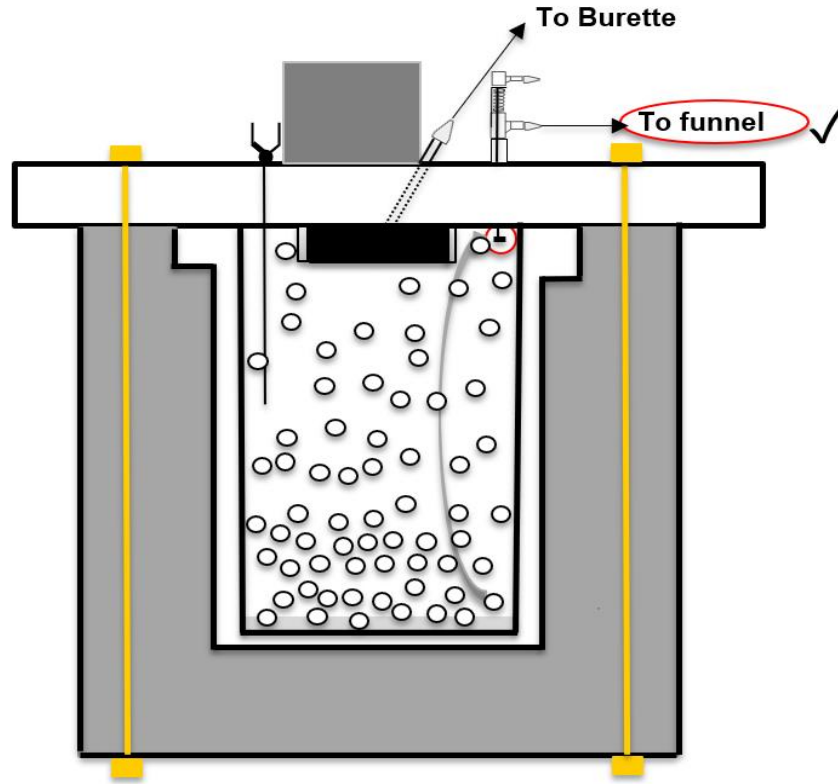


Figure 28. Heat Supply: glass beads motions and hydrocarbon phase transition and venting

Once the system has reached to the desired temperature set-point and remained steadily (30-45 minutes to recover the expected condensed hydrocarbon in the funnel, this should be approximately two-thirds of the volume of the liquid hydrocarbon which was inserted initially), the open valves to the atmosphere from crucible (pneumatic valve) and solids-cup (valve 2 in figure 27) are closed.

4.3.2.3 Step 3: Gas-Solid Contact

The gas-solid contact is initiated by disabling the electromagnet. Figure 29 shows that the solids-cup is dropped after unplugging the electromagnet and creates the gas-solid contact at the time when we are ensured the vaporization vessel is presented at 1 atmosphere gaseous phase.

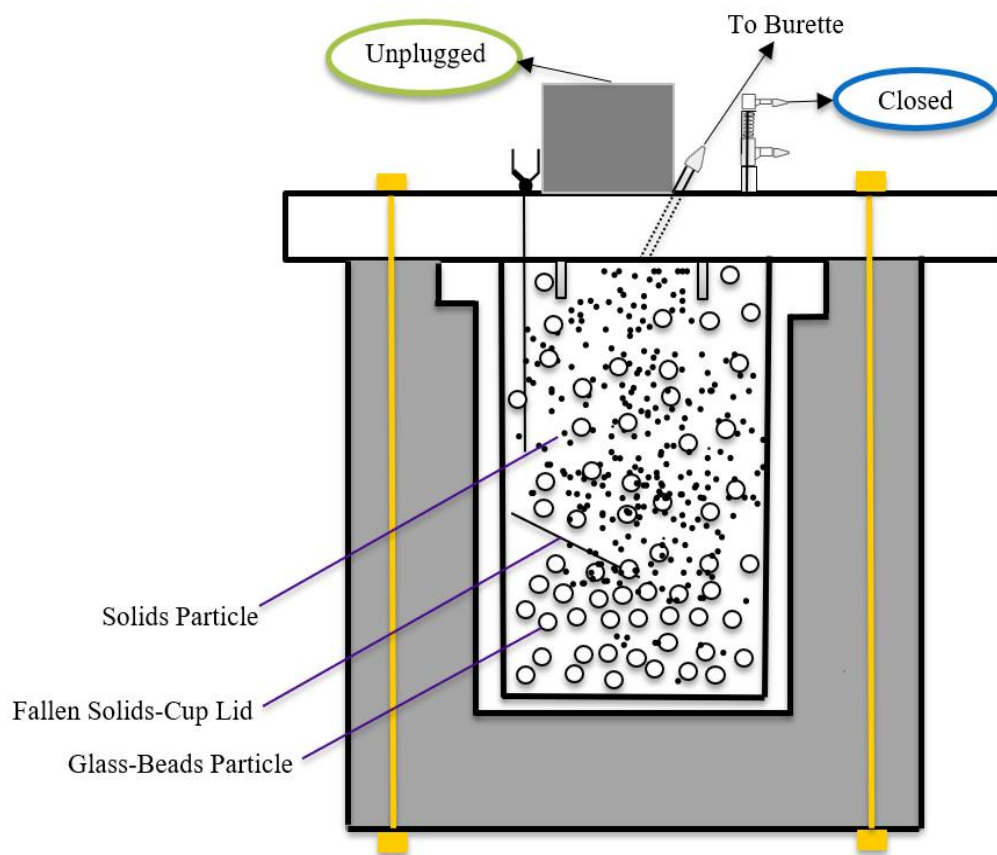


Figure 29. Gas-solid contact step in hydrocarbon adsorption kinetics measurement

4.3.2.4 Step 4: Kinetic Measurement

A Burette is used as a volumetric measurement system with the accuracy of reading the adsorption of 0.005 mmol/g (0.1 mL volume change). It is important to note that the measurement is independent of the absolute internal volume of the vessel. However, the ratio of solids-cup to the total volume of the vessel is critical and should satisfy the ratio in the actual coker. The adsorption kinetics are measured by recording the volumetric changes in the burette (requirement 4). This step usually takes more than 1 hour (1-1.5 hours) to reach the level in the burette which means that equilibrium has obtained. The data is recorded seeing the volumetric change of 0.1 mL (unit accuracy) and continues until equilibrium is attained. Duplicates gathered for most of the runs, and both sets are shown in graphs.

4.3.3 Operating Conditions and Phase Physical Properties

Table 8 provides a summary of the physical property and chemical structure of hydrocarbon adsorbates used in this study.

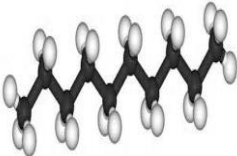
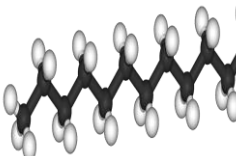
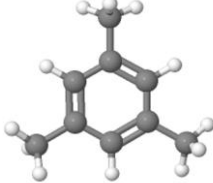
Properties	N-decane	N-dodecane	Mesitylene
Formula	C ₁₀ H ₂₂	C ₁₂ H ₂₆	C ₉ H ₁₂
Chemical Structure			
Molar Mass (g/mole)	142.29	170.34	120.19
Normal Boiling Point (°C)	174.1	216.3	164.7

Table 8. Physical Properties of hydrocarbon adsorbates

In each run, 1 gram of particles is inserted inside the solids-cup. As mentioned earlier hydrocarbon partial pressure for every run is kept at 1 atmosphere and operating temperatures are set to satisfy models with boiling point distributions (i.e., hydrocarbons boiling point +10 °C, +30 ° C, and +50 °C)

4.4 Results and Discussion

Activated carbon was used initially as a commercially well-known adsorbent during the system validation since the measured adsorption based on the volumetric method was showing higher adsorption (i.e., higher volumetric changes in burette). Thus, based on this, the approach for experiments was set to initially investigate the impact of temperature on the adsorption kinetics and test the validation of results, secondly impact of molecular weight and shape of hydrocarbon adsorbates was studied, then the adsorption kinetics of fluid coke was studied and finally comparison of different carbonaceous materials in adsorption kinetics is illustrated.

The pseudo-first-order kinetic model which was explained in chapter 2 and fitted with liquid-solid adsorption kinetics results in chapter 3 is used here again to fit with the experimental results. The equation is shown below.

$$q_t = q_e(1 - e^{-t k_1}) \quad (11)$$

Where in this model q_t is the adsorption capacity at the specified time (mg/g), q_e is the adsorption capacity at equilibrium (mg/g), K_1 is the pseudo-first-order rate adsorption constant (s^{-1}), and t is time (s) (Qiu et al., 2009). The excel solver is used to fit the experimental results with the pseudo-first-order rate kinetics model. The solver is used to minimize the sum of residual squares obtained from the experimental q_t and estimated q_t from the model. To fit the pseudo-first-order rate kinetic model with results in the graphs, model was fitted with both series. However, it also fitted separately with individual sets to compare the kinetic of the experimental set and the replicate.

4.4.1 The Effect of Temperature on Adsorption Kinetics

To investigate the effect of temperature on adsorption kinetics, adsorption of normal decane was studied with coconut shell activated carbon based on the difference between the operating temperature and n-decane normal boiling point (normal boiling point +10°C, +30°C, and +50°C). The reproducibility of the experimental results is shown in Figure 30 by providing data sets for replicate experiments at each set point temperature. The two data sets in each temperature are fitted with a Pseudo-first order rate kinetic model. Decreasing the temperature from 224°C to 184°C resulted in an increase of equilibrium adsorption uptake from 106 (mg/g) to 156 (mg/g), which is following the expected adsorption equilibrium trend with temperature.

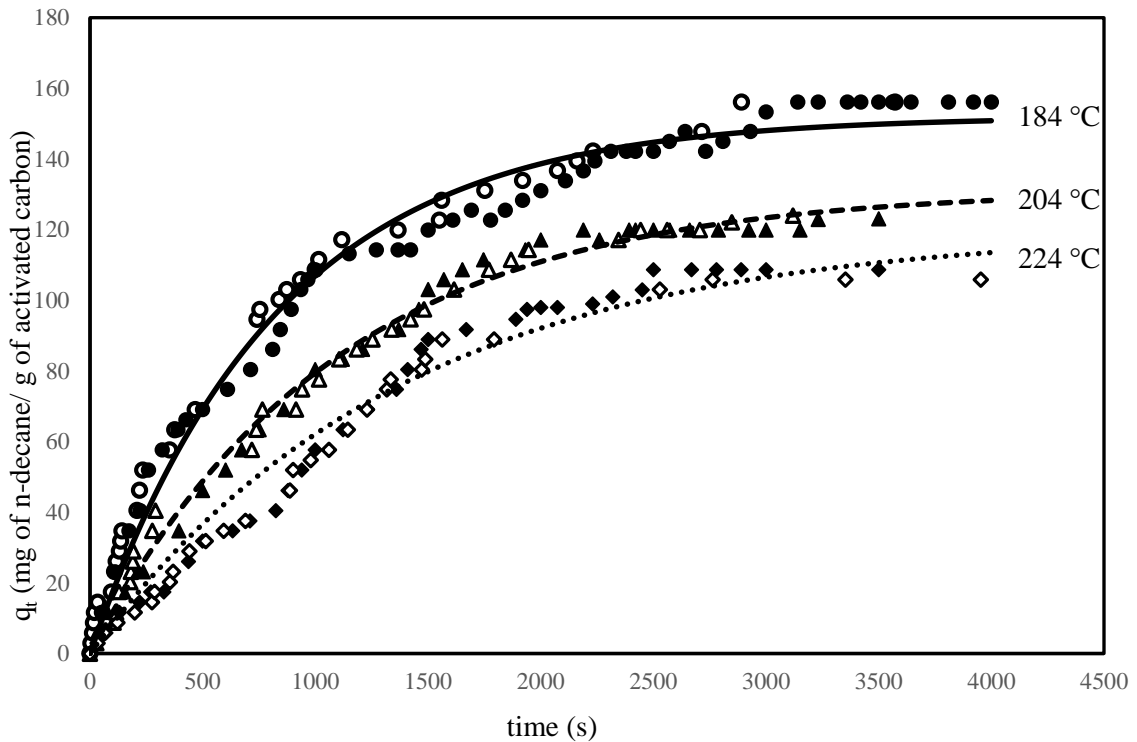


Figure 30. Adsorption kinetics of n-decane with coconut shell activated carbon. Hollow and filled in data points are used to compare duplicate runs. Pseudo-first order rate model was used to fit with experimental results.

Figure 30 shows a good adsorption kinetics reproducibility for each studied temperature. The reproducibility is proven in the following table by comparing the pseudo first order

adsorption rate constants (K_1), measured separately and compared for individual sets in each temperature. The model was fitted for each data-set individually to examine the reproducibility of results. Table 9 compares the reproducibility of results via measured adsorption rate constants relative error.

Table 9. Reproducibility of the model parameters

T-T _b (°C)	Experimental Equilibrium Adsorption (mg/g)	K ₁ (Set 1)	K ₁ (Set 2)	Relative Error %
50	105.8	0.000729	0.000678	7.0
30	123.1	0.000928	0.000925	0.3
10	156.1	0.0013	0.0011	15.3

The adsorption kinetics of n-decane with coconut shell activated carbon is illustrated in the time scale more relevant to the Fluid Coker in figure 31. In the initial 600 seconds of the experiment, 30-40 percent of the equilibrium uptake was adsorbed for coconut shell activated carbon adsorption run with n-decane. The adsorption kinetics follow a similar expected trend along with the equilibrium values (i.e., lower temperatures result in more adsorption for a given residence time).

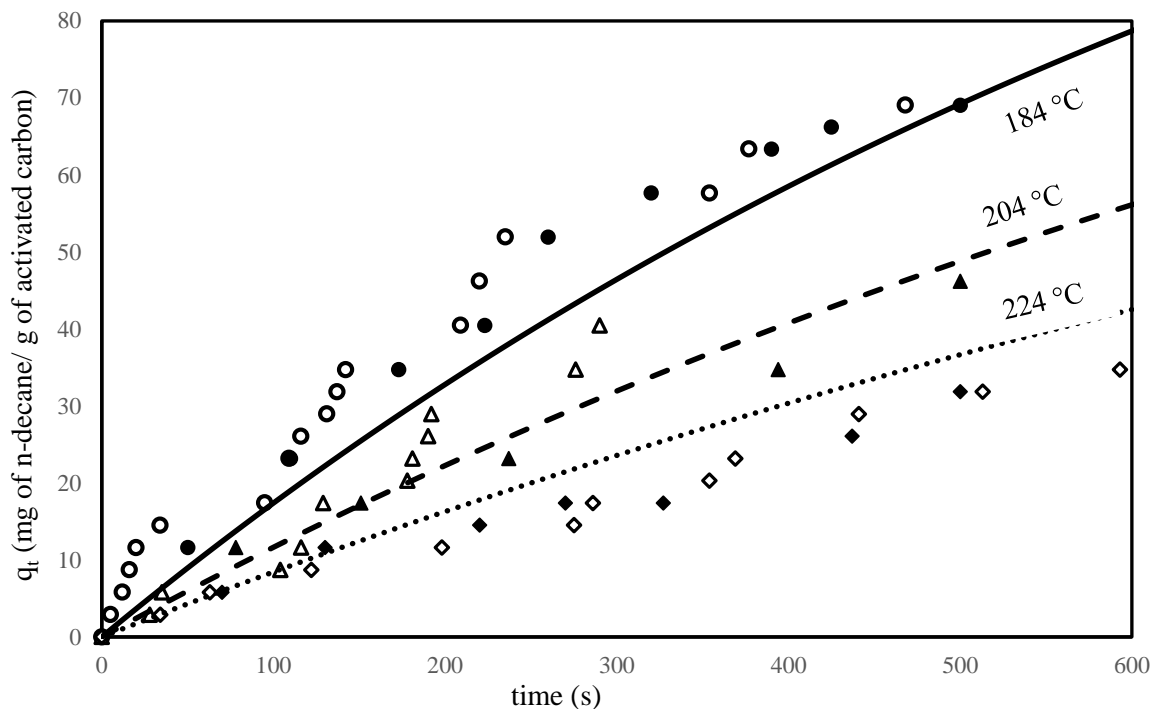


Figure 31. N-decane adsorption kinetics in the first 600 seconds with coconut shell activated carbon. Hollow and filled in data points are used to compare duplicate runs. Pseudo-first order rate model used to fit with experimental results.

4.4.2 The Impact of Molecular Weight and Shape

The effect of molecular weight on hydrocarbon adsorption kinetics with coconut shell activated carbon is shown in figure 32. The measurements were carried out at the same difference between adsorption temperature and normal boiling point. The previous was completed to be compatible with the hydrocarbon assay used in a separate modeling project using Aspen Plus. The results compare the adsorption of aliphatic hydrocarbons including n-decane ($C_{10}H_{22}$), n-dodecane ($C_{12}H_{26}$) with Mesitylene (C_9H_{12}) as an aromatic. Figure 32 illustrates adsorption kinetics in mass basis, where n-dodecane (heaviest adsorbate) adsorbs preferentially in equilibrium due to having a higher molar mass. It is worth stating that n-decane shows faster kinetics compared to others which agree with Laredo et al. study where they concluded that the heavier hydrocarbon in one family, adsorbs relatively slower (the adsorption of n-dodecane (heavier adsorbate) is slower than n-decane).

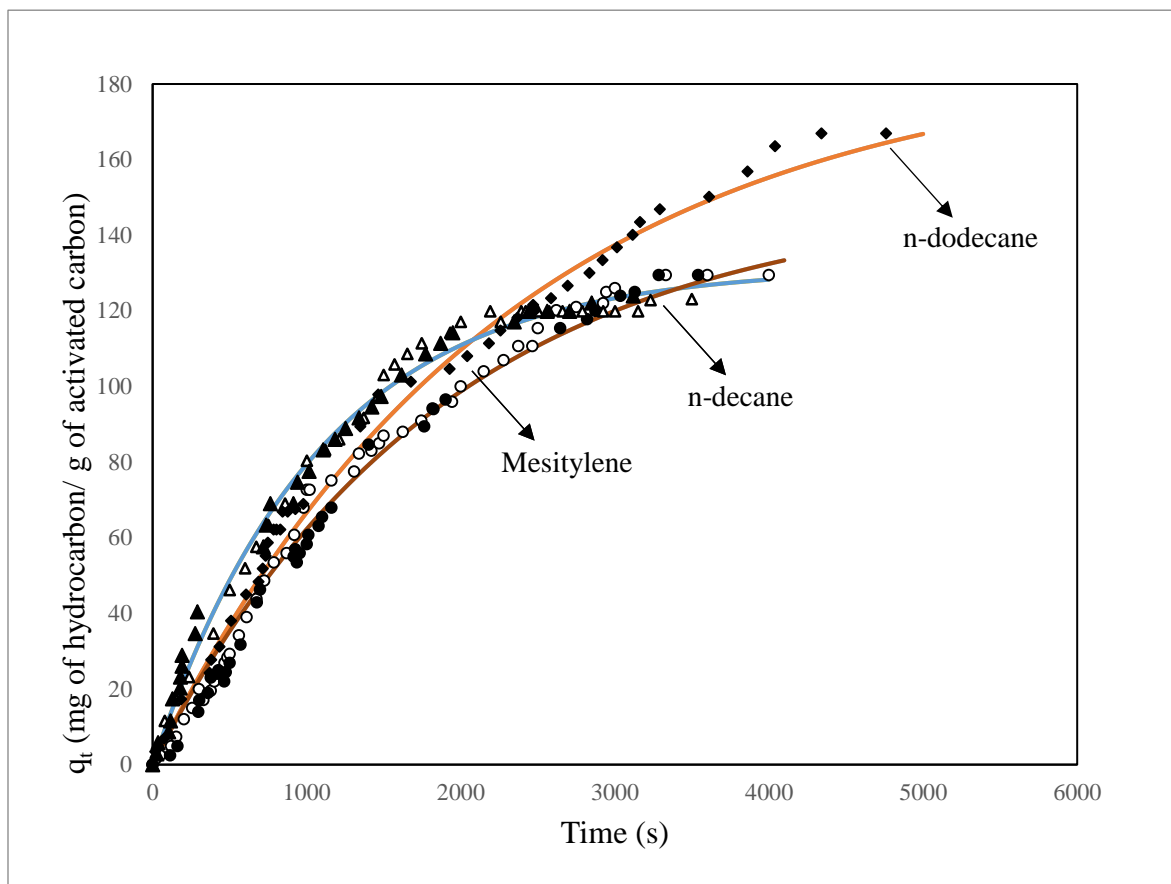


Figure 32. Hydrocarbons adsorption kinetics (mg/g) with activated carbon in boiling point +30 °. Pseudo-first order rate model used to fit with experimental results.

Figure 32. shows that in the same temperature variance with the hydrocarbon normal boiling point (+30 °C), n-dodecane is adsorbed more than others in equilibrium (mass basis) due to having a heavier molecule. Adsorption uptake after 4000 seconds falls within the range 119-165 mg/g for these three compounds in the chosen operating temperatures. By conversion of values in molar basis, this range will get quite tighter (0.86-1.07 mmole/g). Figure 33 suggests that on a molar basis, mesitylene gives the highest adsorption uptake at equilibrium, whereas n-decane and n-dodecane give similar equilibrium adsorption uptakes: these differences are likely caused by different molecular structures,

with mesitylene being aromatic. The Pseudo-first order kinetic model is fitted with experimental results in both figure 32 and 33.

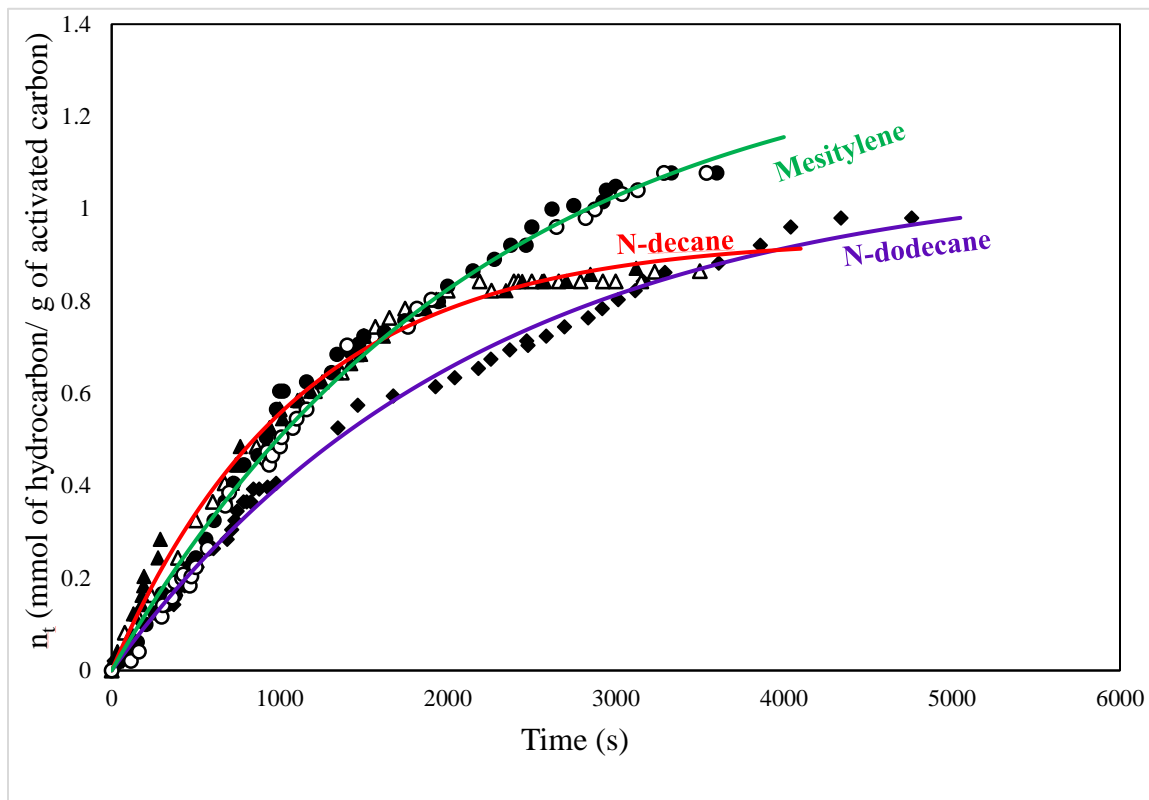


Figure 33. Hydrocarbons adsorption kinetics (mmol/g) with activated carbon in boiling point +30 °C. Pseudo-first order rate model used to fit with experimental results.

4.4.3 Hydrocarbon Adsorption Kinetics with Coke

The adsorption capacity of the coke has been compared with coconut shell activated carbon in chapter 3 via liquid-solid adsorption and BET. Both methods suggested that surface area and pore volume of coke and even activated fluid cokes, and flexicoke is 1 to 2 orders of magnitude less than coconut shell activated carbon. Therefore, knowing the gas-solid result obtained with coconut shell activated carbon and coke adsorption capacity, we did not expect to see the volumetric change of higher than 2 mL in equilibrium with the burette. Therefore, the optimal condition for detecting hydrocarbon adsorption kinetics with coke

was chosen here. The normal dodecane adsorption at 226 °C is the operating condition (heaviest compound, lowest temperature variance with the boiling point) which has the most expected adsorption uptake with coconut shell activated carbon. Therefore, to detect changes with coke, these operating conditions have been chosen for coke adsorption kinetics experiments. Figure 34 compares the adsorption kinetic of flexicoke (this is combination of flexicoke and burner coke, the particles are taken from the burner of the fluid coker) and SBC coke (Simulated burner condition for fluid coke which has gone through pretreatment with the nitrogen at 650 °C) with normal dodecane in 226 °C.

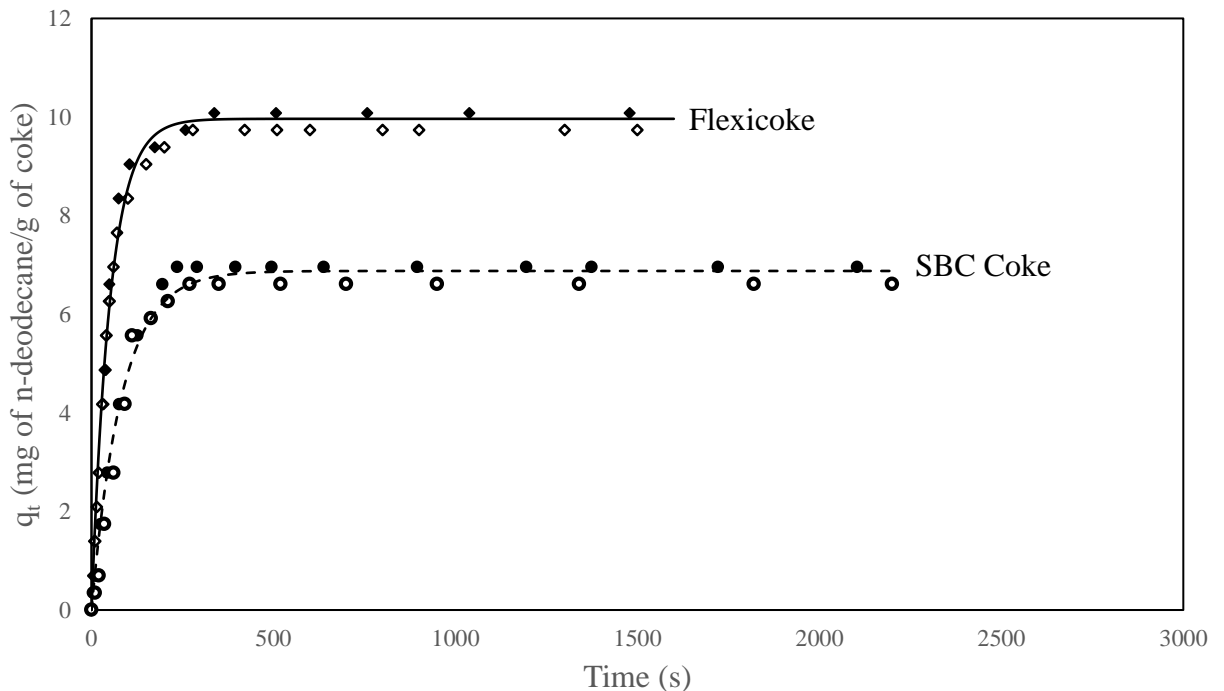


Figure 34. Adsorption kinetics comparison of SBC coke and flexicoke with normal dodecane at 226 °C. Pseudo-first order rate model used to fit with experimental results.

It takes approximately 300 seconds to reach the adsorption equilibrium, with a value for raw SBC coke of 6.9 mg/g and flexicoke at 9.96 mg/g. The replicate experiment carried out with both SBC Coke and flexicoke to confirm the accuracy of the results and Pseudo-first order rate kinetic model used as a fit with experimental results. The initial 100 seconds of the adsorption kinetics for these runs are shown in figure 35. The graph shows that the Pseudo-first order rate kinetic model still fits very well in the initial contacting time.

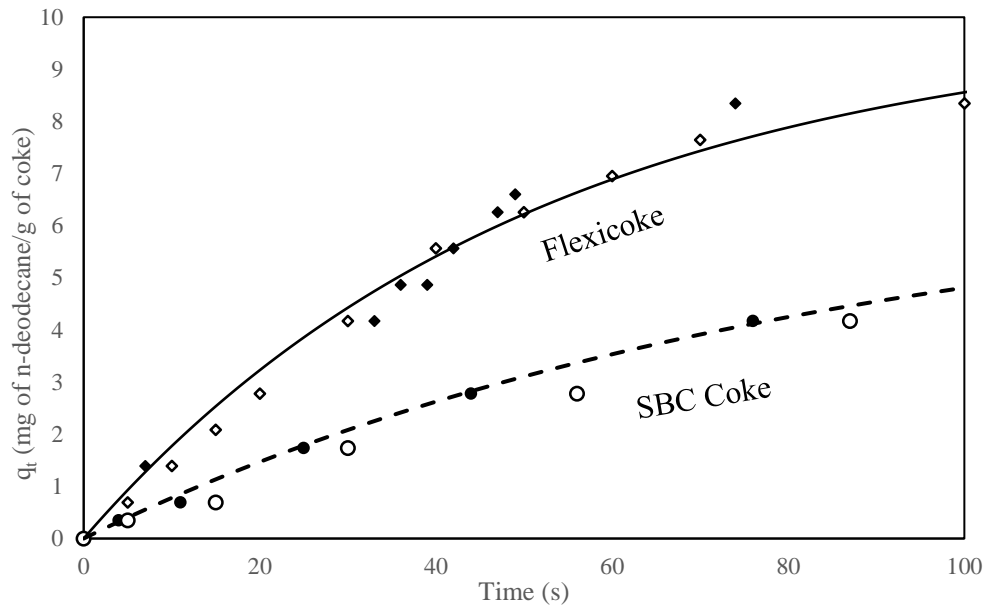


Figure 35. Initial 100 seconds of coke adsorption kinetics experiment with normal dodecane at 226 °C. Pseudo-first order rate model used to fit with experimental results.

The result shows that approximately 0.7 mg/g (10% of the equilibrium) and 1.6 mg/g (16 % of the equilibrium) is adsorbed respectively with SBC coke and flexicoke in the initial 10 seconds. These values are critical since they refer to the potential adsorption uptakes in the residence time of coke particles inside the horn chamber before entering the cyclone, as needed for cyclone fouling model. After 100 seconds of the experiments, 73, and 84 percent of the equilibrium uptake takes place respectively for raw fluid coke and flexicoke.

4.4.4 Comparison of Adsorption Kinetics with Different Carbonaceous Materials

The adsorption kinetics of coconut shell activated carbon is compared with SBC coke and flexicoke at 226 °C in figure 36. Since the equilibrium adsorption values vary by orders of magnitudes, a logarithmic scale graph was used for comparison.

The equilibrium adsorption values for SBC coke and flexicoke are 6.9 mg/g and 9.9 mg/g, in comparison with 190.2 mg/g for coconut shell activated carbon, which is 28 times higher than SBC coke and 19 times higher than flexicoke equilibrium uptake with n-dodecane.

SBC coke and flexicoke reach a plateau at about 300 seconds; however, the equilibrium is reached for activated carbon after more than 4000 seconds. Two potential reasons for this is that coke does not have internal pores as much as activated carbon. The fewer seconds takes for SBC coke and flexicoke to reach the equilibrium; this suggests that the adsorption is likely only taking place on mostly surface (surface diffusion). Therefore, the rate-limiting step for the adsorption process of coconut shell activated carbon is due to internal pore diffusion. However, the rate-limiting step in case of coke adsorption is the surface pore diffusion. The contacting time in the Fluid Coker is likely to only result in adsorption on the outside surface of the particles. The internal pores are filled at much longer times but do not occur with the coke particles (since there are much fewer pores). The BET has shown that coconut shell activated carbon has the total pore volume of 0.43 mL/g, but SBC coke has only 0.006 mL/g (71 times less). The second potential reason is that the size of activated carbon particles are approximately 3-4 times bigger than that of the flexicoke and SBC coke (640 μm -220 μm -163 μm) and relatively faster adsorption is expected with finer particles (explained in appendices in section 6-9 and 6-19).

The results obtained from coke hydrocarbon adsorption kinetics are a significant factor for the Fluid Coker essentially the first few seconds of experiments are crucial because of referring to the residence time of vapor-particles contact in the horn chamber before entering the cyclones. One of the factors contributing to cyclone fouling is the adsorption of coke particles in the horn chamber, and this potentially can be related along with other factors to the cyclone fouling model.

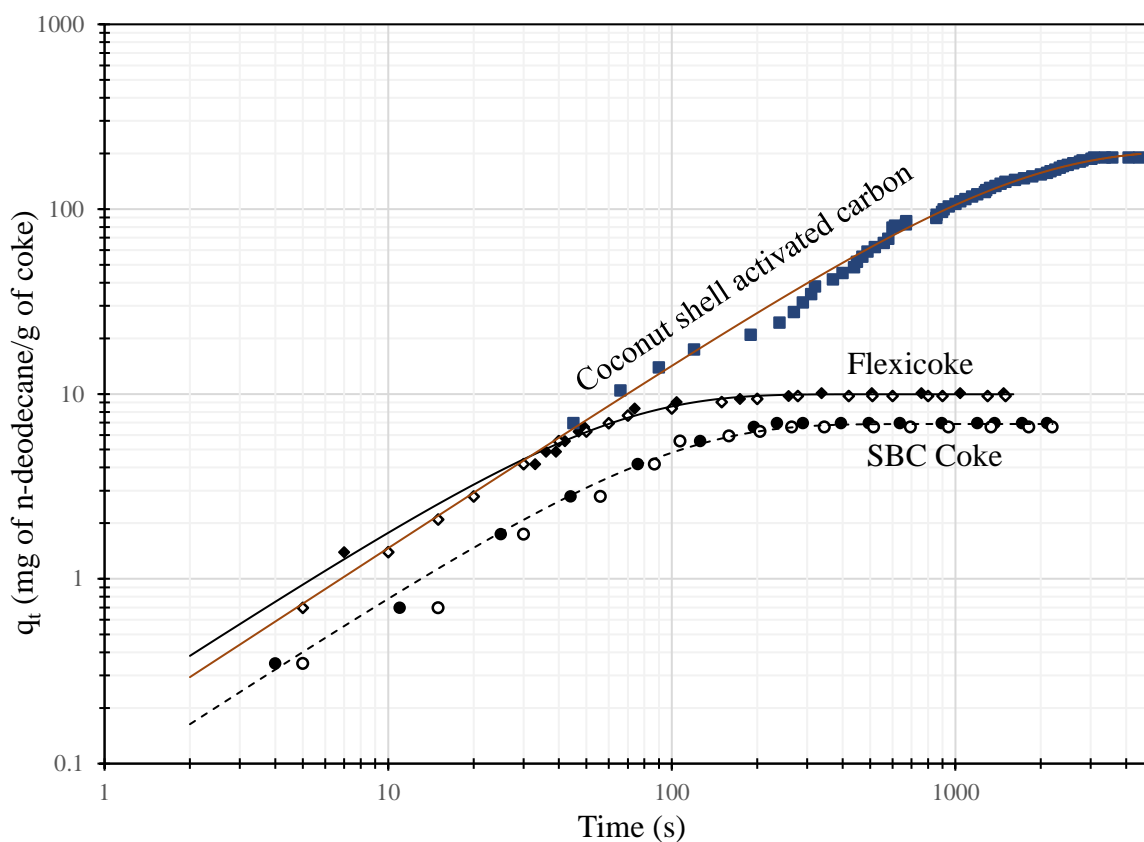


Figure 36. Adsorption kinetics comparison of raw coke, flexicoke, and coconut shell activated carbon with normal dodecane at 226 °C on a logarithmic scale. Pseudo-first order rate model used to fit with experimental results.

4.4.5 Gas-Solid Results Comparison with BET and Liquid-Solid Adsorption Results

Here, the equilibrium gas-solid results obtained from this chapter is compared with BET results and the liquid-solid adsorption results from the previous chapter. The BET suggests the surface area of 12.35 m²/g, 23.67 m²/g, and 809.254 m²/g respectively for SBC coke, flexicoke and coconut shell activated carbon. Also, BET represented that surface area of coconut shell activated carbon is 65 and 34 times higher than SBC coke and flexicoke. Liquid-solids adsorption also was shown that the adsorption capacity of coconut shell activated carbon is 138.9 times higher than that of the flexicoke.

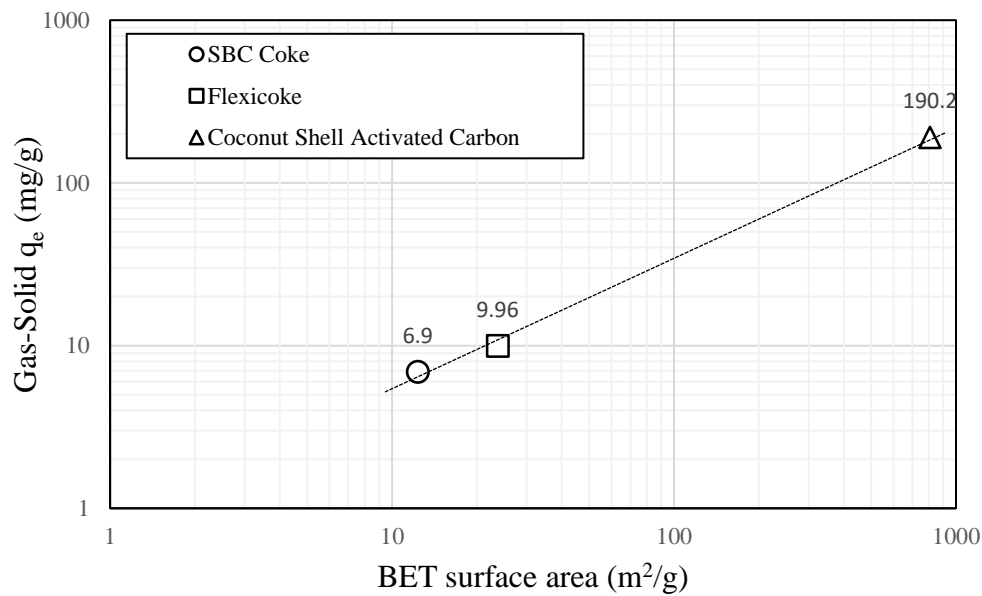


Figure 37. Comparison of gas-solid adsorption equilibrium with BET surface area

Figure 37 suggests that a reasonable correlation is associated with the obtained equilibrium values from hydrocarbon adsorption results and the BET surface area for SBC coke, flexicoke and coconut shell activated carbon. Figure 38 also shows the equilibrium gas-solid adsorptions versus equilibrium liquid-solid adsorption which was obtained in chapter 3.

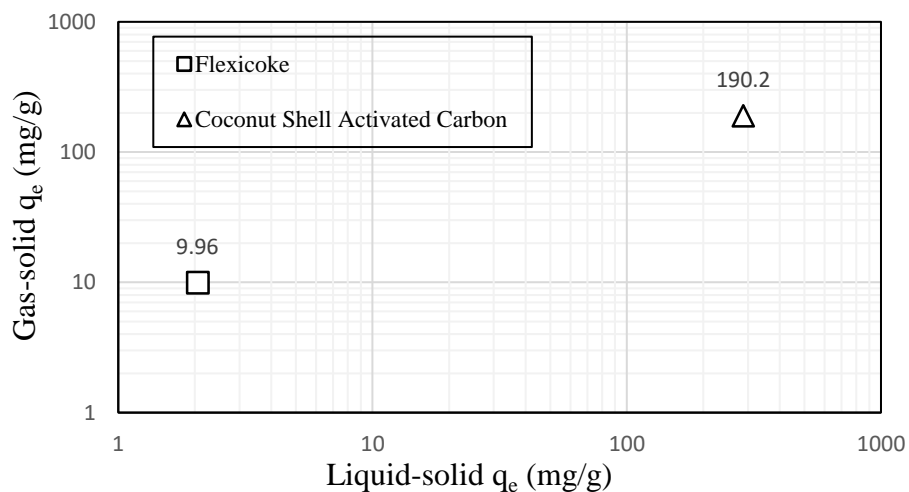


Figure 38. Equilibrium gas-solid results versus equilibrium liquid-solid results.

4.5 Summary of the Chapter

A vertically oscillating gas-solid contacting unit is developed and proposed for hydrocarbon adsorption kinetics with a new technique utilizing electromagnet to provide a proper gas-solid contact at the required moment. The system is capable of measuring adsorption kinetics at the time resolution of seconds while providing a near atmosphere undiluted hydrocarbon environment at elevated temperatures ranging from 184 °C to 246 °C.

Experiments carried out to see the impact of temperature on adsorption kinetics of n-decane with coconut shell activated carbon. The reproducibility of the results tested with the equipment via reasonable temperature trend on adsorption kinetics and obtaining similar equilibrium values and close kinetics with replicates at each temperature.

The effect of molecular weight and hydrocarbon adsorbate shape was also investigated on adsorption kinetics. Results were shown in the boiling +30 °C for different adsorbates. Adsorption kinetics was compared both in molar and mass basis.

The adsorption kinetics of SBC coke and flexicoke carried out in the equipment limit conditions (normal dodecane at 226 °C). Obtained results compared with coconut shell activated carbon adsorption kinetics at the same operating conditions. The equilibrium results compared and correlated with surface area and total pore volume obtained from BET also compared with liquid-solid adsorption results.

Chapter 5

5 Conclusion

A review of the literature on gas-solid adsorption, focusing on measurement methods, showed that no readily available method could perform accurate measurements of adsorption kinetics for high-boiling point vapors, with precise temperature control, isothermal conditions, and at a time scale relevant to the freeboard of the Fluid Cokers. It was thus decided to adopt an existing reactor configuration; the JBR was developed to study fast catalytic reactions, to measure adsorption kinetics.

As expected, commercial activated carbon was found to be a much better adsorbent than any tested coke materials (fluid coke, activated coke, flexicoke). The studied flexicoke adsorbed approximately 2.5 times more liquid adsorbate than fluid coke, based on methylene blue measurements. Activating fluid coke with carbon dioxide at elevated temperature produced an activated coke that nearly matched the liquid-solid adsorbent characteristics of flexicoke.

The vertically oscillating gas-solid contacting unit developed for this study performed as designed and provided reproducible results. Tests with a commercial activated carbon, fluid coke, and flexicoke gave equilibrium adsorption uptakes that correlated well with BET and liquid adsorption results. Flexicoke adsorbed 46% more n-dodecane vapors than fluid coke.

Adsorption kinetics of all the tested adsorbents could be well correlated with a pseudo-first order rate model. The time at which the adsorbate uptake reached 63.2 % of its equilibrium value ranged from 83s for fluid coke to 51 s for flexicoke and 1220 s for activated carbon. This confirmed that adsorption for the activated carbon occurs within small pores, thus slowed by internal pore diffusion. With fluid coke and flexicoke, most hydrocarbon vapor adsorption occurred at time scales that are comparable to the freeboard region of the Fluid Cokers.

From the measured adsorption kinetics of hydrocarbons on raw fluid coke and flexicoke, accompanied with knowledge of the approximate total amount of gaseous phase and residence time of scouring coke particles in the fluid coker's horn chamber, a rough ratio of gas adsorbed by particles can be anticipated. The calculation concludes that 0.53% of vapor phase residing in the horn chamber can be expected to be adsorbed with raw fluid coke. However, this ratio is predicted to increase to 1.25 % in case of switching raw fluid coke to flexicoke.



Title: Classification of Gibbs adsorption isotherms
Author: M.D Donohue,G.L Aranovich
Publication: Advances in Colloid and Interface Science
Publisher: Elsevier
Date: 1 July 1998
 Copyright © 1998 Elsevier Science B.V. All rights reserved.

Logged in as:
 ERFAN PAZOKI TOROUDI

[LOGOUT](#)

Order Completed

Thank you for your order.

This Agreement between Western University ("You") and Elsevier ("Elsevier") consists of your license details and the terms and conditions provided by Elsevier and Copyright Clearance Center.

Your confirmation email will contain your order number for future reference.

[printable details](#)

License Number	4477320425045
License date	Nov 27, 2018
Licensed Content Publisher	Elsevier
Licensed Content Publication	Advances in Colloid and Interface Science
Licensed Content Title	Classification of Gibbs adsorption isotherms
Licensed Content Author	M.D Donohue,G.L Aranovich
Licensed Content Date	Jul 1, 1998
Licensed Content Volume	76
Licensed Content Issue	n/a
Licensed Content Pages	16
Type of Use	reuse in a thesis/dissertation
Portion	figures/tables/illustrations
Number of figures/tables/illustrations	1
Format	electronic
Are you the author of this Elsevier article?	No
Will you be translating?	No
Original figure numbers	Figure 1
Title of your thesis/dissertation	Adsorption Kinetics of C9-C12 Hydrocarbons on Carbonaceous Materials
Expected completion date	Dec 2018
Estimated size (number of pages)	130

SPRINGER NATURE

Title: Measurement of Gas Mixture Adsorption Equilibria of Natural Gas Compounds on Microporous Sorbents

Author: J.U. Keller, F. Dreisbach, H. Rave et al

Publication: Adsorption

Publisher: Springer Nature

Date: Jan 1, 1999

Copyright © 1999, Kluwer Academic Publishers

Logged in as:
ERFAN PAZOKI TOROUDI
Account #:
3001372578

[LOGOUT](#)

Review Order

Please review the order details and the associated [terms and conditions](#).

No royalties will be charged for this reuse request although you are required to obtain a license and comply with the license terms and conditions. To obtain the license, click the Accept button below.

Licensed Content Publisher	Springer Nature
Licensed Content Publication	Adsorption
Licensed Content Title	Measurement of Gas Mixture Adsorption Equilibria of Natural Gas Compounds on Microporous Sorbents
Licensed Content Author	J.U. Keller, F. Dreisbach, H. Rave et al
Licensed Content Date	Jan 1, 1999
Licensed Content Volume	5
Licensed Content Issue	3
Type of Use	Thesis/Dissertation
Requestor type	academic/university or research institute
Format	electronic
Portion	figures/tables/illustrations
Number of figures/tables/illustrations	3
Will you be translating?	no
Circulation/distribution	<501
Author of this Springer Nature content	no
Title	Adsorption Kinetics of C9-C12 Hydrocarbons on Carbonaceous Materials
Institution name	n/a
Expected presentation date	Dec 2018
Portions	Figure3, figure 4, and figure 7 is used in the thesis.



Title: A novel fluidized and induction heated microreactor for catalyst testing
Author: Mohammad Latifi, Franco Berruti, Cedric Briens
Publication: AICHE Journal
Publisher: John Wiley and Sons
Date: Jun 2, 2014
Copyright © 2014, John Wiley and Sons

Logged in as:
ERFAN PAZOKI TOROUDI
Account #:
3001372578

LOGOUT

Review Order

Please review the order details and the associated [terms and conditions](#).

No royalties will be charged for this reuse request although you are required to obtain a license and comply with the license terms and conditions. To obtain the license, click the Accept button below.

Licensed Content Publisher	John Wiley and Sons
Licensed Content Publication	AICHE Journal
Licensed Content Title	A novel fluidized and induction heated microreactor for catalyst testing
Licensed Content Author	Mohammad Latifi, Franco Berruti, Cedric Briens
Licensed Content Date	Jun 2, 2014
Licensed Content Volume	60
Licensed Content Issue	9
Licensed Content Pages	16
Type of use	Dissertation/Thesis
Requestor type	University/Academic
Format	Electronic
Portion	Figure/table
Number of figures/tables	1
Original Wiley figure/table number(s)	Figure 1
Will you be translating?	No
Title of your thesis / dissertation	Adsorption Kinetics of C9-C12 Hydrocarbons on Carbonaceous Materials
Expected completion date	Dec 2018
Expected size (number of pages)	130

Bibliography

- Akkimaradi, B.S., Prasad, M., Dutta, P., Srinivasan, K., 2001. Adsorption of 1,1,1,2-tetrafluoroethane on activated charcoal. *J. Chem. Eng. Data* 46, 417–422.
- Aksu, Z., Kabasakal, E., 2004. Batch adsorption of 2,4-dichlorophenoxy-acetic acid (2,4-D) from aqueous solution by granular activated carbon. *Separation and Purification Technology*, **35**(3):223-240. [doi:10.1016/S1383-5866(03)00144-8]
- Al-Muhtaseb, S. A.; Holland, C. E.; Ritter, J. A. Adsorption of C₁ – C₇ Normal Alkanes on BAX- Activated Carbon . 2. Statistically Optimized Approach for Deriving ... Statistically Optimized Approach for Deriving Thermodynamic Properties from the Adsorption Isotherm. **2001**, No. September 2017.
- Álvarez, A.; Borges, M.; Corral-Pérez, J. J.; Olcina, J. G.; Hu, L.; Cornu, D.; Huang, R.; Stoian, D.; Urakawa, A. CO₂ Activation over Catalytic Surfaces. *ChemPhysChem* **2017**, *18* (22), 3135–3141.
- Aly, Z.; Graulet, A.; Scales, N.; Hanley, T. Characterisation, Kinetics, Equilibrium and Thermodynamic Studies Removal of Aluminium from Aqueous Solutions Using PAN-Based Adsorbents : Characterisation, Kinetics, Equilibrium, and Thermodynamic Studies. **2013**, No. December.
- Atias, J. A.; Tonetto, G. . de L. Modeling Fluid Catalytic Cracking in a Novel CREC Riser Simulator: Adsorption Parameters under Reaction Conditions. *Int. J. Chem. React. Eng.* **2003**, 1 (A-50), 1-25.
- Atias, J. A.; De Lasa, H. Adsorption and Catalytic Reaction in FCC Catalysts Using a Novel Fluidized CREC Riser Simulator. *Chem. Eng. Sci.* **2004**, *59* (22–23), 5663–5669.
- Bi, H.T, Grace, J.R., Lim, C.J., Rusnell, D., Bulbuc, D., McKnight, C.A, 2008. Hydrodynamics of the Stripper Section of Fluid Cokers, 2008.

Blaser, D. Fluid Coking with Improved Stripping, 1986.

Chiang, Y.-C.; Chiang, P.-C.; Huang, C.-P. Effects of Pore Structure and Temperature on VOC Adsorption on Activated Carbon. *Carbon N. Y.* **2001**, 39 (4), 523–534.

Choi, B.; Choi, D.; Lee, Y.; Lee, B.; Kim, S. Hydrogen onto Activated Carbon. **2003**, *m*, 603–607.

Co, E. FUELS TECHNOLOGIES FLUID COKING™ Conversion Technology Client Integration for Power / Steam.

Colomba, A. Production of Activated Carbons from Pyrolytic Char for Environmental Applications. **2015**, No. August, 193.

Corma. Transformation of Hydrocarbons on Zeolite Catalyst. **1993**, 22, 33–52.

Costa, E.; Sotelo, J. L. Adsorption Of Binary And Ternary Hydrocarbon Gas Mixtures On Activated Carbon : Experimental Determination And Theoretical Prediction Of The Ternary Equilibrium Data. **1981**, 27 (1), 5–12.

Donohue, M. Classification of Gibbs Adsorption Isotherms Classification of Gibbs Adsorption Isotherms. **2017**, 8686 (July 1998).

Ellis, P. J.; Paul, C. A. Delayed Coking Fundamentals. *AIChE 1998 Spring Natl. Meet.* **1998**, 1–20.

Falabella Sousa-Aguiar, E.; Liebsch, A.; Chaves, B. C.; Costa, A. F. Influence of the External Surface Area of Small Crystallite Zeolites on the Micropore Volume Determination. *Microporous Mesoporous Mater.* **1998**, 25 (1), 185–192.

Farneth, W. E.; Gorte, R. J. Methods for Characterizing Zeolite Acidity. *Chem. Rev.* **1995**, 95 (3), 615–635.

Ginsburg, J. M.; Lasa, H. I. De. INTERNATIONAL JOURNAL OF CHEMICAL The CREC Fluidized Riser Simulator. Characterization of Mixing Patterns The CREC Fluidized Riser Simulator. Characterization of Mixing Patterns. **2003**, 1.

Hamdaoui, O.; Naffrechoux, E. Modeling of Adsorption Isotherms of Phenol and Chlorophenols onto Granular Activated Carbon. Part II. Models with More than Two Parameters. *J. Hazard. Mater.* **2007**, *147* (1–2), 401–411.

Ho, Y. S.; Mckay, G. Pseudo-Second Order Model for Sorption Processes. **1999**, *34*, 451–465.

Jankovic, J. Simulation of the Scrubber Section of a Fluid Coker. **1996**.

Jiménez-Cruz, F.; Hernández, J. A.; Laredo, G. C.; Mares-Gallardo, M. T.; García-Gutierrez, J. L. Adsorption of N-Heptane and 2-Methylheptane in the Gas Phase on Polyvinylidene Chloride-Based Microporous Activated Carbon. *Energy and Fuels* **2007**, *21* (5), 2929–2934.

Karimi, A.; Thinon, O.; Fournier, J.; Hill, J. M. Activated Carbon Prepared from Canadian Oil Sands Coke by CO₂ Activation: I. Trends in Pore Development and the Effect of Pre-Oxidation. *Can. J. Chem. Eng.* **2013**, *91* (9), 1491–1499.

Keller, J. U.; Dreisbach, F.; Rave, H.; Staudt, R.; Tomalla, M. Measurement of Gas Mixture Adsorption Equilibria of Natural Gas Compounds on Microporous Sorbents. *Adsorption* **1999**, *5* (3), 199–214.

Laredo, G. C.; Castillo, J.; Marroquin, J. O. Gas-Phase Diffusion of Linear and Multi-Branched Alkanes on a Carbon Molecular Sieve by the ZLC Method. *Sep. Purif. Technol.* **2013**, *103*, 36–42.

Latifi, M. Gasification of Bio-Oils to Syngas in Fluidized Bed Reactors Gasification of Bio-Oils to Syngas In. **2012**, No. April.

Lee, C. K.; Ashtekar, S.; Gladden, L. F.; Barrie, P. J. Adsorption and Desorption Kinetics of Hydrocarbons in FCC Catalysts Studied Using a Tapered Element Oscillating Microbalance (TEOM). Part 1: Experimental Measurements. *Chem. Eng. Sci.* **2004**, *59* (5), 1131–1138.

Lewis, W. K.; Gilliland, E. R.; Chertow, B.; Cadogan, P. HYDROCARBON GAS

MIXTURES. 1319–1326.

Li, C.; Chen, Y. W.; Yang, S. J.; Yen, R. B. In-Situ FTIR Investigation of Coke Formation on USY Zeolite. *Appl. Surf. Sci.* **1994**, *81* (4), 465–468.

Malek, A. Kinetics of Hydrocarbon Adsorption on Activated Carbon and Silica Gel. **1997**, *43* (3).

Mallory, D. G.; Mehta, S. A. R.; Moore, R. G. The Role of the Vapour Phase in Fluid Coker Cyclone Fouling: Part 2. Liquid and Vapour Yields and Compositions. *Can. J. Chem. Eng.* **2000**, *78* (2), 337–342.

McCoy, B. J.; Madras, G. I International Journal of Chemical. *Int. J. Chem. React — Eng.* **2003**, *1*, 1–15.

Murray R. Gray. *Upgrading Oil Sands Bitumen and Heavy Oil*; 2014.

Nunes, C. A.; Guerreiro, M. C. Estimation of Surface Area and Pore Volume of Activated Carbons by Methylene Blue and Iodine Numbers. *Quim. Nova* **2011**, *34* (3), 472–476.

Pfeifer, R.W., Borey, D.S., Jahnig, C. E. Pfeifer, R.W., Borey. U.S Patent No. 2,881,130, 1959.

Qada, E. N. El; Allen, S. J.; Walker, G. M. Adsorption of Methylene Blue onto Activated Carbon Produced from Steam Activated Bituminous Coal : A Study of Equilibrium Adsorption Isotherm. **2006**, *124* (1385), 103–110.

Qiu, H.; Lv, L.; Pan, B.; Zhang, Q.; Zhang, W.; Zhang, Q. Critical Review in Adsorption Kinetic Models. *J. Zhejiang Univ.* **2009**, *10* (5), 716–724.

Rao, K. S. Adsorption Kinetics for the Removal of Fluoride from Aqueous Solution by Activated Carbon Adsorbents Derived from the Peels of Selected Citrus Fruits. **2010**, *7*.

Reactors, M.; Tracers, I. And With. **1970**, *48*, 151–157.

- Rouquerol, J.; Kenneth, S. W.; Maurin, G.; Llewellyn, P. *1 Introduction Franc*; 2014.
- Saha, B. B.; Habib, K.; El-sharkawy, I. I.; Koyama, S. Adsorption Characteristics and Heat of Adsorption Measurements of R-134a on Activated Carbon ' Ristiques d ' Adsorption et Mesures de La Chaleur Caracte ' Gage ' e Par l ' Adsorption Du R-134a Par Le Charbon Actif De. *Int. J. Refrig.* **2009**, *32* (7), 1563–1569.
- Santamarina, J. C.; Klein, K. A.; Wang, Y. H.; Prencke, E. Specific Surface : Determination and Relevance. **2002**, *241*, 233–241.
- Simonin, J. On the Comparison of Pseudo-First Order and Pseudo-Second Order Rate Laws in the Modeling of Adsorption Kinetics. *Chem. Eng. J.* **2016**, *300*, 254–263.
- Siperstein, F.; Gorte, R. J.; Myers, A. L. Measurement of Excess Functions of Binary Gas Mixtures Adsorbed in Zeolites by Adsorption Calorimetry. *Adsorption* **1999**, *5* (2), 169–176.
- Siperstein, F.; Engelhard, M.; Myers, A. L. Comparison of Experimental Techniques for Measuring Isothermic Heat of Adsorption. **2000**, No. 1, 275–286.
- Solnordal, C. B.; Reid, K. J.; Hackman, L. P.; Cocco, R.; Findlay, J. Modeling Coke Distribution above the Freeboard of a FLUID COKING Reactor. *Ind. Eng. Chem. Res.* **2012**, *51* (47), 15337–15350.
- Song, X.; Bi, H.; Jim Lim, C.; Grace, J. R.; Chan, E.; Knapper, B.; McKnight, C. Hydrodynamics of the Reactor Section in Fluid Cokers. *Powder Technol.* **2004**, *147* (1–3), 126–136.
- Speight, A. and. The Fact on Oil Sands; CAPP,2014.
- Umasankar, D. P.; Kumar, D. S. S. A General Approach for Direct Conversion of Single Phase AC to AC Converter for Induction Heating System. *Circuits Syst.* **2016**, *07* (11), 3896–3910.
- Wang, K.; Do, D. D. Sorption Equilibria and Kinetics of Hydrocarbons onto Activated

Carbon Samples Having Different Micropore Size Distributions. *Adsorption* **1999**, 5 (1), 25–37.

Zimmermann, W.; Keller, J. U. A New Calorimeter for Simultaneous Measurement of Isotherms and Heats of Adsorption. *Thermochim. Acta* **2003**, 405 (1), 31–41.

6 Appendices

6.1 Delayed Coking Process

Delayed coking is an upgrading technology which is viable at current oil prices. This technology is characterized by low production cost and profound conversion which allows

increased production of the more significant amount of heavy crude oil. The process is operating using a furnace at temperatures range of 480-520 °C and low pressure (25-30) psi. Then feedstocks are moved to two or more coke drums used to hold and delay (24 hr residence time) the heated feed, while thermal cracking is taking place there at a pressure of (25-75 psi). At the end vapors from the coke-drums transfer to a fractionator where gas, naphtha, and gas oils are separated, and heavy hydrocarbons from the bottom of the fractionator recycled back to the furnace.

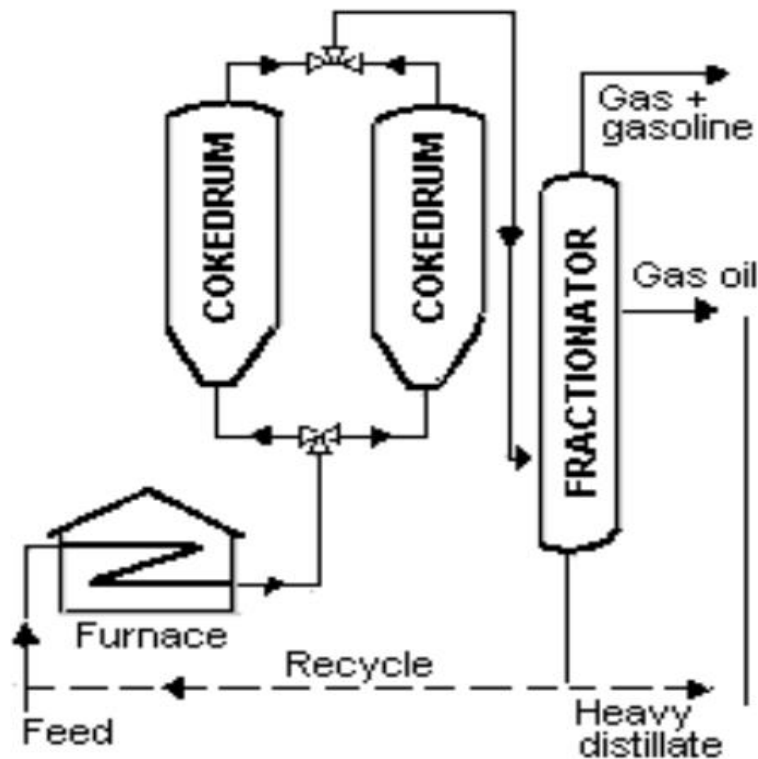


Figure 39. The schematic of the delayed coking process

6.2 Fluid Catalytic Cracking (FCC) Process

The Fluid Catalytic Cracking process plays a crucial role in the primary conversion of high-boiling petroleum fractions (gas oil) to high-value transportation fuels (gasoline, jet fuel, and diesel). In the FCC process feed reacts with powder zeolites in the fluidized bed reactor and riser in relatively lower residence time to fluid coking. To reduce the cracking of vapors in fluid coking, it may be suggested to reduce residence time using a scouring coke line

with higher upward velocity(Murray R. Gray, 2014) The FCC catalyst particles contain zeolite crystallites embedded in a matrix of alumina, clay and sometimes silica(Lee et al., 2004). Steaming to generate mesopore sites is required since without steaming, Bronsted acid sites in catalysts are inaccessible to hydrocarbon molecules. Besides, defects generated by steaming lead to diffusion of reactant into micropores of zeolite crystals and products out of it and also it increases the external surface area. (Atias and De Lasa, 2004).

Although there have been numerous studies on catalytic cracking reactions, including reaction mechanism (Corma, 1993; Li et al., 1994; Farneth and Gorte, 1995) also molecular transport within zeolites has been studied (Karger and Ruthven, 1992; Chen et al., 1994), very few studies have been done on adsorption and transport properties of commercial FCC catalyst particles. Understanding of adsorption and desorption kinetics of FCC process is crucial not only to understand what chemical reactions are occurring but also to know the design of riser and stripper where adsorption and desorption of heavy hydrocarbons are happening respectively. Catalytic cracking occurs on the active sites of a catalyst which means that reactant molecules must diffuse through the pore network of the catalyst and then be adsorbed on the surface for the conversion. Adsorption of 1,3,5-TIPB by the difference concentration between thermal and catalytic experiment was investigated (Atias and De Lasa, 2004). They performed an analysis with and without a catalyst under the same condition and found a high rate of adsorption and nearly occurrence of instantaneous equilibrium conditions. To study the kinetics of the surface-catalyzed reaction, they obtained a quantitative relation between the amount adsorbed and corresponding gas-phase partial pressure. Gas-phase catalytic cracking occurs at a temperature high enough that relatively small fraction of adsorption sites are occupied. It was shown that under the condition of FCC reactions, adsorption of chemical species at equilibrium can be represented by Henry's law (Atias, J. A.; Tonetto, 2003). Lee et al. have done experiment on adsorption equilibrium and kinetic behavior of n-hexane, n-heptane, n-octane, toluene and p-xylene in a rare-earth exchanged zeolite Y using a tapered element oscillating microbalance (TEOM) which is an inertial balance in which the mass change can be measured by calculating the natural resonance frequency of tapered quartz element containing the sample of interest. They lead to the conclusion that adsorption and desorption rates for FCC catalyst are almost the same for pure zeolite Y which means that

mass transport in the matrix component of the FCC catalyst is rapid and is not a limiting step in the adsorption process. (Falabella Sousa-Aguiar et al., 1998) carried out cracking of 1,3,5-TIPB over two zeolites, considering that the cracking reactions took place only at the outer surface of the zeolite and concluded that the external surface plays a vital role in cracking of alkyl aromatic compounds. (Atias and De Lasa, 2004) found diffusion-controlled regime at a temperature range of 350-450 °C and a kinetically controlled regime at higher temperature 450-550 °C on the study of the catalytic conversion of 1,3,5-TIPB over Y-zeolite catalysts.

6.3 Freundlich adsorption isotherm

Freundlich proposed an empirical equation for measurement of adsorption. It is mathematically expressed as

$$\frac{x}{m} = Kp^{\frac{1}{n}} \quad (1)$$

Therefore, the conventional logarithmic type of Freundlich is expressed as;

$$\text{Log}\left(\frac{x}{m}\right) = \text{Log}(K) + \frac{1}{n} \text{Log}(p) \quad (2)$$

Where x = mass of adsorbed material, m = mass of adsorbent, and p = equilibrium pressure of the adsorbate, and k , n are Freundlich constant for a known adsorbent and adsorbate at a given temperature.

According to Freundlich correlation, the amount of adsorption of low pressure can be predicted, but it fails to represent accurate amount in case of using high pressure. Freundlich isotherm only can work at a pressure lower than saturation pressure, and beyond this pressure, it fails (Levan et al., 2014).

6.4 The Brunauer-Emmet-Teller (BET) Isotherm

By considering some simplifying assumption, Brunauer, Emmet, and Teller could extend Langmuir method for multilayer adsorption which works correctly in case of having type II adsorption isotherm. Some of these assumptions are provided below;

1. Ideal gaseous molecule behavior
2. Each adsorbed molecule provides a site for the adsorption of the molecule in the upper layer
3. All sites are considered to be equivalent
4. No adsorbate-adsorbate interactions
5. The adsorbed molecule is immobile
6. In the second and higher layers, the energy of adsorption has the same value as the liquefaction energy.
7. The multilayer has an infinite thickness at $p/p^\circ=1$.

Here they defined different fractional occupancy of adsorption sites. Where,

$$\theta_i = \frac{\text{Number of sites with } i \text{ adsorbed molecules}}{\text{Total number of sites}} \quad (3)$$

Considering equilibrium condition and equalizing energy of adsorption and desorption in the i^{th} layer we have:

$$a_i P \theta_{i-1} = b_i \theta_i \exp\left(\frac{-E_i}{RT}\right), \quad (4)$$

Total adsorbed amount:

$$n = n_m [1\theta_1 + 2\theta_2 + \dots + i\theta_i + \dots] \quad (5)$$

where a_i and b_i are adsorption and desorption constants respectively and θ_{i-1} , θ_i are fraction of surface covered by $i-1$ and i layers (Brunaur, 1945).

Considering this correlation they lead to linear transformed BET equation which provides a basis for BET plot of experimental data,

$$\frac{P}{n(P^\circ - p)} = \frac{1}{n_m} \times \frac{1}{C} + \frac{C-1}{C n_m} \times \frac{P}{P^\circ} \quad (6)$$

Where,

$$C \approx \exp\left(\frac{E_1 - E_L}{RT}\right) \quad (7)$$

And E_1-E_L is known as the net heat of adsorption (Lamb and Coolidge, 1920)

6.5 Dubinin-Astakhov (D-A) Isotherm

The isotherm is expressed by the following equation:

$$W = W_0 \exp\left[- \left\{ \frac{RT}{E} \ln\left(\frac{P_s}{p}\right) \right\}^n\right] \quad (8)$$

In equation 9, W (m³/kg) is the adsorption volumetric uptake, W_0 (m³/kg) is the limiting volumetric uptake, R shows the universal gas constant, E (J/mole) is the characteristic energy, P is the pressure and P_s is the saturation pressure, T is the operating temperature and n is the heterogeneity constant (Saha et al., 2009)

The equation can also be expressed based on the adsorption mass uptake C (kg/kg):

$$C = C_0 \exp\left[- \left\{ \frac{RT}{E} \ln\left(\frac{P_s}{p}\right) \right\}^n\right] \quad (9)$$

The adsorbed phase volume is defined in the following equations:

$$v_a = v_b \exp[\Omega(T_{des} - T_b)] \quad (10)$$

Which v_a is the adsorbed phase volume, v_b is the volume at boiling point temperature, and Ω is a constant which is defined by the following equation (Akkimaradi et al., 2001)

$$\Omega = \frac{\ln\left(\frac{b}{v_b}\right)}{T_c - T_b} \quad (11)$$

$$b = RT_c / 8P_c \quad (12)$$

Where T_c and P_c are critical temperatures and pressure respectively, and T_b is adsorbent boiling point temperature.

The D-A isotherm equation with and without volume correction can be used for desorption data in the following equations:

$$\Delta C_{T_{des}} = W_0 \frac{\exp\left[-\left\{\left(\frac{RT_{des}}{E}\right) \ln\left(\frac{P_s}{P_i}\right)\right\}^n\right] - \exp\left[-\left\{\left(\frac{RT_{des}}{E}\right) \ln\left(\frac{P_s}{P_f}\right)\right\}^n\right]}{v_a} \quad (13)$$

$$\Delta C_{T_{des}} = C_0 \left(- \exp\left[-\left\{\left(\frac{RT_{des}}{E}\right) \ln\left(\frac{P_s}{P_f}\right)\right\}^n\right] \right) \quad (14)$$

6.6 Multi-component Adsorption

There is a large volume of pure gas and some binary gas adsorption equilibrium and kinetic data in the published literature, but multicomponent adsorption data are rare. It should be considered that most adsorptive deal with competitive adsorption of a multicomponent gas mixture of varied sizes. This can create complexity in the behavior of multicomponent adsorption equilibria, kinetics, and heats of adsorption. In this section, we are providing some methodologies utilized for the investigation of multicomponent adsorptive.

Multicomponent Adsorption study is of important priority, especially for the design of industrial separation processes (D.M. Ruthven, 1984; R.T. Yang 1987). Whereas, multicomponent adsorption kinetics and equilibria study are much more complicated than single component adsorptive research and there are few studies in this field as opposed to a single component. Therefore, we look forward to finding theories to estimate the behavior of multicomponent from the data of a single component. In the literature, there are some models for multicomponent adsorption kinetics as well as equilibria models such as the Langmuir kinetics model (R. Srinivasan, 1995), Pore and surface diffusion model (W. Rudzinski et al., 1997) and stochastic theory (W.R. Qureshi, 1990)

In our study, we are looking for preferential adsorption of heavier hydrocarbon on particles. There are a few studies that prove if we use a mixture of hydrocarbon, it is the heavier that adsorbs preferentially. There is no previous such study on fluid coke particles. However, there are some which have been investigated the adsorption of hydrocarbon mixture on activated carbon and silica gel.

Few studies have been done on mixture hydrocarbons adsorption on activated carbon (Myers, 1965; Friedrich and Mullins, 1972; Szepeszy and Illes, 1963). Because of

thermodynamics complexity of mixed adsorptive, they simplified equations to ideal gas conditions, and they do not coincide with experimental data. E. Costa et al. used Wilson and unique equations to calculate activity coefficients which show closeness to the ideality (activity closer to 1 corresponds to ideality). Their predicted and experimental data are close enough, and they illustrated preferential adsorption of the heavier hydrocarbon using binary and a ternary mixture of Methane, Ethane, Propylene, and Propane(Costa and Sotelo, 1981).

W.K Lewis et al., investigated the relative volatility of binary and ternary lower gaseous hydrocarbons (Ethane-Ethylene-Propane-Propylene) on silica gel and activated carbon. They concluded that at a specific partial pressure, the amount of gas adsorbed in the single component is higher compared to present of other hydrocarbons and having a gas mixture. In their results, they have represented mole fraction of more volatile component (Lighter hydrocarbon) in gas versus in the adsorbate and it is shown that for each gas mole fraction, there is less mole fraction in the adsorbate which means that it is replaced by a heavier component in the binary mixture and proves the preferential adsorption. In the Ethane Ethylene mixture test, they compared silica gel with activated carbon regarding selectivity, and silica gel is more selective for the unsaturated compound. Relative volatility of the binary system is defined by (y_1x_2/ y_2x_1) which y is the mole fraction in gas and x is the mole fraction in adsorbate. It is shown that relative volatility is higher in activated carbon. In the ethylene-propylene and ethylene-propane tests by the same method, they have shown preferential adsorption of heavier hydrocarbons which are Propylene and Propane. They have also shown the effect of temperature and pressure in the study. Increasing pressure and temperature is affecting on lowering the relative volatility. It has also been shown that the amount of gas mixture adsorbed at a certain pressure lies between maximum (heaviest hydrocarbon) and minimum (Lightest) adsorption quantity of pure gases. Finally, the relative volatility of each two components selection of a ternary combination is the same as relative volatility of a binary mixture, thus, they use data obtained for binary mixtures for ternary ones(Lewis et al.)

6.7 The Heat of Adsorption Measurement

Three different methods are widely used to calculate the heats of adsorption (Siperstein et al., 2000):

1. Differentiation of adsorption isotherms at a constant loading
2. Measurement base on isosters
3. Calorimetry

Isosteric heat of a pure gas thermodynamically is defined by the molar enthalpy of the gas phase minus the differential enthalpy in the adsorbed phase.

$$q_{sT} = h^g - \left[\frac{\partial H^m}{\partial n^m} \right] T \quad (15)$$

In which, H^m is the specific enthalpy [J/Kg] for the adsorbate which has been adsorbed and n^m is the specified amount adsorbed (mol/kg). For the ideal gas law, the equation can be written as follows:

$$q_{sT} = -R \left[\frac{\partial \ln(P)}{\partial \left(\frac{1}{T}\right)} \right] n^m \quad (16)$$

Adsorption isosters are defined by plots of $\ln(p)$ versus absolute temperature at a constant loading.

The other method for calculation of heat of adsorption in the calorimetry method is described by the following equation

$$-q_{sT} = \frac{Q + \Delta PV^t}{\Delta n^m} \quad (17)$$

Q is the heat released in the process of the change of gaseous mole equal to Δn^m in the calorimeter cell. V^t is the dead space volume. Q is a negative term and ΔPV^t is smaller compared to Q.

For the binary mixture of adsorptive, heats of adsorption is measured base on the temperature coefficient of selectivity at fixed loading (Siperstein et al., 1999).

$$R\left[\frac{\partial \ln S_{1,2}}{\partial\left(\frac{1}{T}\right)}\right]=q_1-q_2 \quad (18)$$

In which $S_{1,2}$ is equal to $(x_1y_2)/(x_2y_1)$ which is selectivity of component 1 divided by the selectivity of component 2. Thermodynamic excess functions describe Vapor-liquid equilibria (VLE) (Smith et al.,1996). Activity coefficients are given by excess Gibbs free energy function which temperature is given by Gibbs-Helmholtz equation.

Molar integral enthalpy of vaporization is calculated as follows

$$\Delta h = \left(\frac{1}{n}\right) \int_0^n q dn \quad (19)$$

And for a binary mixture:

$$\Delta h = \left(\frac{1}{n_1+n_2}\right) \int_0^{n_1} \int_0^{n_2} q_1 dn_1 \quad (20)$$

The heat of mixing (excess enthalpy) is given by

$$\Delta h^e = \Delta h - \sum_i x_i \Delta h_i^0 \quad (21)$$

In which Δh_i^0 is the enthalpy of vaporization for a pure component. Excess enthalpy is also described by the Gibbs-Helmholtz equation:

$$\Delta h^e = -T^2 \left[\frac{\partial \left(\frac{\Delta g^e}{T}\right)}{\partial T} \right] \quad (22)$$

The excess Gibbs free energy is:

$$(\Delta g^e / RT) = x_1 \ln \gamma_1 + x_2 \ln \gamma_2 \quad (23)$$

Which γ_1 and γ_2 are activity coefficients.

For an adsorbed quadratic mixture we will have (Valenzuela and Myers,1989; Talu et al., 1995):

$$\Delta g^e = \Delta h^e = Cx_1x_2(1 - e^{-B\Psi}) \quad (24)$$

In which,

$$\Psi = -\phi/RT \quad (25)$$

$$\Psi = \int_0^P \frac{n}{p} dP = \int_0^P \frac{d \ln(P)}{d \ln(n)} dn \quad (26)$$

Adsorbed phase activity (γ) and change of total loading (n_t)

$$\ln(\gamma_1) = Cx_2^2(1 - e^{-B\Psi}) \quad (27)$$

$$\ln(\gamma_2) = Cx_1^2(1 - e^{-B\Psi}) \quad (28)$$

$$\frac{1}{n_t} - \frac{x_1}{n_1^0} - \frac{x_2}{n_2^0} = \frac{CB}{RT} x_1x_2(e^{-B\Psi}) \quad (29)$$

Conditions for phase equilibrium in ideal gas phase is

$$Py_1 = P_1^0 \gamma_1 x_1 \quad (30)$$

$$Py_2 = P_2^0 \gamma_2 x_2 \quad (31)$$

In ideal adsorbed solution (IAS) we have

$$C = B = 0 \quad (32)$$

$$\gamma_1 = \gamma_2 = 1 \quad (33)$$

And mixture heat is calculating as following equation (Karavias and Myers, 1992)

$$q_1 = \Delta h_1^0 + \frac{1}{n_1^0} \left[\frac{\sum_i x_i (q_i^0 - \Delta h_i^0) G_i^0 n_i^0}{\sum_i x_i G_i^0} \right] \quad (34)$$

$$q_2 = \Delta h_2^0 + \frac{1}{n_1^0} \left[\frac{\sum_i x_i (q_i^0 - \Delta h_i^0) G_i^0 n_i^0}{\sum_i x_i G_i^0} \right] \quad (35)$$

In which,

$$G_i^0 = (d \ln n / d \ln P)^0 / (n_i^0)^2 \quad (36)$$

6.8 Liquid-solid experimental procedure and Error Analysis

In this section, we cover error analyses rules and explain an exact method on liquid-solid adsorption measurement and implement the error analyses rules for liquid-solid error measurement.

If $R = X + Y - Z$; then

$$\Delta R = (\Delta X^2 + \Delta Y^2 + \Delta Z^2)^{0.5} \text{ or,}$$

$$\Delta R \approx \Delta X + \Delta Y + \Delta Z$$

1) $R = \frac{X \cdot Y}{Z}$; then

$$\Delta R = |R| \times \left(\left(\frac{\Delta X}{X} \right)^2 + \left(\frac{\Delta Y}{Y} \right)^2 + \left(\frac{\Delta Z}{Z} \right)^2 \right)^{0.5}$$

2) $R = c \cdot X$

$$\Delta R = |c| \cdot \Delta X$$

3) $R = X^n$

$$\Delta R = |R| \cdot |n| \cdot \frac{\Delta X}{|X|}$$

Procedure:

Stage 1:

A sample of 2000 ppm methylene blue in a 100mL glass flask is made.

Mass of solid methylene blue= 200 mg

Error of preparing mass= $m_1=0.1$ mg

$$\text{Relative error\%} = \frac{\Delta m_1}{m_1} = 0.05 \%$$

We neglect the error associated to make up the volume in the glass flask.

Stage 2:

Preparing 100, 200, 300, 400, 500, 600, 700, 800 ppm samples from the 2000 ppm source sample. A 10mL pipette is used to transfer from the source methylene blue to a 50mL glass flask.

Relative error for each for pipette usage=

$$\frac{\text{accuracy of pipette} \times \text{number of time using pipette}}{\text{volume of source methylene blue} \times \text{Volume of total sample}} \times 100$$

Solution relative error= source methylene blue relative error+ pipette relative error

Solution concentration (ppm)	Volume of source Methylene blue (mL)	Absolute error (mL)	Relative error %	DI Water Volume (mL)	Volume of Total Sample(mL)	Pipette relative error %	Solution relative error%
100	2.5	0.1	4	47.5	50	0.080	0.13
200	5	0.1	2.000	45	50	0.040	0.09

300	7.5	0.1	1.333	42.5	50	0.027	0.077
400	10	0.1	1.000	40	50	0.020	0.070
500	12.5	0.2	1.600	37.5	50	0.032	0.082
600	15	0.2	1.333	35	50	0.027	0.077
700	17.5	0.2	1.143	32.5	50	0.023	0.073
800	20	0.2	1.000	30	50	0.020	0.070

Table 10. Step 1 in liquid-solid error analysis

Stage 3:

A certain amount of activated carbon for each sample is prepared. A balance with the accuracy of 0.1 mg is used to measure the amount of activated carbon from coal.

$$\text{Relative error for the mass of activated carbon} = \frac{\text{Accuracy of balance}}{\text{mass of activated carbon}}$$

Table 11. Step 2 in liquid-solid error analysis

Sample concentration	Mass of activated carbon	Relative error%
100	12.2	0.82
200	12.6	0.79
300	12.5	0.80
400	12.9	0.77
500	12.9	0.77
600	12.5	0.80
700	12.5	0.80
800	12.5	0.80

Stage 4:

For each concentration, we make (1) blank sample and (2) a sample with activated carbon.

The volume of each sample is 10 mL. pipette with an accuracy of 0.1 mL is used to make all samples

$$\text{Volume relative error} = \frac{\text{Accuracy of Burette}}{\text{volume of sample}} \times 100 = 1\%$$

Stage 5:

Samples are kept in the shaker at 25 °C at 500 rpm for five days to reach their equilibrium concentrations.

Stage 6:

The centrifuge is used at 4500 rpm to separate liquid and solid phase for 2 hours.

Stage 7:

Estimate of samples initial concentration from the blank samples using a UV spectrophotometer. The range which is readable for methylene blue by UV spectrophotometer is 0-25 ppm. Therefore we need to dilute each sample. Balance is used to measure how much each sample is diluted by deionized water.

Table 12. Step 3 in liquid-solid error analysis

C_0 (ppm)	Mass of Methylene Blue (mg)	Total Mass (mg)	Dilution	Dilution relative error %
100	96	3324.3	0.028	0.104
200	110.5	3291.9	0.033	0.091
300	86.5	3271	0.026	0.116
400	69.7	3411	0.02	0.144
500	68.5	3288.8	0.02	0.146
600	48	3310.7	0.014	0.208
700	36.5	3392.7	0.011	0.274
800	47.8	3367	0.014	0.209

Table 13. Step 4 in liquid-solid error analysis

Absorbance	Concentration	Dilution relative error%	Relative error of initial concentration %
0.375	96.63	0.104	0.234
0.876	203.79	0.091	0.181
1.028	305.15	0.116	0.193
1.066	409.94	0.144	0.214
1.325	502.70	0.146	0.228
1.122	608.99	0.208	0.285
0.989	720.76	0.274	0.347
1.434	799.60	0.209	0.279

The error associated with a spectrophotometer is neglected, and we assume the same relative error for initial concentrations as for dilution relative error.

Total relative error for the initial concentration measurement= Dilution relative error + solution relative error

Stage 8:

Measurement of absorption and consequently final concentration of samples containing activated carbon.

Table 14. Step 5 in liquid-solid error analysis

C ₀ (ppm)	Mass of Methylene Blue (mg)	Total Mass (mg)	Dilutio n ratio	Dilution relative error %	Absor bance	Final Concentrat ion (ppm)	Total relative error%
100	N/A	N/A	1	0	0.189	1.28	0.13
200	397.9	3238.3	0.122	0.025	0.357	21.52	0.115
300	340.5	3328.6	0.102	0.029	0.161	10.37	0.106
400	108.5	3237.5	0.033	0.092	0.461	104.01	0.162
500	75.4	3226.4	0.023	0.132	0.459	148.47	0.214
600	62.7	3468.1	0.018	0.159	0.429	178.50	0.236
700	54.5	3276.4	0.016	0.183	0.519	237.75	0.256
800	73.7	3319.4	0.022	0.136	0.948	334.32	0.206

Total relative error for the final concentration measurement= Dilution relative error + solution relative error.

Stage 9:

Calculation of equilibrium adsorption and its associated error according to the equation below.

$$q_e(\text{mg/g}) = \frac{(C_0 - C_e) \times V}{M}$$

6.9 Particles Size Distributions

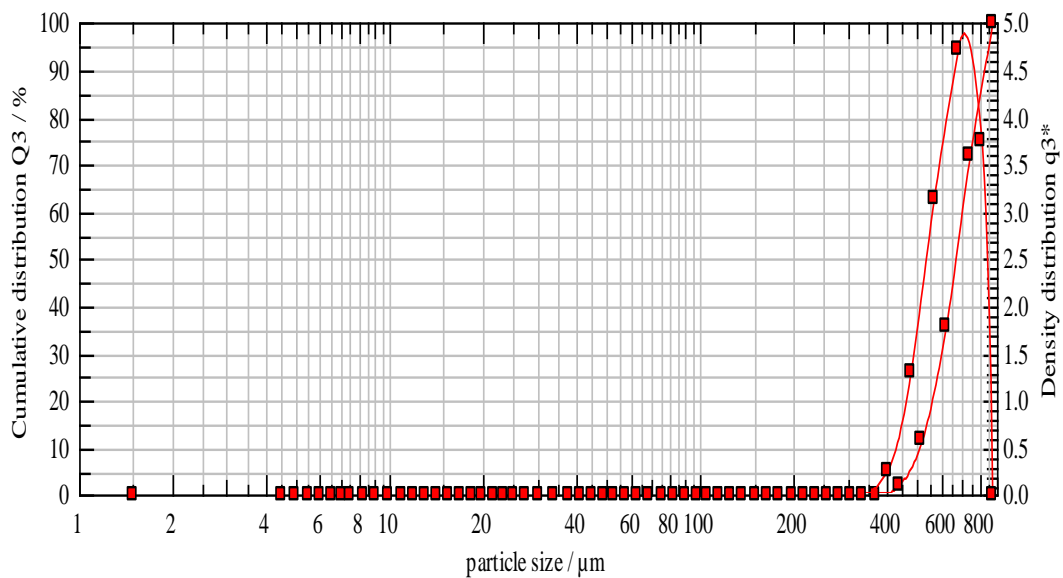


Figure 40. Coconut Shell Activated Carbon size distribution

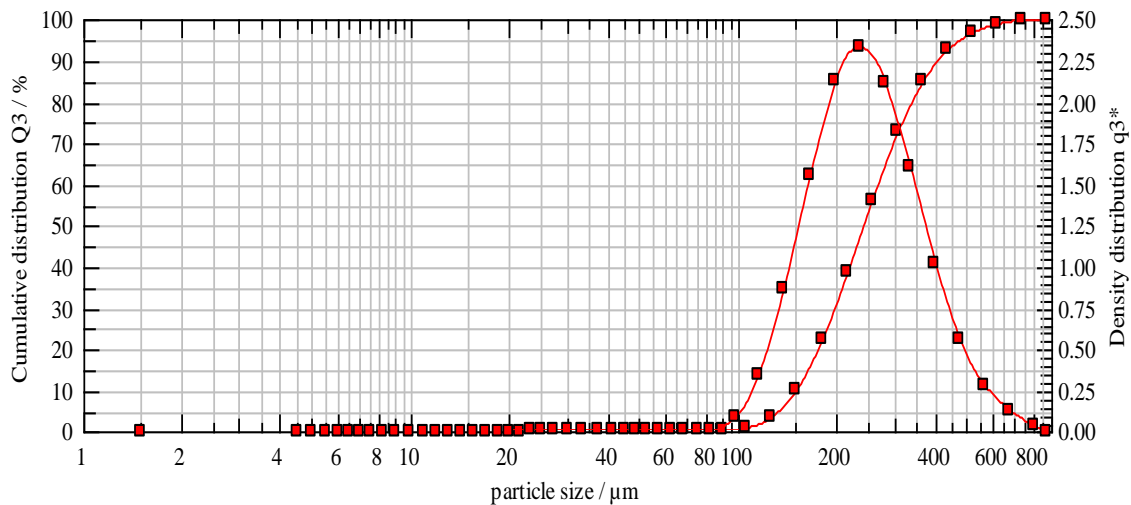


Figure 41. Flexicoke size distribution

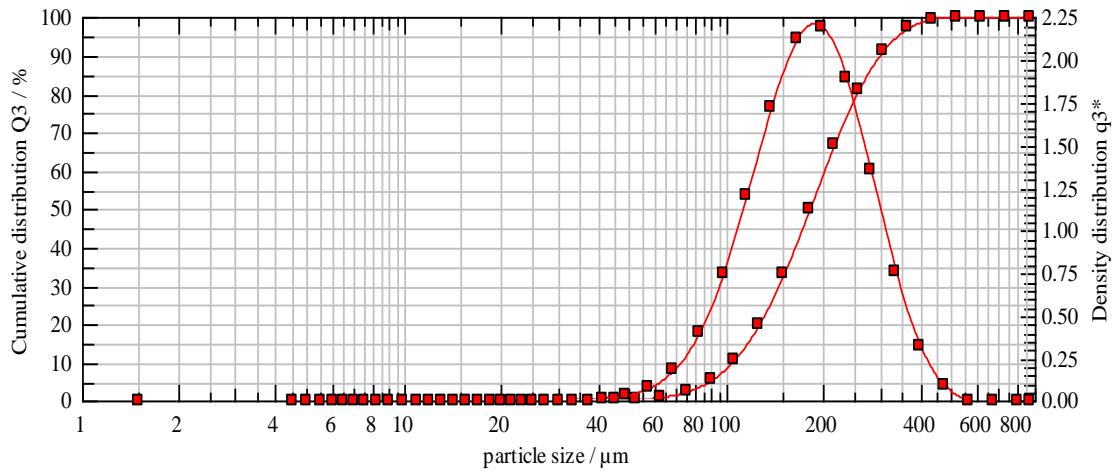


Figure 42. Raw Fluid Coke size distribution

6.10 Elemental Analysis

Elemental Analysis was performed to measure the proportion of N, C, H and S for the raw coke and activated coke following the CO_2 activation. The result for each element is the average of triplicates. A table showing every single experiment with the equipment along with the average and standard deviation is shown in the section 6-10 of appendices. Figure 19 shows a consistent trend of decreasing hydrogen content during activation. Hydrogen portion is decreasing during CO_2 activation due to the removal of volatile hydrocarbons. It should be noted that the values used for each element are an average of three replicates.

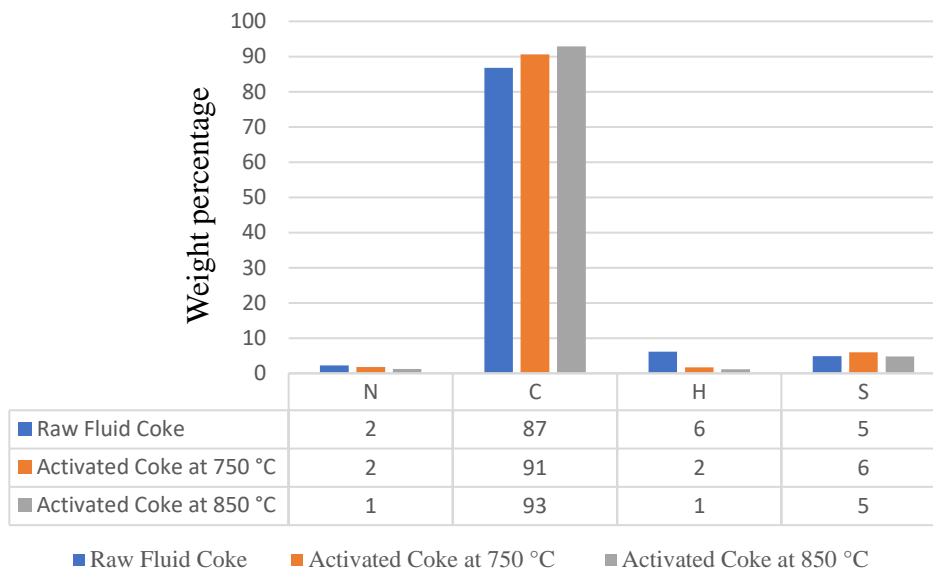


Figure 43. Elemental Analysis for coke and activated coke

From the obtained weight percentages of the elements, H/C ratio is calculated and is shown in table 15. A much higher H/C for raw coke (0.071) has been found compared to activated coke at 750 °C (0.019). Activated coke at 850 °C has even less H/C atomic ratio (0.012).

Table 15. H/C mass ratio comparison of raw coke with activated coke

	Coke	Activated Coke at 750 °C	Activated Coke at 850 °C
Run 1	0.073	0.021	0.010
Run 2	0.073	0.018	0.015
Run 3	0.067	0.017	0.012
Average	0.071	0.019	0.012
Standard Deviation	0.004	0.002	0.002

Table 16. Elemental analysis with replicates, average and standard deviation

	N	C	H	S
Raw Fluid Coke-1	2.63	86.34	6.28	4.73
Raw Fluid Coke-2	2.13	87.24	6.38	4.24
Raw Fluid Coke-3	1.89	86.67	5.78	5.65
Average	2.21	86.75	6.15	4.87
Standard Deviation	0.38	0.45	0.32	0.71
Activated Coke at 750 °C-1	2.02	90.11	1.85	6.01
Activated Coke at 750 °C-2	1.56	90.22	1.64	6.56
Activated Coke at 750 °C-3	1.71	91.37	1.55	5.36
Average	1.76	90.57	1.68	5.98
Standard Deviation	0.23	0.69	0.15	0.60
Activated Coke at 850 °C-1	1.13	91.70	0.93	6.23
Activated Coke at 850 °C-2	1.38	92.89	1.37	4.34
Activated Coke at 850 °C-3	1.12	93.90	1.10	3.87
Average	1.21	92.83	1.13	4.81
Standard Deviation	0.14785717	1.099588	0.225397	1.248193

Table 17. H/C molar ratio comparison of raw coke with activated coke

	Coke	Activated Coke at 750 °C	Activated Coke at 850 °C
Run 1	0.87	0.25	0.12
Run 2	0.88	0.22	0.18
Run 3	0.80	0.20	0.14
Average	0.85	0.22	0.15
Standard Deviation	0.04	0.02	0.03

6.11 Methylene Blue, Phenol Calibration Curve

A source methylene blue sample with a concentration of 1000 mgL^{-1} was prepared. From the source methylene blue sample, 6 different samples with concentrations of 2.5, 5, 10, 15, 20, 25 mgL^{-1} were prepared. The absorbance of each sample was measured with the UV spectrophotometer. The calibration curve is provided in Figure 4. It is important to note that for absorbance above 3 and consequently concentrations above 25 mgL^{-1} , the trend shows a plateau. Therefore, to use the UV spectrophotometer properly, it is required to stay in this boundary of concentrations (0-25 mg/L). To obtain the concentration of samples with higher concentrations, samples need to be diluted and be used in UV spectrophotometer.

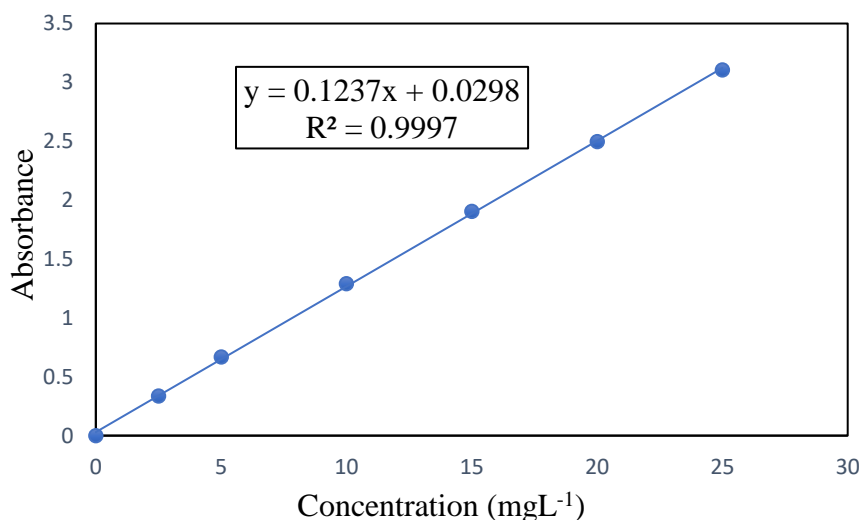


Figure 44. Methylene Blue Calibration Curve

For the phenol calibration curve, 6 samples with concentrations of 10,20,30,40,50 and 60 were made and used in UV spectrophotometer. Like methylene blue calibration curve, for phenol, only samples with concentrations between 0-60 mg/L are readable with UV spectrophotometer and any samples with higher concentrations should be diluted prior using with UV spectrophotometer.

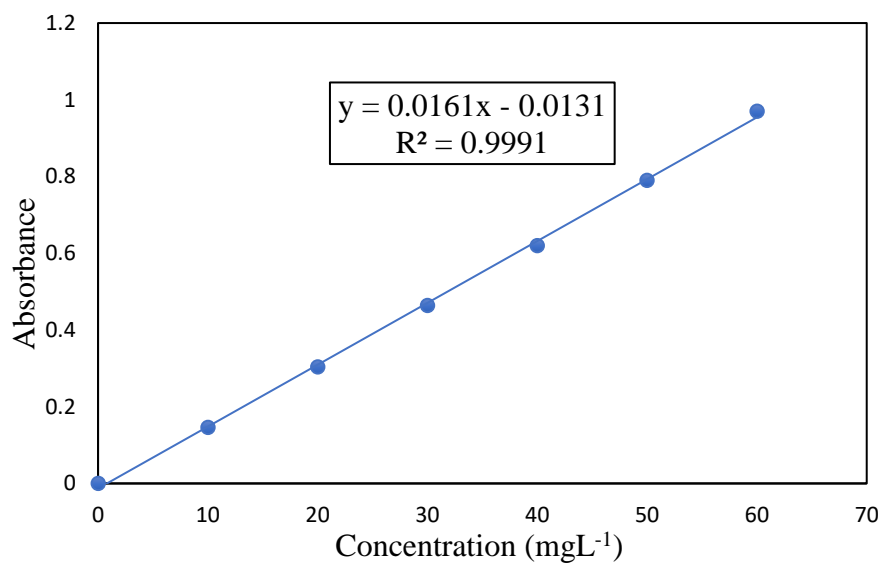


Figure 45. Phenol Calibration Curve

6.12 Equilibrium Isotherm and Kinetic Models

Table 18. 2 parameter equilibrium isotherm models

Models	Equation	Parameters	Assumptions/ Applications
Langmuir	$q_e = \frac{q_m \cdot K_L \cdot C_e}{1 + K_L \cdot C_e}$	<p>q_m: maximum uptake per unit mass of carbon (mg/g)</p> <p>K_L : Langmuir constant (L/g)</p> <p>C_e: The equilibrium concentration of adsorbate (mg/L)</p> <p>q_e: The equilibrium adsorption(mg/g)</p>	<p>Homogeneous surface</p> <p>Monolayer Adsorption</p> <p>No Interaction between adsorbed molecules</p> <p>4-adsorption is a reversible process</p>
Freundlich	$q_e = K_F \cdot C_e^{\frac{1}{n}}$	<p>K_F: Freundlich Adsorption Capacity (mg/g) . (L/mg)^{1/n}</p> <p>1/n: Intensity of adsorption (generally 1/n >1)</p> <p>C_e: The equilibrium concentration of adsorbate (mg/L)</p> <p>q_e: The equilibrium adsorption(mg/g)</p>	<p>Empirical Model</p> <p>No assumption for being reversible or irreversible model</p> <p>Heterogenous adsorbent surface</p>
BET	$q_e = \frac{K_B \cdot C_e \cdot q_m}{(C_s - C_e) \left[1 + (K_B - 1) \left(\frac{C_e}{C_s} \right) \right]}$	<p>C_s: Saturation Concentration (mg/L)</p> <p>K_B: binding intensity</p> <p>C_e: The equilibrium concentration of adsorbate (mg/L)</p> <p>q_e: The equilibrium adsorption(mg/g)</p>	<p>General multilayer model</p> <p>An uncompleted layer can be covered with next layer</p> <p>The same adsorption energy for all molecules other than first layer</p>

Table 19. 3 parameter equilibrium isotherm models

Models	Equation	Parameters	Assumptions/ Applications
Redlich Peterson	$q_e = \frac{A.C_e}{1+B.C_e^\beta}$	<p>A: Redlich Peterson isotherm constant (Lg^{-1})</p> <p>B: Constant(Lmg^{-1})$^\beta$</p> <p>C_e: The equilibrium concentration of adsorbate (mg/L)</p> <p>q_e: The equilibrium adsorption(mg/g)</p>	<p>Empirical isotherm</p> <p>Combines Langmuir and Freundlich</p> <p>Do not follow monolayer coverage</p> <p>At high concentration follows Freundlich</p> <p>At $\beta=1$ reduces to Langmuir</p>
Stips	$q_e = \frac{q_{ms}.k_s.C_e^{m_s}}{1+k_s.C_e^{m_s}}$	<p>K_s: Stips equilibrium constant (Lag^{-1})m_s</p> <p>m_s: Stips model exponent</p> <p>m_{ms}: Maximum steps adsorption capacity (mg/g)</p> <p>C_e: The equilibrium concentration of adsorbate (mg/L)</p> <p>q_e: The equilibrium adsorption(mg/g)</p>	<p>This model solves the Freundlich model limit once concentration goes to infinite, here, despite the Freundlich model, it has a finite limit</p>
Toth	$q_e = \frac{q_{mT}.C_e}{(1/K_T + C_e^{mT})^{1/mT}}$	<p>q_{mT}: Maximum Toth adsorption capacity (mg/g)</p> <p>K_s: Toth equilibrium constant</p> <p>m_T: Toth model exponent</p> <p>C_e: The equilibrium concentration of adsorbate (mg/L)</p> <p>q_e: The equilibrium adsorption(mg/g)</p>	<p>Toth model developed to reduce the Langmuir error with predicted values</p>

Table 20. Kinetic Models

Kinetic Model	Equation	Parameters
Pseudo first order	$q_t = q_e(1 - e^{-t.k_1})$	<p>q_e: adsorption capacity at equilibrium (mg/g)</p> <p>q_t: adsorption capacity at t (mg/g)</p> <p>K_1: Pseudo-first order rate adsorption constant</p> <p>t: time (min)</p>
Pseudo-second order	$q_t = \frac{t.K_2.q_e^2}{1 + q_e.K_2.t}$	<p>q_e: adsorption capacity at equilibrium (mg/g)</p> <p>q_t: adsorption capacity at t (mg/g)</p> <p>K_1: Pseudo-first order rate adsorption constant</p> <p>t: time (min)</p>
Elovich	$q_t = \frac{1}{\beta} \ln(\alpha\beta) + \frac{1}{\beta} \ln(t)$	<p>α: The rate of chemisorption at zero coverage ($mg.g^{-1}.min^{-1}$)</p> <p>β: The extent of surface coverage and activation energy for chemisorption ($g.mg^{-1}$)</p> <p>q_t: adsorption capacity at t (mg/g)</p> <p>t: time (min)</p>
Modified Second Order	$q_t = q_e(1 - \frac{1}{k_2t + \beta_2})$	
nth-order kinetics	$q_t = q_e \left\{ 1 - \left[\frac{1}{\beta_n + k_n(n-1)t} \right]^{1/(n-1)} \right\}$	
Intraparticle diffusion	$q_t = k_{dif}t^{1/2} + C$	

6.13 Vaporization Vessel

The ceramic has been used as a thermal insulator sleeve. The crucible is contained of an internal thin cup inside the ceramic crucible. An O-ring was applied between the crucible and the lid as well as six brass bolts for the closure of the system to make a proper seal for the equipment. The schematics of the crucible with dimensions for its kinetics is provided in the following figures. The total internal volume of the crucible is 500 mL with the thickness of 2.15 cm and 3.3 cm in the side and bottom respectively.

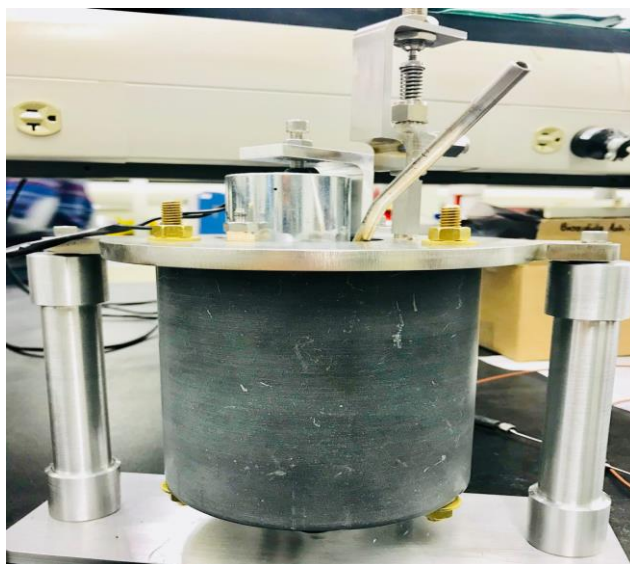


Figure 46. The actual Ceramic Crucible

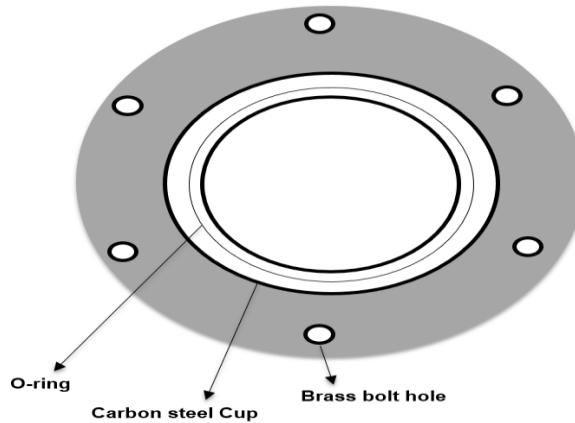


Figure 47. Crucible view from the top

6.14 Solids-Cup

A stainless steel cylindrical char-cup is welded to the lid to contain particles inside the crucible and release them at the required time. The char-cup is designed to satisfy coke to hydrocarbon ratio in the Fluid Coker (This value is 2% in volumetric basis). Therefore internal diameter is 40 mm with a height of 8 mm which gives us the interior volume of 10 mL and its wall thickness is approximately 3mm.

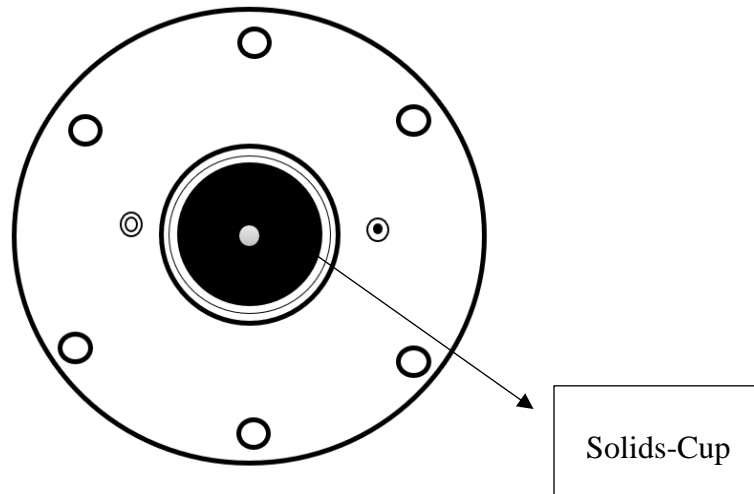


Figure 48. Solids-cup configuration relative to the lid

6.15 Round DC Electromagnet

A 2-inch diameter round 24V/5.6 W DC electromagnet with a maximum pull of 180 lbs is utilized to pull up a stainless-steel lid of the char-cup, seal it using an O-ring between the char-cup and its lid and release the lid and particles at the proper time by disabling it.

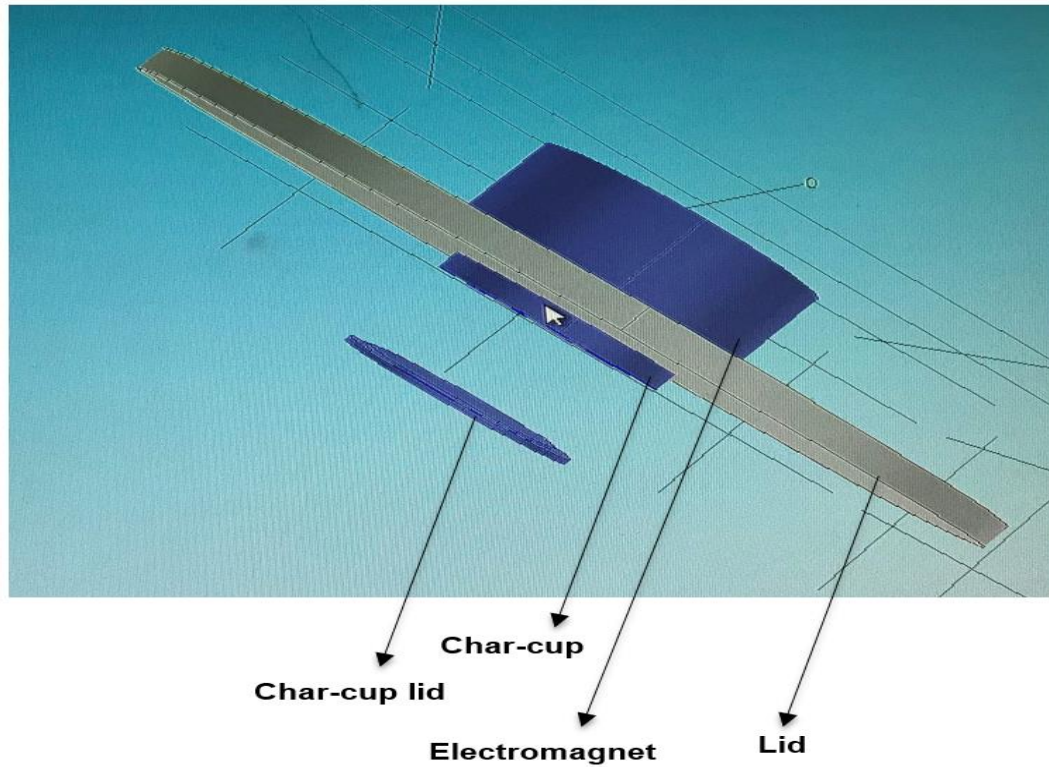


Figure 49. Electromagnet position relative to the crucible lid and char cup

6.16 Pneumatic Valve

Preliminary experiments with hydrocarbons suggest that hydrocarbon condensations and its circulation in the system will make it challenging to establish hydrocarbon vapor adsorption results due to the change in partial pressure. Hence, to be in the safe side for experiments, an internal closure of the system is required to avoid any risk of hydrocarbons condensation and liquid droplets in the closed system before measurement. A pneumatic

valve (“Anti-condensation” valve) is designed, therefore, to close the system internally using pressurized air and a spring rod.

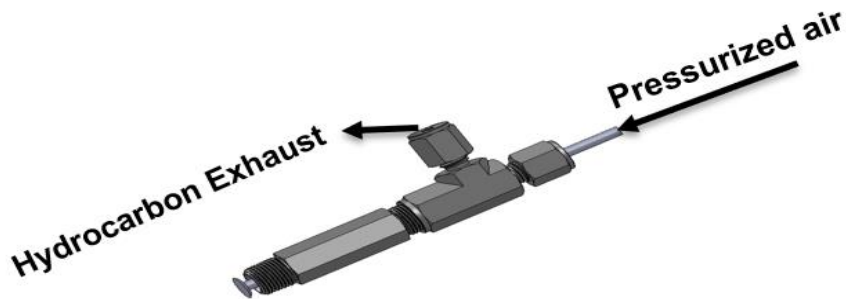


Figure 50. Pneumatic Valve

6.17 Induction Heating Supply

Induction heating is a flame-free, non-contacting, efficient and very fast paced method which is used in industry for numerous usages and advantages such as hardening, melting and welding of conductive materials (Latifi, 2012).

Induction induces a high-frequency altering current through electromagnetic forces. A magnetic field is generated, once any high conductive material is placed in between the coil. The altering electromagnetic field creates eddy currents in the object in between the coil and results in resistive losses and consequently heat the material. The reason why ferromagnetic materials heat up with induction easier than the others is that by altering magnetic field, these materials are magnetized and demagnetized rapidly which causes magnetic domains to flip back and forth and creates hysteresis losses and result in heat (Umasankar and Kumar, 2016).

In our study, a 48 VDC/ 1 KW power supply is used to generate power for the induction system. The internal cup inside the ceramic sleeves gets hot, whereas, the Ceramic and brass bolts do not heat up in this process.

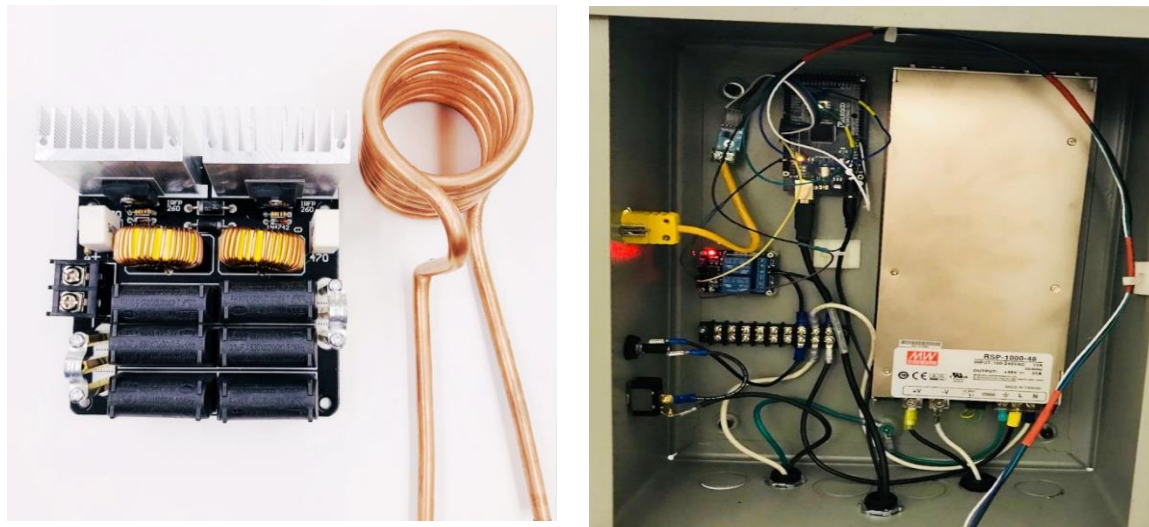


Figure 51. Induction power board, copper coil and power supply box for induction heat generation

6.18 Pneumatic Actuator

In our study, we aim to have the adsorption of gaseous hydrocarbons on solid particles. Therefore, to have a better mass transfer and to eliminate the effect of external mass transfer, proper gas-solid mixing is essential. Adequate gas-solid mixing in the system results in better mass transfer and provides uniform temperature. In this study, we run isothermal experiments. Hence, the unit should be capable of being operated in uniform and constant temperatures.

The required amplitude of the pneumatic actuator is required to be almost the same as the height of the crucible for proper mixing. Once the particles of the bed expand over the height of the crucible, the gas which was initially located at the top of the vessel moves downward. The opposite of this happens while the bed contracts downward, so this time gas is moving upward and required contact is taking place (Latifi, 2012)

To provide agitations, a single rod air cylinder is utilized which works by a solenoid valve and is activated by reed switches. A controller box is controlled the alternative motion of the unit. The amplitude of the unit is altered by changing the position of the reed switches, and the required frequency is set by the air pressure regulator attached to the controller box. Inert glass-bead particles are used in the system to better mix the particles and gas and have a better heat transfer prior gas-solid contact. The required frequency and amplitude for the system are tested with a transparent vessel (with almost the same mass as the real ceramic crucible) and using stainless steel balls. The required amplitude and frequency are set in the condition where steel balls are hitting the top of the vessel. The frequency of the system with ceramic crucible is estimated to be 3 Hz.

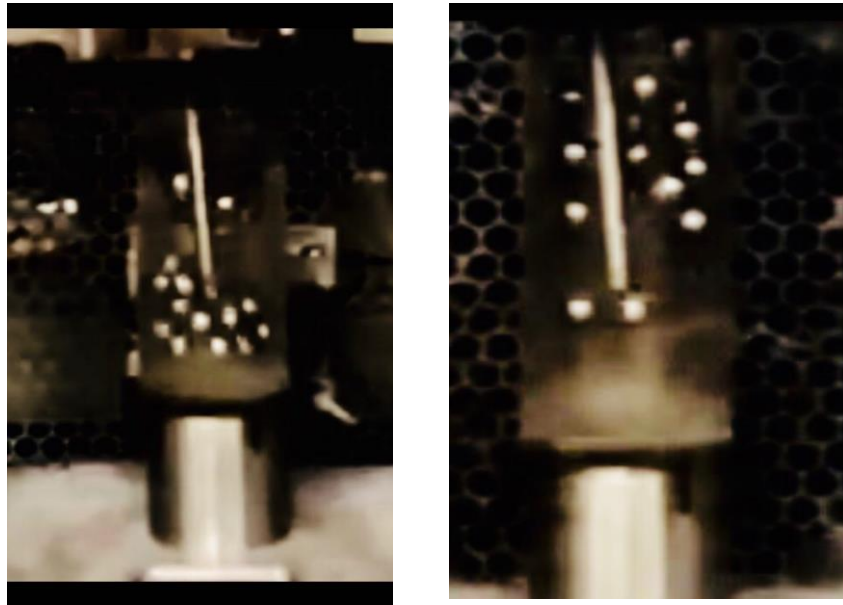


Figure 52. A scan of motions of stainless steel balls in the transparent vessel

6.19 Sauter Mean Diameter of Adsorbents

A Sympa Tec Helos particle size analyzer is used to measure the particle size distribution of different adsorbents. Table 6 is comparing the Sauter mean diameter for the adsorbents which are used in the thesis. The coconut shell activated carbon has a Sauter mean diameter of approximately three times higher than that of the flexicoke and four times higher than that of the raw fluid coke. CO₂ activation and pretreatments had a negligible effect on the particle size.

Table 22. Sauter Mean diameter of different adsorbents

	Coconut Shell Activated Carbon	Flexicoke	Raw Fluid Coke	Activated Coke at 850 °C	SBC Coke
Sauter Mean Diameter (μm)	634.1	224.2	162.8	158.2	156.5

Curriculum Vitae

Name: Erfan Pazoki Toroudi

Post-secondary Education and Degrees: University of Tehran
Tehran, Iran
2012-2016 B.Sc

The University of Western Ontario
London, Ontario, Canada
2016-2018 M.E.Sc

Honors and Awards: Ranked among top 0.2 % of national entrance exam, Iran
2012

Mathematics and Computer national Olympiad award
2011

Related Work Experience

Teaching Assistant
Advanced Fluidization in Engineering (CBE 3550)
The University of Western Ontario
Sep 2017-Jan 2018

Teaching Assistant
Computational Method in Engineering
The University of Western Ontario
Jan 2018-May 2018

Research Assistant
Syncrude Fluid Coker Cyclone Fouling Project
ICFAR, Ilderton, Ontario, Canada
Sep 2016-Sep 2018